

PL-TR-96-2290

SSS-DTR-96-15568

# **APPLICATION OF SOVIET PNE DATA TO THE ASSESSMENT OF THE TRANSPORTABILITY OF REGIONAL DISCRIMINANTS**

**J. R. Murphy  
D. D. Sultanov  
B. W. Barker**

**I. O. Kitov  
M. E. Marshall**

**Maxwell Technologies, Incorporated  
8888 Balboa Avenue  
San Diego, CA 92123-1506**

**October 1996**

**Scientific Report No. 1**

**Approved for public release; distribution unlimited**

**19970328 006**



**PHILLIPS LABORATORY  
Directorate of Geophysics  
AIR FORCE MATERIEL COMMAND  
HANSCOM AFB, MA 01731-3010**

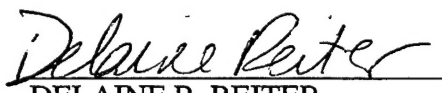
**DTIC QUALITY INSPECTED 1**

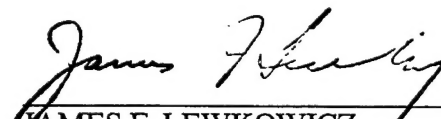
SPONSORED BY  
Air Force Technical Applications Center  
Directorate of Nuclear Treaty Monitoring  
Project Authorization T/5101

MONITORED BY  
Phillips Laboratory  
CONTRACT No. F19628-95-C-0109

The views and conclusions contained in this document are those of the authors and should not be interpreted as representing the official policies, either express or implied, of the Air Force or U.S. Government.

This technical report has been reviewed and is approved for publication.

  
DELAINE R. REITER  
Contract Manager  
Earth Sciences Division

  
JAMES F. LEWKOWICZ  
Director  
Earth Sciences Division

This report has been reviewed by the ESD Public Affairs Office (PA) and is releasable to the National Technical Information Service (NTIS).

Qualified requestors may obtain copies from the Defense Technical Information Center. All others should apply to the National Technical Information Service.

If your address has changed, or you wish to be removed from the mailing list, or if the addressee is no longer employed by your organization, please notify PL/IM, 29 Randolph Road, Hanscom AFB, MA 01731-3010. This will assist us in maintaining a current mailing list.

Do not return copies of this report unless contractual obligations or notices on a specific document requires that it be returned.

REPORT DOCUMENTATION PAGE			Form Approved OMB No. 0704-0188	
Public reporting burden for this collection of information is estimated to average 1 hour per response, including the time for reviewing instructions, searching existing data sources, gathering and maintaining the data needed, and completing and reviewing the collection of information. Send comments regarding this burden estimate or any other aspect of this collection of information, including suggestions for reducing this burden, to Washington Headquarters Services, Directorate for Information Operations and Reports, 1215 Jefferson Davis Highway, Suite 1204, Arlington, VA 22202-4302, and to the Office of Management and Budget, Paperwork Reduction Project (0704-0188), Washington, DC 20503.				
1. AGENCY USE ONLY (Leave blank)		2. REPORT DATE October, 1996	3. REPORT TYPE AND DATES COVERED Scientific No.1	
4. TITLE AND SUBTITLE APPLICATION OF SOVIET PNE DATA TO THE ASSESSMENT OF THE TRANSPORTABILITY OF REGIONAL DISCRIMINANTS			5. FUNDING NUMBERS Contract No. F19628-95-C-0109  PE 35999F  PR 5101  TA GM WU AE	
6. AUTHOR(S)  J. R. Murphy, D. D. Sultanov*, B. W. Barker, I. O. Kitov* and M. E. Marshall				
7. PERFORMING ORGANIZATION NAME(S) AND ADDRESS(ES)  Maxwell Technologies, Inc. 8888 Balboa Avenue San Diego, CA 92123-1506			8. PERFORMING ORGANIZATION REPORT NUMBER  SSS-DTR-96-15568	
9. SPONSORING/MONITORING AGENCY NAME(S) AND ADDRESS(ES)  Phillips Laboratory 29 Randolph Road Hanscom AFB, MA 01731-3010  Contract Manager: Delaine Reiter/GPE			10. SPONSORING/MONITORING AGENCY REPORT NUMBER  PL-TR-96-2290	
11. SUPPLEMENTARY NOTES  *Institute for Dynamics of the Geospheres, Russian Academy of Sciences				
12a. DISTRIBUTION/AVAILABILITY STATEMENT  Approved for public release; distribution unlimited			12b. DISTRIBUTION CODE	
13. ABSTRACT (Maximum 200 words)  This project represents a joint research investigation being carried out by scientists from Maxwell Technologies, Inc. and the Russian Institute for Dynamics of the Geospheres (IDG). The objective of the study is to use regional seismic data recorded from Soviet PNE tests to derive improved, quantitative bounds on the ranges of seismic signal characteristics which could be expected from underground nuclear explosions which might be conducted under the wide variety of source and propagation path conditions which must be considered in global test monitoring. A digital database of regional seismic data recorded from 63 selected Soviet PNE events at the Borovoye Geophysical Observatory in Central Asia has been acquired from IDG for use in this study and these data are being systematically analyzed to define the effects of source and propagation path variables on the spectral characteristics of the different observed regional phases. The results of these analyses are being used to derive improved constraints on the transportability of various proposed regional discriminants as they apply to underground nuclear explosions conducted over a wide range of testing conditions.				
14. SUBJECT TERMS Seismic Discrimination Nuclear Explosion Regional Borovoye Soviet PNE CTBT Monitoring			15. NUMBER OF PAGES 108 16. PRICE CODE	
17. SECURITY CLASSIFICATION OF REPORT UNCLASSIFIED	18. SECURITY CLASSIFICATION OF THIS PAGE UNCLASSIFIED	19. SECURITY CLASSIFICATION OF ABSTRACT UNCLASSIFIED	20. LIMITATION OF ABSTRACT UNLIMITED	

## Table of Contents

1.0	Introduction.....	1
2.0	Overview of Regional Seismic Data Recorded From Soviet PNE Tests .....	3
3.0	Regional Phase Spectra and Discrimination .....	30
4.0	Summary and Conclusions.....	56
4.1	Summary .....	56
4.2	Conclusions .....	57
	References .....	59
	Appendix A .....	63
	Appendix B .....	69
	Appendix C.....	83

## List of Illustrations

1	Locations of representative Soviet PNE events (large squares) shown as overlays to a shaded topographic map of the former Soviet Union and surrounding countries. The small squares correspond to the ISC seismicity for the region for the period 1988-1990.....	2
2	Map locations of selected Soviet PNE tests which were recorded at the Borovoye digital station in Kazakhstan.....	6
3	Distributions of selected Soviet PNE tests with respect to epicentral distance from Borovoye, source medium, explosion yield and depth of burial.....	8
4	Broadband, vertical component seismograms recorded at Borovoye from selected Soviet PNE tests. The vertical arrows above these traces mark the group arrival times associated with apparent velocities of 4.5 and 3.5 km/sec....	9
5	Example of a data spike on the Borovoye recording of the PNE event of 6/18/85. Such discontinuities in the data can be easily identified using the high frequency bandpass filter output (center trace).....	14
6	Example of a data dropout on the Borovoye recording of the PNE event of 10/04/79. Such discontinuities in the data can be easily identified using the high frequency bandpass filter output (center trace).....	15
7	Locations of selected Soviet PNE events with respect to the Borovoye (BRV) station in North Kazakhstan. The open circles correspond to six explosions at an average epicentral distance of about 8°; the filled circles correspond to six explosions at an average epicentral distance of about 10.5°....	16

8	Vertical component regional signals recorded at Borovoye from six Soviet PNE events located at a common epicentral distance of about $8^{\circ}$ .....	18
9	Vertical component regional signals recorded at Borovoye from six Soviet PNE events located at a common epicentral distance of about $10.5^{\circ}$ .....	19
10	Comparison of the broadband vertical component recordings and associated bandpass filter outputs for two of the PNE events from the 8 degree distance group.....	21
11	Comparison of the broadband vertical component recordings and associated bandpass filter outputs for two of the PNE events from the $10.5^{\circ}$ degree distance group.....	22
12	Vertical component regional signals recorded at Borovoye from six Soviet PNE events located at a common epicentral distance of about $8^{\circ}$ . Here the data have been approximately normalized to a common yield of 10 kt and plotted at a fixed absolute amplitude scale.....	24
13	Vertical component regional signals recorded at Borovoye from six Soviet PNE events located at a common epicentral distance of about $10.5^{\circ}$ . Here the data have been approximately normalized to a common yield of 10 kt and plotted at a fixed absolute amplitude scale.....	25
14	Noise levels as a function of frequency at the Borovoye station estimated from the pre-signal noise samples for the 12 selected Soviet PNE tests in the distance ranges of 8 and $10.5$ degrees.....	27
15	Maximum P wave amplitudes as a function of distance for the 7/21/84 PNE test. These amplitude data were taken from the Soviet Bulletin data for this event which is listed in Appendix A.....	28
16	Borovoye broadband peak amplitudes as a function of yield for the selected Soviet PNE events.....	30

17	Normalized Borovoye PNE broadband peak amplitudes as a function of yield at a reference source depth of 1000 m (left) and as a function of source depth at a reference yield of 10 kt (right).....	31
18	Borovoye regional phase spectra corresponding to the 10/04/79 (left) and 12/10/80 (right) PNE events from the 8° distance group. ....	36
19	Borovoye regional phase spectra corresponding to the 8/15/73 (left) and 9/02/81 (right) PNE events from the 10.5° distance group .....	37
20	Comparison of Borovoye $P_n$ (left) and $L_g$ (right) spectra for the selected PNE events in the 8° distance group.....	39
21	Comparison of Borovoye $P_n$ (left) and $L_g$ (right) spectra for the selected PNE events in the 10.5° distance group. ....	40
22	Comparison of yield (n) and depth (m) scaling exponents as a function of frequency for the different regional phases determined from least-squares analysis of the selected Borovoye data. ....	42
23	Comparison of yield (top) and depth (bottom) frequency dependent scaling exponents determined for the different regional phases recorded at Borovoye from the selected PNE events. ....	43
24	Comparison of theoretical (Mueller/Murphy) and observed bounds on the yield (top) and depth (bottom) frequency dependent scaling exponents determined for the regional phases for the selected PNE events.....	45
25	Comparison of predicted (dashed) and observed (solid) Borovoye $P_n$ amplitude spectra for the selected PNE events in the 8° distance range.....	46

26	Comparison of predicted (dashed) and observed (solid) Borovoye $L_g$ amplitude spectra for the selected PNE events in the $8^\circ$ distance range.....	47
27	Comparison of predicted spectra as a function of source depth for the $P_n$ (left) and $P_g$ (right) regional phases at Borovoye, $W = 10$ kt.....	49
28	Comparison of predicted spectra as a function of source depth for the $S_n$ (left) and $L_g$ (right) regional phases at Borovoye, $W = 10$ kt.....	50
29	Observed Borovoye $L_g$ spectral ratios with respect to $P_n$ (left) and $P_g$ (right).....	52
30	Observed Borovoye $S_n$ spectral ratios with respect to $P_n$ (left) and $P_g$ (right).....	53
31	Predicted Borovoye $L_g$ spectral ratios as functions of source depth computed with respect to $P_n$ (left) and $P_g$ (right).....	54
32	Predicted Borovoye $S_n$ spectral ratios as functions of source depth computed with respect to $P_n$ (left) and $P_g$ (right).....	55

## 1. INTRODUCTION

In order to discriminate the regional seismic signals produced by underground nuclear explosions from those produced by earthquakes, rockbursts and conventional mining explosions of comparable magnitude, it is necessary to know the range of nuclear explosion signal variation that can be expected as a function of source and propagation path conditions over the entire ranges of these conditions which may be encountered in global test monitoring under the CTBT. However, most of the empirical regional discrimination studies which have been conducted to date have focused on analyses of seismic signals recorded from underground tests conducted at the few major nuclear test sites, and these sample only limited ranges of the variables of interest. This constitutes a serious limitation in that existing theoretical simulation models have not yet proven capable of fully explaining the observed characteristics of the various proposed empirical discriminants and, therefore, their extrapolation to applications in new environments is subject to considerable uncertainty. In an attempt to overcome these limitations of previous analyses, we have been working with scientists from the Russian Institute for Dynamics of the Geospheres (IDG) to use regional seismic data recorded from the extensive Soviet Peaceful Nuclear Explosion (PNE) testing program to better quantify the variability of regional discriminants over ranges of explosion source and propagation path conditions which may be more representative of the diversity which will be encountered in global CTBT monitoring.

From its inception in the mid 1960's, the Soviet PNE program utilized nuclear explosions in a variety of commercial and scientific applications. Over 120 explosions were conducted in this series up until its cessation in 1988 and the locations of these tests were widely dispersed throughout the territories of the former Soviet Union. This fact is graphically illustrated in Figure 1 where the locations of a representative subset of these explosions are shown as overlays (large squares) to a gray-scale topographic map of the former Soviet Union and surrounding countries. The ISC seismicity database for the area for the period 1988-1990 is also included as an overlay (small squares) to this map to illustrate

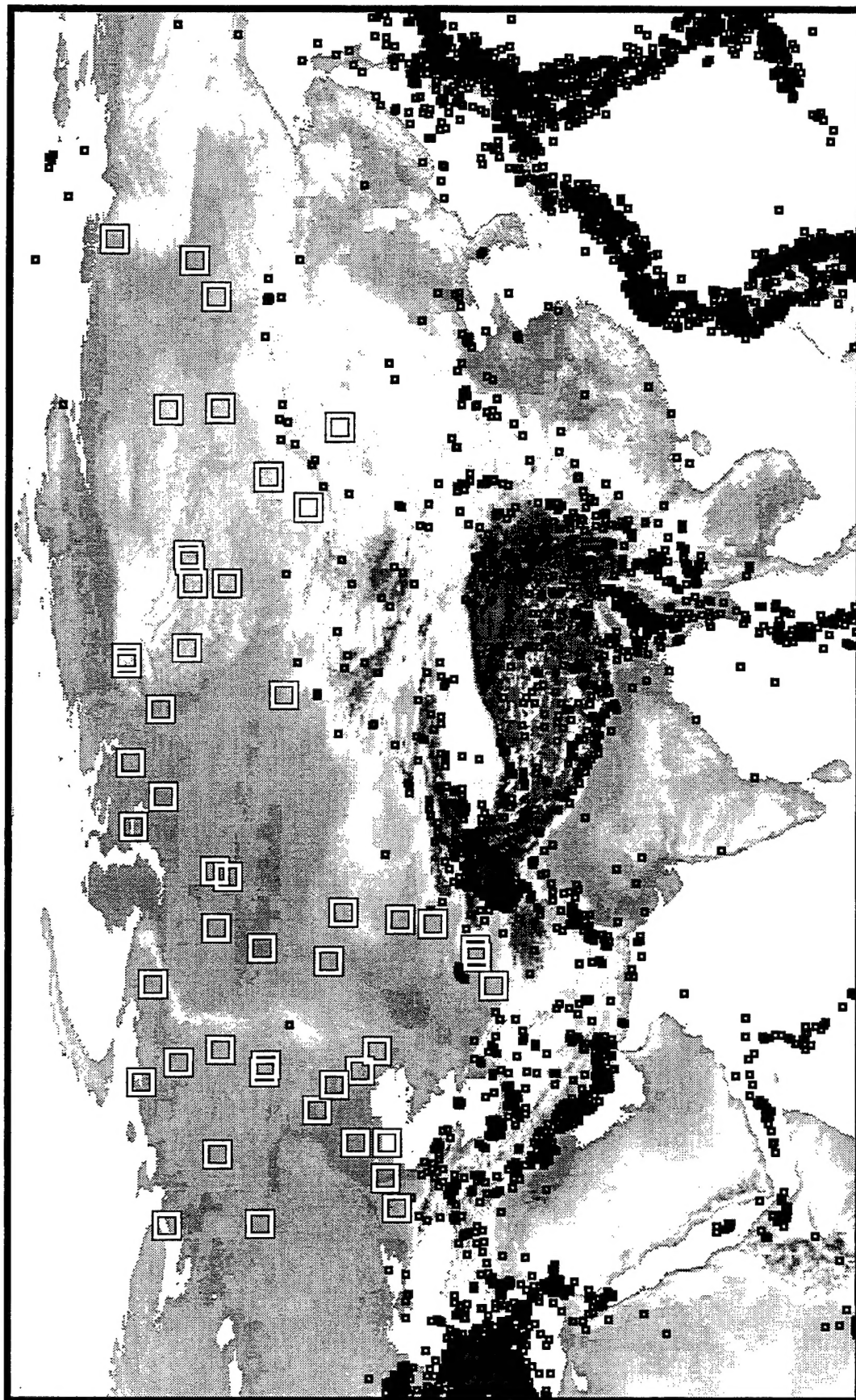


Figure 1. Locations of representative Soviet PNE events (large squares) shown as overlays to a shaded topographic map of the former Soviet Union and surrounding countries. The small squares correspond to the ISC seismicity for the period 1988-1990.

the tectonic variability of the PNE test environments. The PNE explosions were conducted in a wide variety of geologic emplacement media (e.g. salt, clay, sandstone, granite, limestone, dolomite) and are representative of broad ranges in yield (0.01 to 140 kt) and source depth (31 to 2860 m). Moreover, because of the tremendous geologic and tectonic diversity represented within the territories of the former Soviet Union, regional data recorded from these tests sample propagation path characteristics encompassing a range extending from tectonically active to stable continental interior regimes. Thus, regional data recorded from these tests represent a unique resource for use in seismic verification studies of underground nuclear testing. The objective of the research described in this report is to improve seismic discrimination capability through in-depth analyses of regional seismic data recorded from these Soviet PNE tests.

This report presents a summary of the research investigations conducted during the first year of this study program. During this initial phase, the effort has focused primarily on analyses of regional seismic data recorded at the Borovoye Observatory in Central Asia from selected Soviet PNE tests. The source characteristics of these selected PNE tests are summarized in Section 2, where the seismic data recorded from them at the Borovoye station are also reviewed in a preliminary fashion. This is followed in Section 3 by the presentation of a detailed spectral analysis of an initial subsample of these Borovoye data in which the variations of some of the more promising regional discriminants are assessed and quantified. The report concludes with Section 4, which contains a summary and preliminary statement of conclusions regarding the transportability of regional seismic discriminants.

## **2. OVERVIEW OF REGIONAL SEISMIC DATA RECORDED FROM SOVIET PNE TESTS**

Although teleseismic data recorded from Soviet PNE tests have been analyzed in previously reported studies (e.g., Murphy and Barker, 1994), only limited data recorded at regional stations within the former Soviet Union have been available until quite recently. Over the past several years,

Sultanov and his colleagues at the Russian IDG have begun to digitize some near-regional photographic recordings from selected PNE tests and these data have been incorporated into analyses of the seismic source characteristics of some specific underground nuclear explosions of particular interest (e.g., Murphy *et al.*, 1996). In addition, data recorded at the Borovoye digital seismic station in Central Asia from a number of Soviet nuclear tests have now been made available by the IDG (Adushkin and An, 1990; Laushkin *et al.*, 1975) for analysis by the seismic verification community. The Borovoye Geophysical Observatory is located in North Kazakhstan (53.08°N, 70.25°E) and is one of the oldest digitally recording seismic observatories in the world, having initiated digital recording in 1966. A variety of long-period and short-period seismic systems have been deployed at this station over the years (Kim and Ekström, 1996), including some relatively broadband systems which were recorded with digitization rates in the 30-40 sample/second range. Thus, dynamic range permitting, these data provide potential resolution of seismic frequency content to 10 Hz and higher. For most of the Soviet PNE tests, these Borovoye recordings represent the highest quality regional seismic data which are available for detailed analysis.

An initial sample of Borovoye data recorded from 63 different Soviet PNE events has been provided by the IDG seismic group (V. M. Ovtchinnikov, personal communication, 1995) and these data have been carefully reviewed, calibrated and merged into a uniform database. Some of these data were found to be unusable for the purposes of the present investigation and a number of others were found to represent recordings of later explosions in sequences of multiple explosions detonated a few minutes apart at a common location. After elimination of these data, a subsample of 46 PNE explosions remained which appeared suitable for a discrimination analysis. The source parameters of these selected PNE events are listed in Table 1 in order of increasing epicentral distance from the Borovoye station. The map locations of these selected explosions with respect to the Borovoye station are shown in Figure 2 where it can be seen that they are widely distributed throughout the territories of the former Soviet Union. Thus, their regional propagation paths to the Borovoye

**Table 1. Source Parameters For Selected Soviet PNE Events  
Recorded at Borovoye**

Date	Origin Time, UT	North Latitude	East Latitude	Yield, kt	Source Depth, m	Source Medium	Distance to Borovoye, Degrees
08/28/73	03:00	50.53	68.32	6.3	395	argillite	2.8
06/18/85	04:00	60.17	72.50	2.5	2859	argillite	7.2
09/19/73	03:00	45.76	67.83	6.3	615	argillite	7.6
10/04/79	16:00	60.68	71.46	21.0	837	clay	7.7
10/26/73	06:00	53.66	55.38	10.0	2026	dolomite	8.3
12/10/80	07:00	61.69	67.00	15.00	2485	sandstone	8.8
08/25/84	19:00	61.88	72.09	8.5	726	clay	8.9
04/19/87	04:00	60.25	57.08	3.2	2015	limestone	10.4
08/15/73	02:00	42.78	67.41	6.3	600	clay	10.5
10/03/87	15:15	47.61	56.23	8.5	1000	salt	10.5
07/21/84	03:00	51.36	53.32	13.5	846	salt	10.6
10/17/78	14:00	63.19	63.43	23.0	593	sandstone	10.7
09/02/81	04:00	60.62	55.59	3.2	2088	limestone	11.0
08/22/88	16:20	66.28	78.49	16.0	829	clay	13.9
08/11/84	19:00	65.03	55.19	9.5	759	clay	14.2
09/06/88	16:20	61.36	48.09	7.5	793	dolomite	14.6
09/30/77	07:00	48.14	47.85	9.3	1503	salt	15.0
12/18/78	08:00	47.79	48.12	103.0	630	clay	15.0
10/24/79	06:00	47.81	48.16	33.0	982	salt	15.0
07/29/76	05:00	47.78	48.12	58.0	1000	salt	15.1
07/14/79	05:00	47.81	48.10	21.0	982	salt	15.1
09/24/83	05:00	46.78	48.32	8.5	1050	salt	15.4
10/08/80	06:00	46.71	48.22	8.5	1050	salt	15.5
09/26/81	05:00	46.78	48.25	8.5	1050	salt	15.5
10/16/82	06:00	46.73	48.20	8.5	974	salt	15.5
10/27/84	06:00	46.77	48.31	3.2	1000	salt	15.5
09/21/78	15:00	66.60	86.21	16.0	886	sandstone	15.6
09/25/82	18:00	64.31	91.83	8.5	554	gabbro	15.8
04/11/72	06:00	37.37	62.00	14.0	1720	argillite	16.7
11/01/80	13:00	60.82	97.57	8.0	720	dolomite	16.7
09/04/82	18:00	69.21	81.65	16.0	960	sandstone	17.0
05/25/81	05:00	68.21	53.66	37.6	1511	clay	17.2
10/22/81	14:00	63.79	97.55	8.5	581	dolomite	17.7
08/20/77	22:00	64.11	99.56	8.5	592	tuff	18.9
09/29/75	11:00	69.58	90.34	7.6	834	salt	19.0
07/26/77	17:00	69.58	90.38	13.0	879	salt	19.1
09/10/77	16:00	57.25	106.6	7.0	537	marl	21.1
07/09/72	07:00	49.78	35.40	3.8	2483	salt	21.8
09/04/72	07:00	67.69	33.45	2.1	131	apatite	22.9
07/24/87	02:00	61.49	112.75	13.0	1515	limestone	24.0
10/08/78	00:00	61.52	112.88	13.0	1545	dolomite	24.1
10/10/82	05:00	61.55	112.86	16.0	1502	limestone	24.1
10/07/79	21:00	61.85	113.09	13.0	1545	dolomite	24.2
08/24/78	18:00	65.93	112.34	19.0	577	limestone	24.4
08/12/79	18:00	61.87	122.43	6.5	982	dolomite	28.5
08/09/78	18:00	63.68	125.52	22.0	567	sandstone	29.8

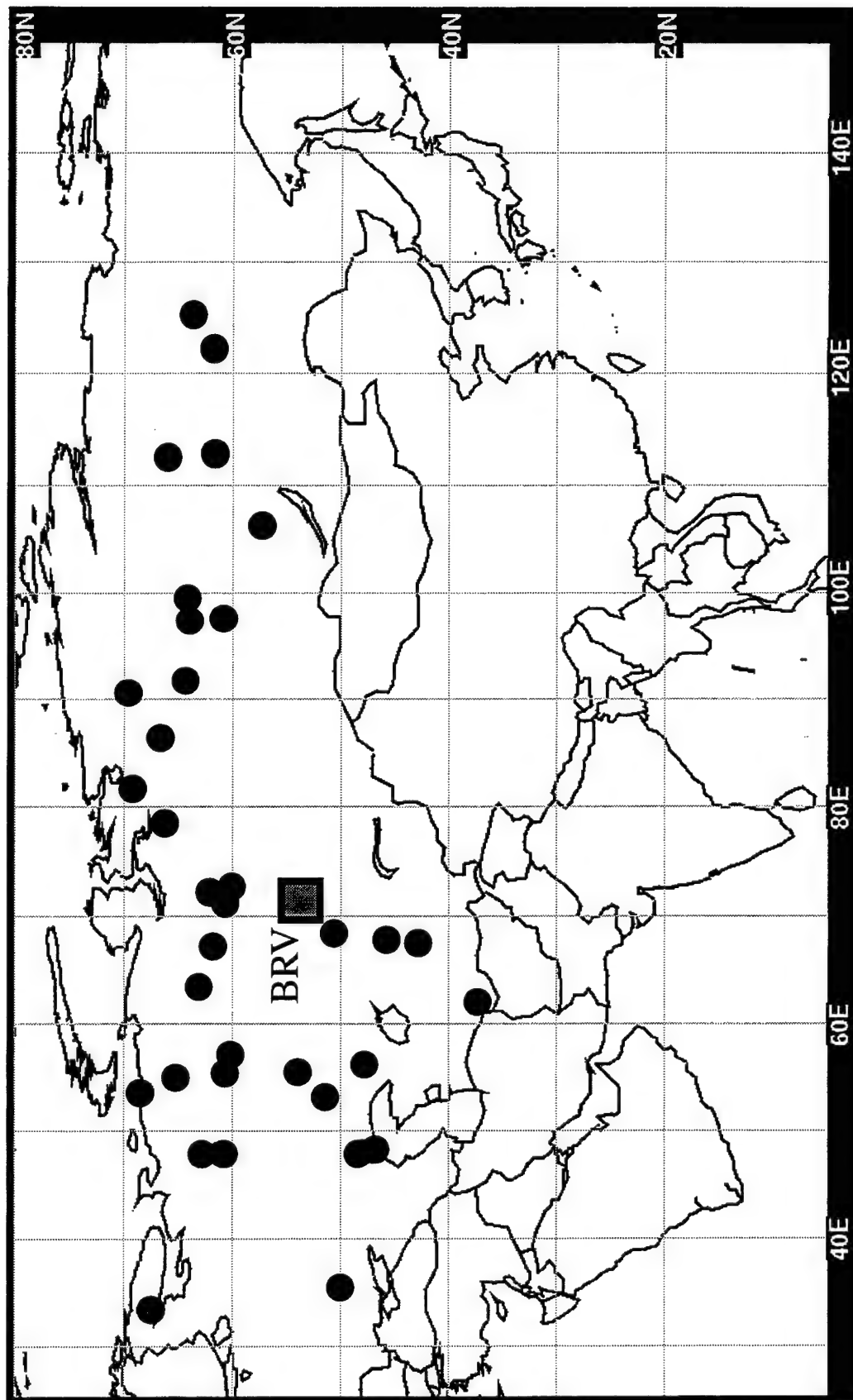


Figure 2. Map locations of selected Soviet PNE tests which were recorded at the Borovoye digital station in Kazakhstan.

station sample diverse ranges of crust and upper mantle structures which can potentially provide some valuable constraints on the types of seismic characteristics which may be expected in global CTBT monitoring. With reference to Table 1, it can also be seen that the selected events represent wide ranges of explosion yield, source medium, source depth and epicentral distance. The distributions of these selected PNE events with respect to these variables are graphically summarized in Figure 3, from which it can be seen that most of the explosions are located in the epicentral distance range extending from 5 to 25 degrees from Borovoye, which represents a most important distance range for regional monitoring of small, clandestine nuclear explosions. It is also evident from Figure 3 that the selected explosions sample wide ranges of source media (i.e., sandstone, clay, salt, limestone/dolomite and other hardrock) and source depth (i.e., 131-2859 m) and that they are predominantly low yield, overburied explosions of the type which represent the greatest challenge to seismic monitoring.

The broadband, vertical component seismic data recorded at Borovoye from the explosions of Table 1 are displayed in order of increasing epicentral distance in Figure 4. The vertical arrows shown over each trace in this display indicate the group arrival times corresponding to apparent group velocities of 4.5 and 3.5 km/sec, which roughly represent the expected arrival times of the regional  $S_n$  and  $L_g$  phases, respectively. Even from the compressed, overview display shown here, it is evident that these data are quite variable, with some having the small broadband S/P and  $L_g$ /P ratios typical of explosion sources (e.g., the 7/21/84 explosion recorded at a distance of 10.6°), while others show much larger S/P and  $L_g$ /P ratios more common to natural earthquake sources (e.g., the 9/02/81 explosion recorded at a distance of 11.0°). As is indicated by the vertical arrows, the data are generally complete through the  $L_g$  phase for the explosions within about 15 degrees of the Borovoye station. However, for the explosions at greater distances, a number of the available data traces terminate prior to the expected  $L_g$  onset time, and some even prior to the expected  $S_n$  onset time. This limits their utility for detailed discrimination analysis to some extent, and attempts are being made to acquire longer time segments of data in those cases for use in the later phases of this study.

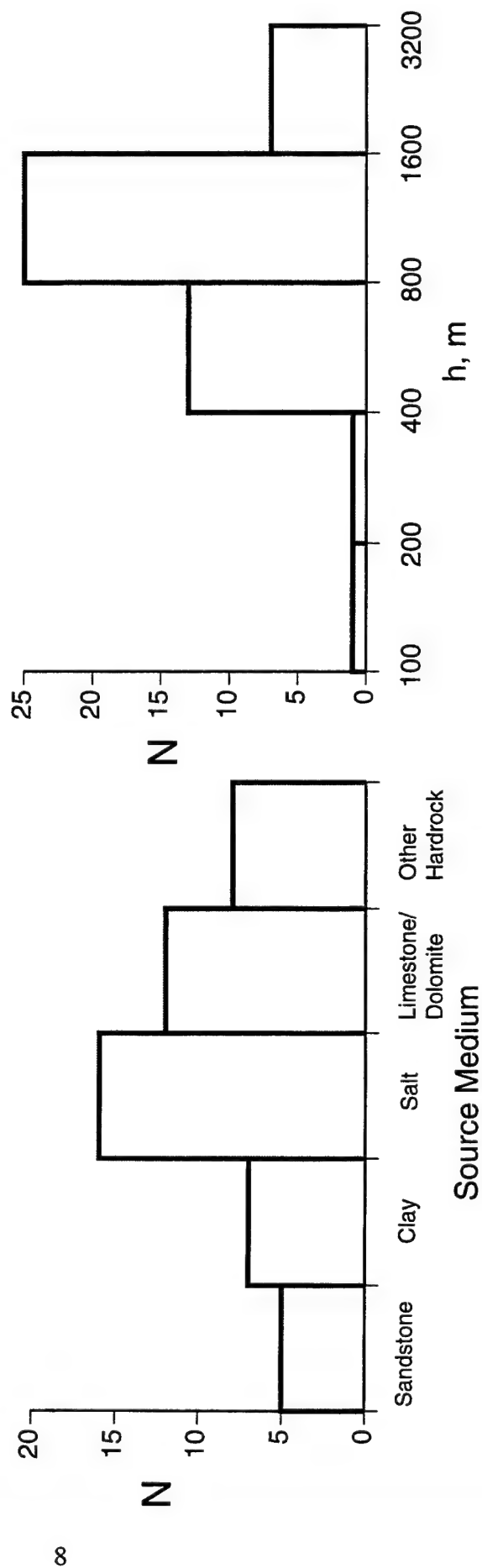
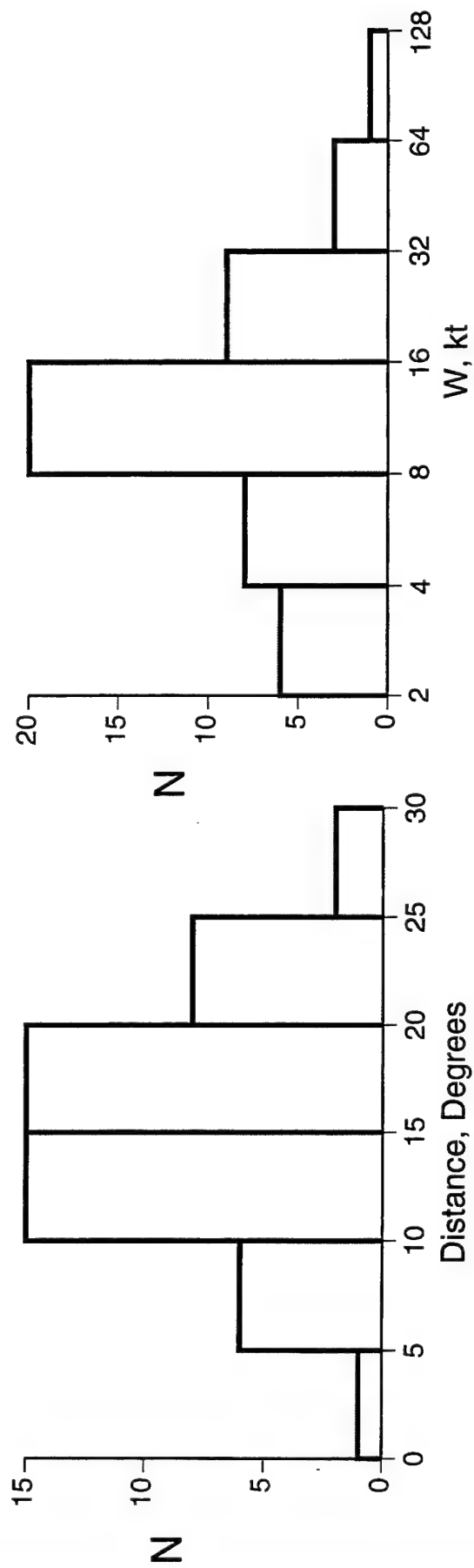


Figure 3. Distributions of selected Soviet PNE tests with respect to epicentral distance from Borovoye, source medium, explosion yield and depth of burial.

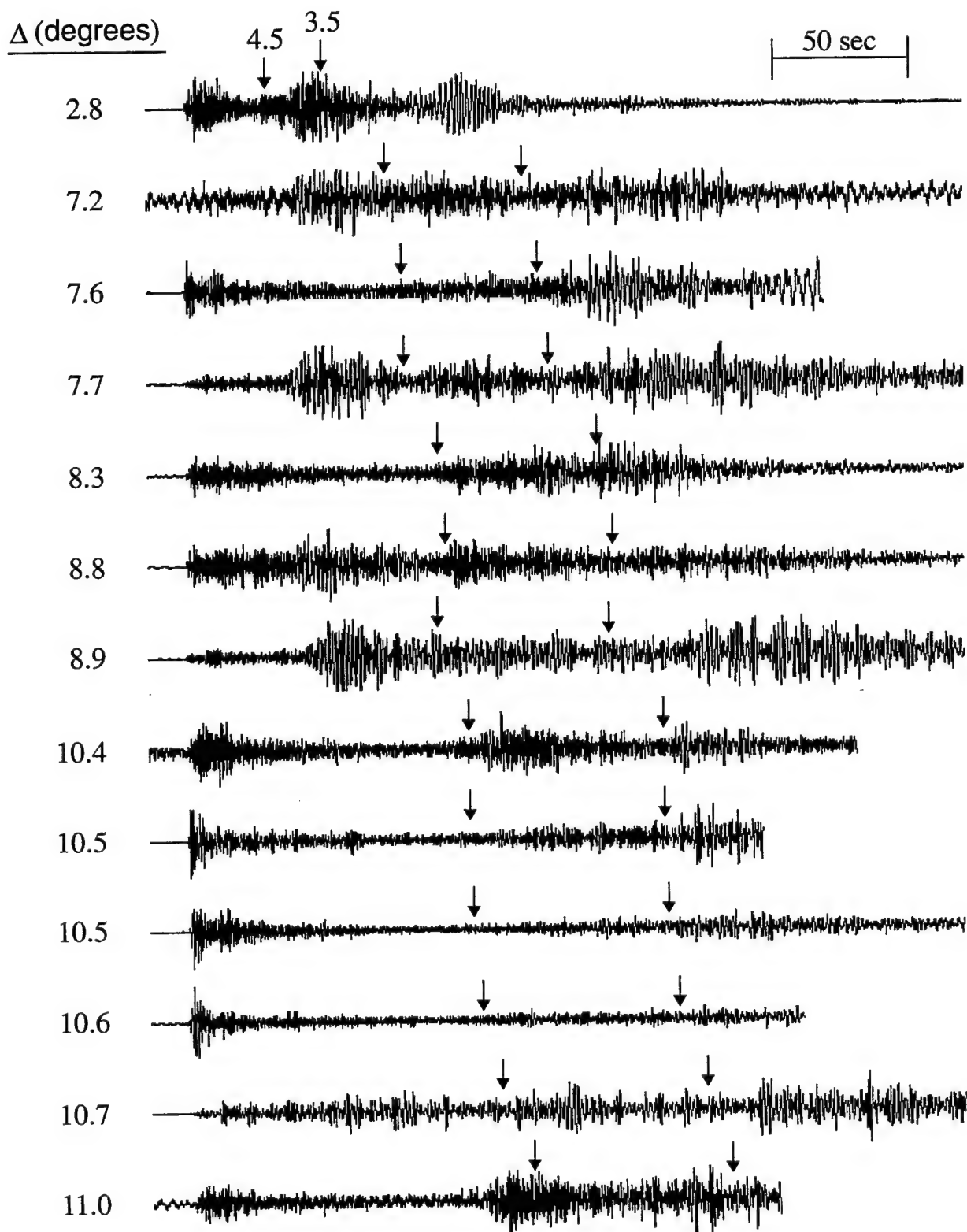


Figure 4. Broadband, vertical component seismograms recorded at Borovoye from selected Soviet PNE tests. The vertical arrows above these traces mark the group arrival times associated with apparent velocities of 4.5 and 3.5 km/sec.

$\Delta$  (degrees)

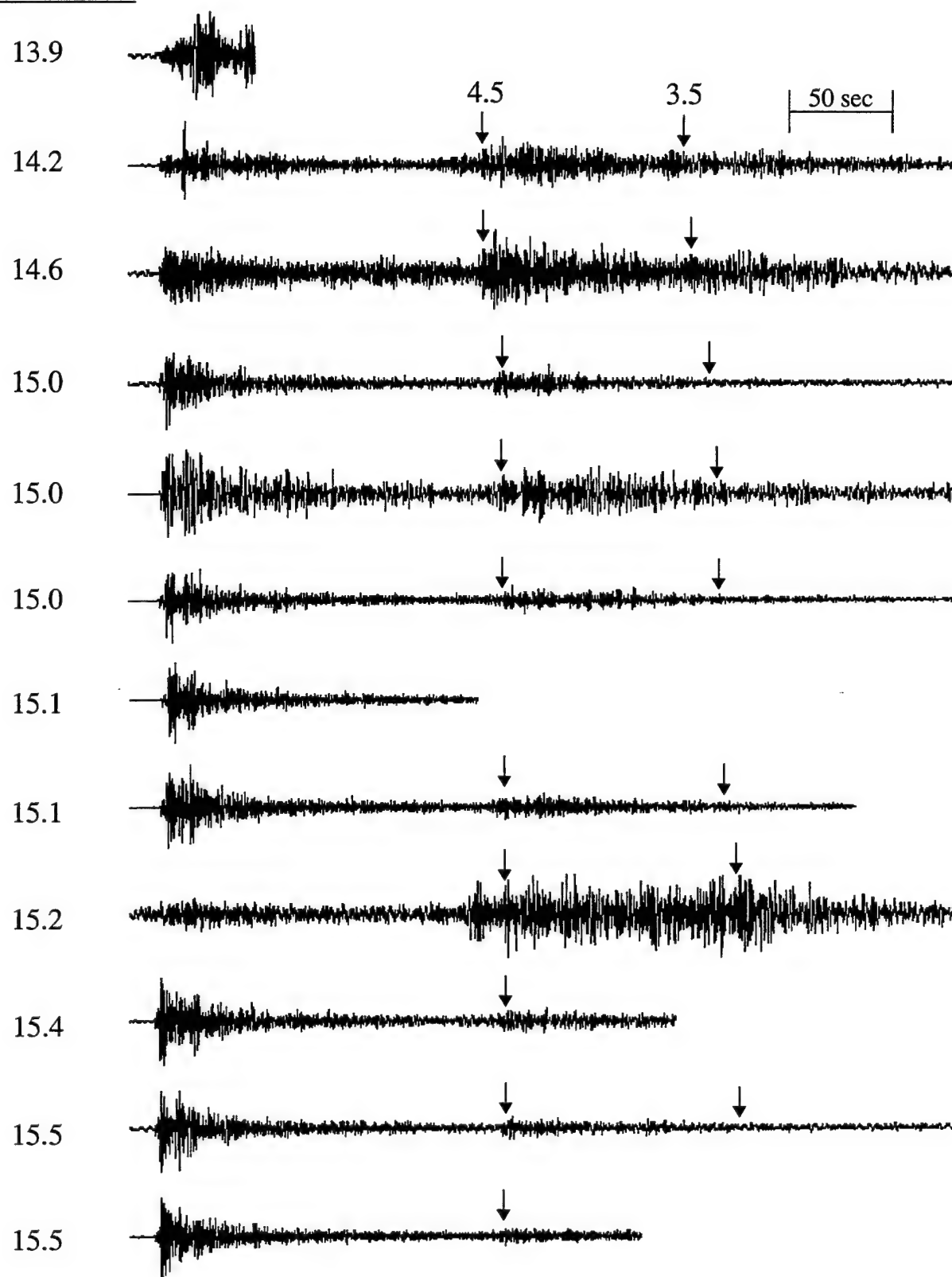


Figure 4. (Continued)

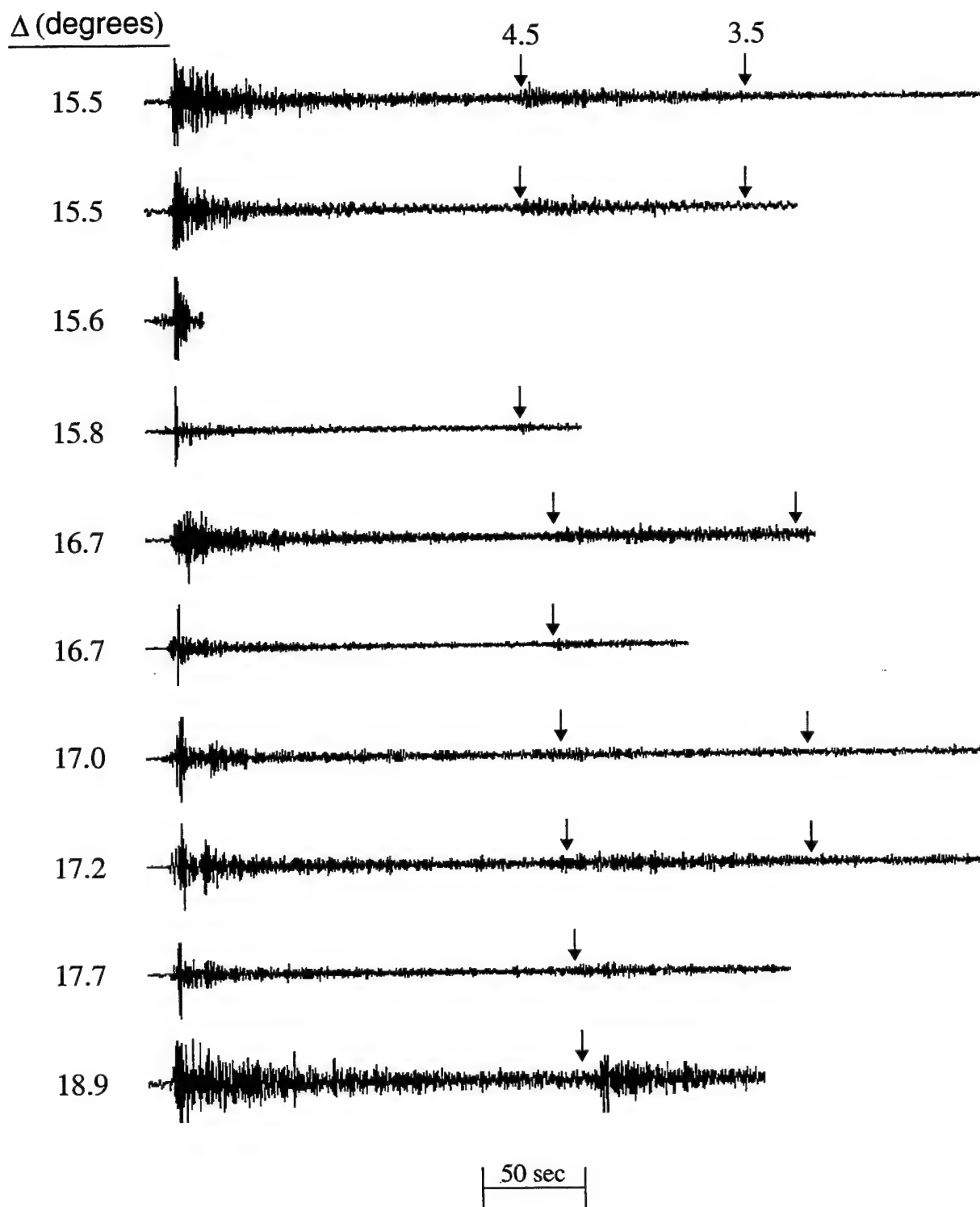


Figure 4. (Continued)

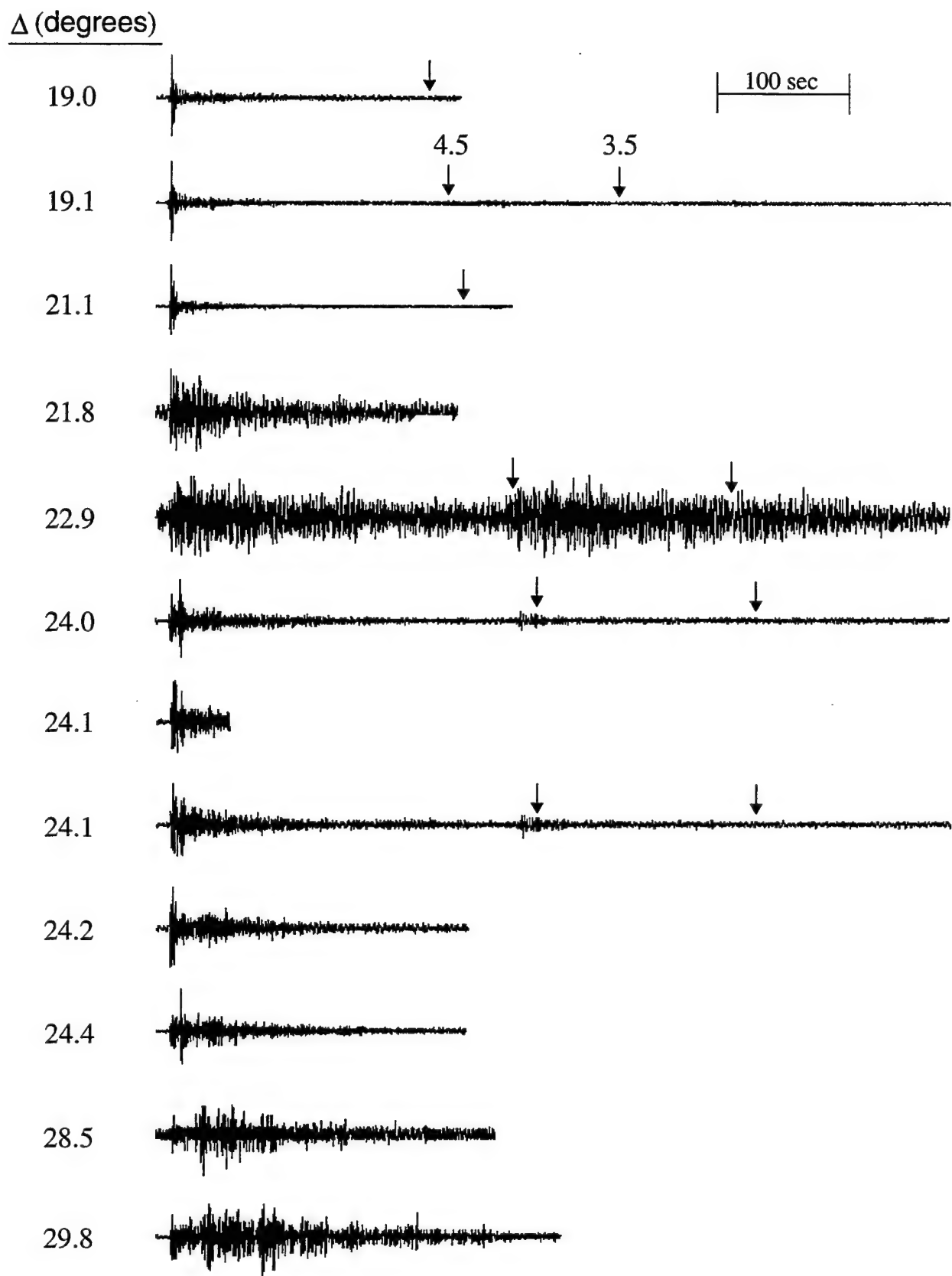


Figure 4. (Continued)

The data of Figure 4 generally appear to be of good quality, although on closer examination there are a number of instances of spikes, data dropouts and clipping which would seriously contaminate any data analysis results at high frequency. Therefore, all the data have been carefully previewed, documented and, where possible, corrected prior to input to the data processing and analysis routines. Examples of the types of data problems encountered are shown in Figures 5 and 6 for the cases of a spike and a data dropout, respectively. In both of these figures the top trace is the original broadband recording, the center trace shows the result of processing the broadband data through a bandpass filter centered at about 8.5 Hz, and the bottom trace shows an expanded plot of the original recording for a time interval surrounding an observed spike on the filter output. In both these cases, a simple interpolation using the adjacent data points effectively eliminates the problem on the high frequency filter output. In more complex cases involving extensive clipping or apparent instrument malfunctions, the time windows containing high frequency spikes are simply recorded and avoided in subsequent spectral analyses of those data traces.

It can be seen from Table 1 and Figure 4 that within the selected data set there are some clusters of PNE events which are located at nearly constant distances from the Borovoye station. Thus, for example, there are six explosions located in a narrow epicentral distance range extending from 7.2 to 8.9 degrees, and another six explosions in a second narrow distance band extending from 10.4 to 11.0 degrees from the Borovoye station. This subset of 12 explosions has been chosen for initial analysis in an attempt to assess the relative importance of propagation path versus source variables with respect to the characteristics of the regional seismic signals observed from explosions at essentially the same distances from the Borovoye station. With reference to Table 1, it can be seen that these 12 explosions encompass representative ranges of source media, explosion yield and source depth. The map locations of these explosions with respect to the Borovoye station are shown in Figure 7, where it can be seen that the two groups of events are characterized by average epicentral distances of about 8 and 10.5 degrees. Moreover, both sets of events encompass about 180

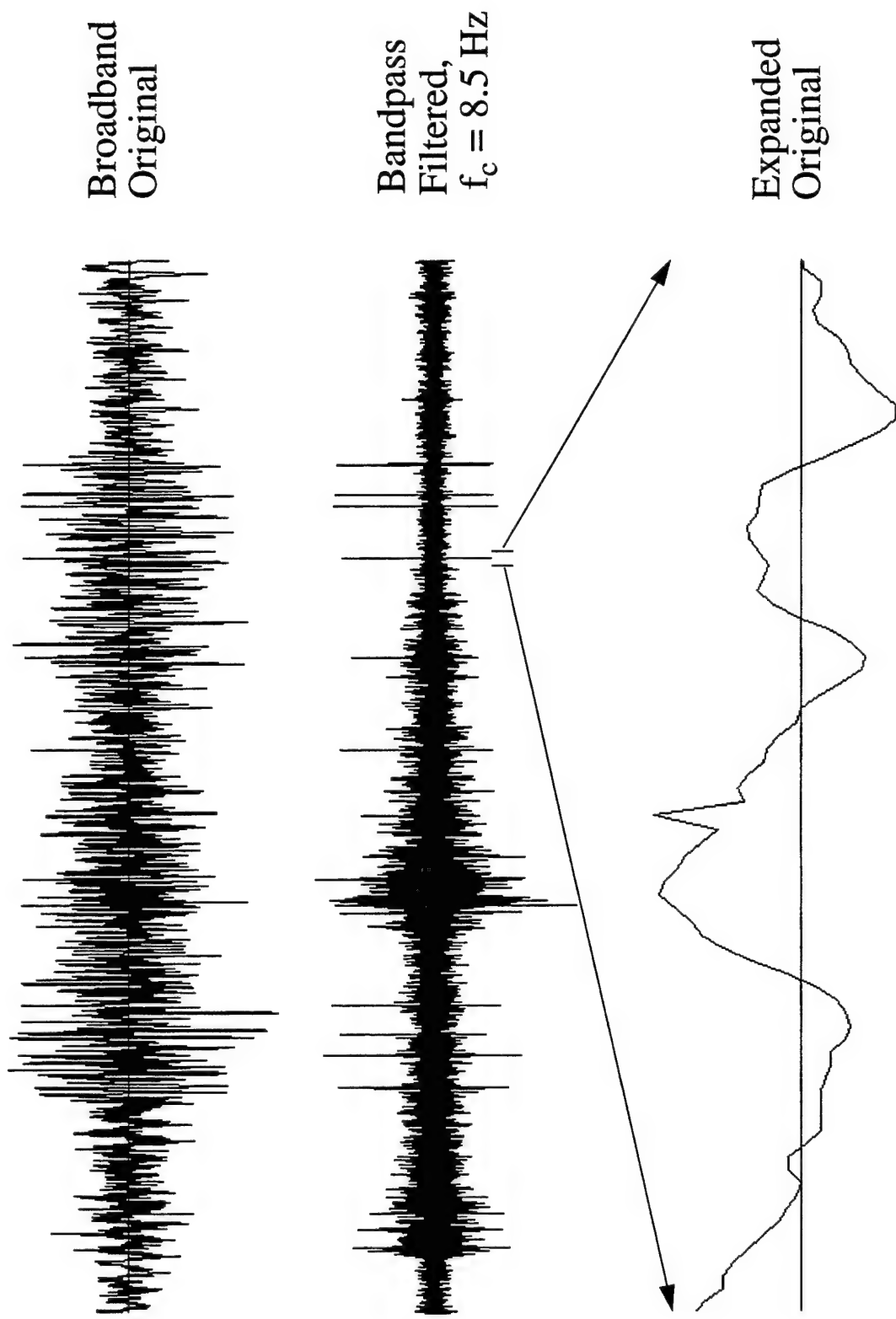


Figure 5. Example of a data spike on the Borovoye recording of the PNE event of 6/18/85. Such discontinuities in the data can be easily identified using the high frequency bandpass filter output (center trace).

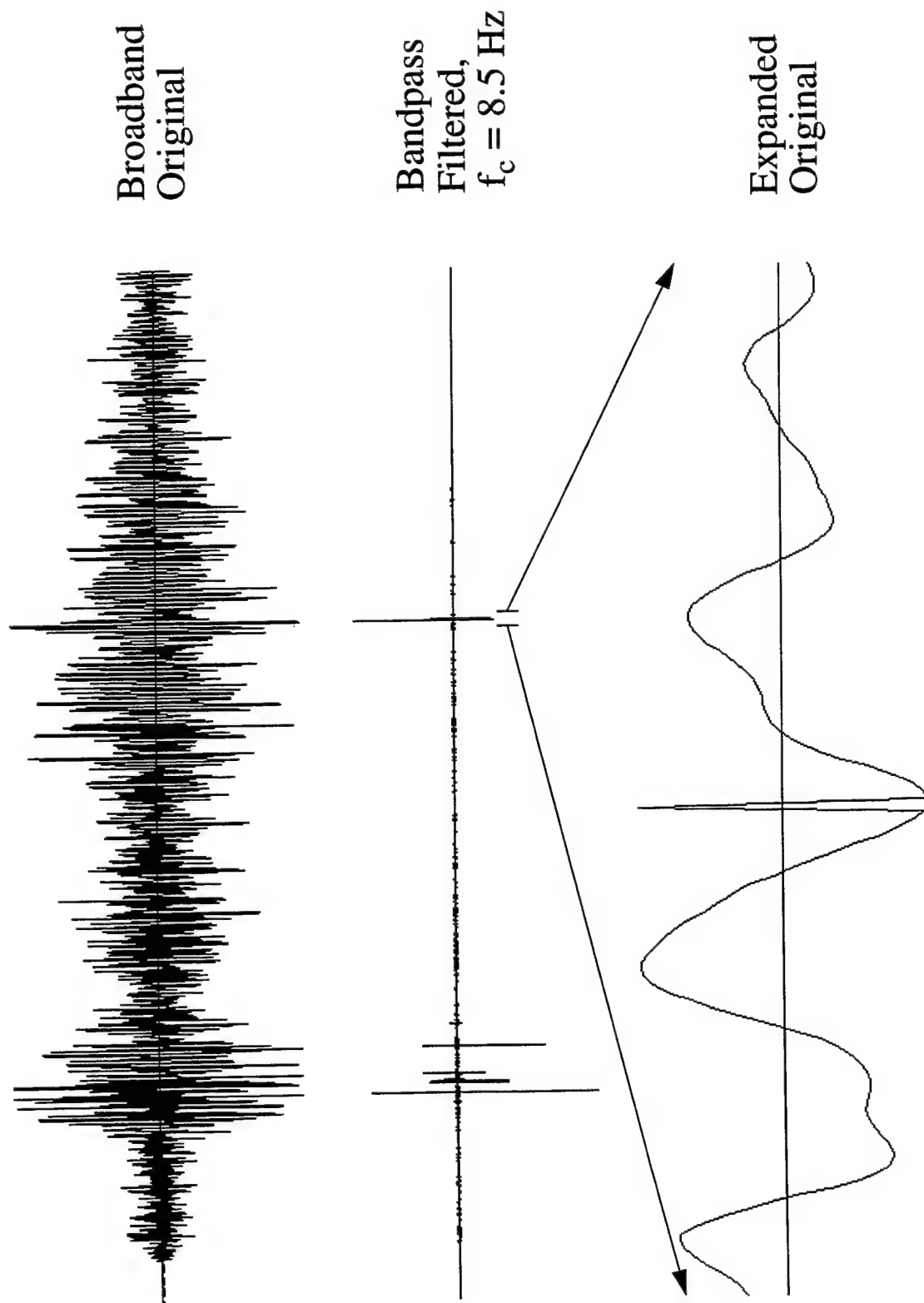


Figure 6. Example of a data dropout on the Borovoye recording of the PNE event of 10/04/79. Such discontinuities in the data can be easily identified using the high frequency bandpass filter output (center trace).

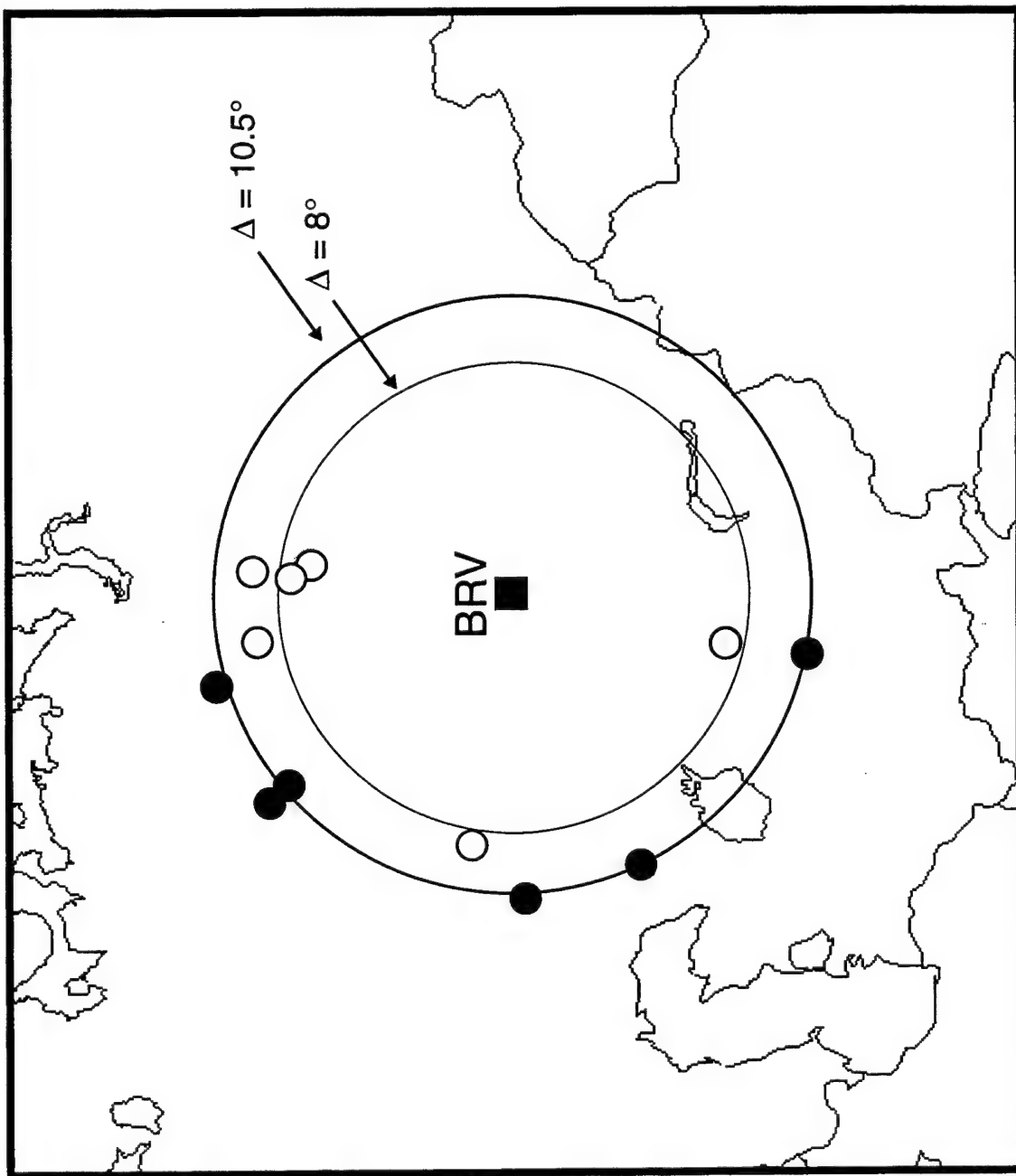


Figure 7. Locations of selected Soviet PNE events with respect to the Borovoye (BRV) station in North Kazakhstan. The open circles correspond to six explosions at an average epicentral distance of about  $8^\circ$ ; the filled circles correspond to six explosions at an average epicentral distance of about  $10.5^\circ$ .

degrees in azimuth with respect to the Borovoye station location and, therefore, data recorded at Borovoye from these PNE tests sample a variety of different regional propagation path conditions, in addition to the previously noted range in source conditions. Thus, this selected data set provides an unusually well-constrained test bed for evaluating the effects of different source and propagation path variables on the transportability of regional discriminants.

The broadband, vertical component data recorded at Borovoye from the six Soviet PNE events located at a common epicentral distance of about  $8^\circ$  are shown in Figure 8, where they are displayed in order of increasing azimuth as measured from Borovoye. In this display, the data are plotted as a function of apparent group velocity, which is useful for qualitative regional phase correlation since the epicentral distance is essentially constant for these events. The corresponding time scale for the average epicentral distance of  $8^\circ$  is indicated by the annotated interval shown at the top of this figure. It can be seen that these data exhibit some significant dependence on azimuth which is presumably related to propagation path differences. The most obvious difference is that the ratio of broadband amplitude in the 5 to 6 km/sec group velocity window (i.e.,  $P_g$ ) to that in the 6 to 8 km/sec group velocity window (i.e.,  $P_n$ ) is much larger for explosions located to the north of Borovoye than for those located south and west of the station. Moreover, if the 3 to 4 km/sec group velocity window is associated with  $L_g$ , it can be seen that the broadband  $L_g/P$  amplitude ratio varies from less than 1.0 (i.e., 12/10/80) to significantly greater than 1.0 (e.g., 10/26/73) for these explosions at an essentially constant distance from Borovoye. Thus, these data once again illustrate that propagation path variability can have a significant effect on the characteristics of the regional seismic signals observed from underground explosions.

The corresponding display of the data recorded at Borovoye from the six Soviet PNE events located at a common epicentral distance of about  $10.5^\circ$  is shown in Figure 9. Here again the data show significant variability as a function of azimuth, with the northernmost 10/17/78 explosion data showing an enhanced  $P_g/P_n$  ratio with respect to the observations at other

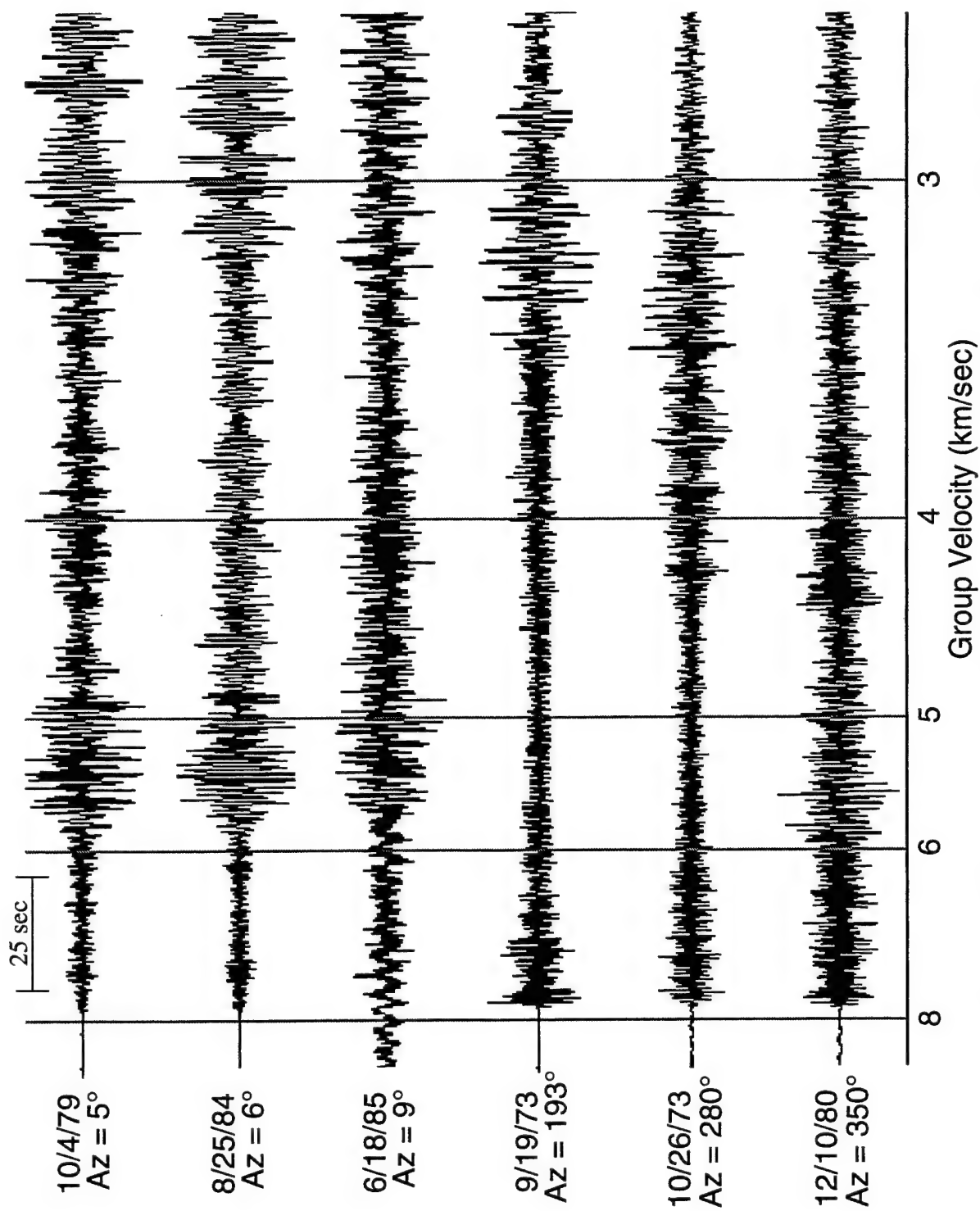


Figure 8. Vertical component regional signals recorded at Borovoye from six Soviet PNE events located at a common epicentral distance of about  $8^\circ$ .

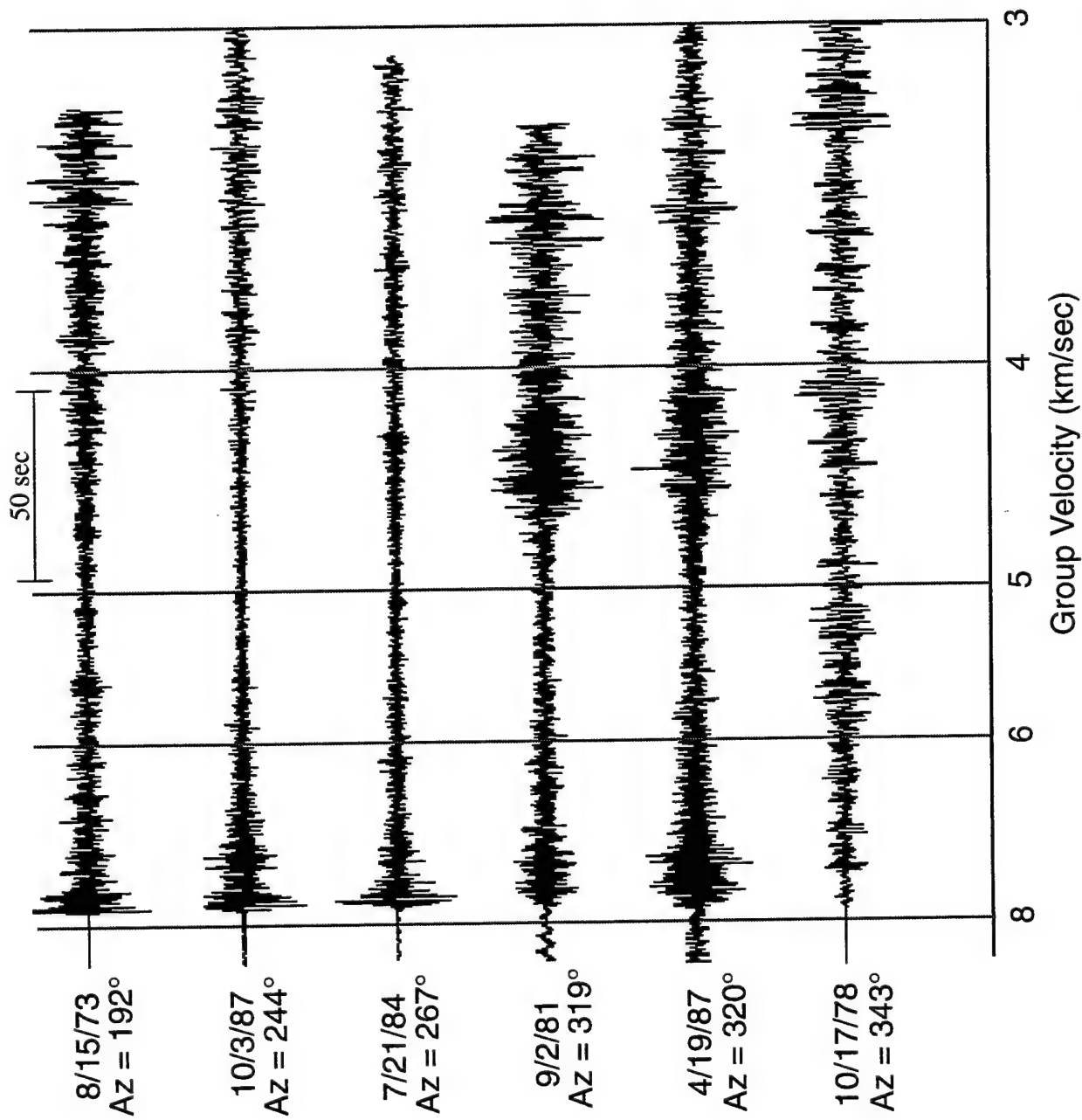


Figure 9. Vertical component regional signals recorded at Borovoye from six Soviet PNE events located at a common epicentral distance of about 10.5°.

azimuths consistent with that observed for the 8° data in Figure 8. A particularly notable recording in this distance range is that from the 9/02/81 explosion which shows evidence of large broadband  $S_n$  (i.e., 4 to 5 km/sec group velocity window) and  $L_g$  amplitude levels with respect to that of P, which is more typical of earthquakes than it is of explosion sources.

Not surprisingly, the variations in regional phase characteristics noted in the broadband data displays of Figures 8 and 9 are also found to be strongly frequency dependent. This fact is graphically illustrated in Figures 10 and 11 where original and bandpass filtered data are compared for several events in the 8 and 10.5 degree distance groups, respectively. In each case, the original broadband data are shown above the outputs obtained by processing these data through bandpass filters centered at about 1 and 9.5 Hz. The example at the top of Figure 10 is for the 10/26/73 event, which was noted previously to be characterized by a large broadband  $L_g/P$  ratio. Note, however, that the  $L_g$  phase has very low amplitude on the high frequency filter output and that the  $L_g/P$  and  $S/P$  ratios in this band are significantly less than one, as expected for explosion sources. On the other hand, the example shown at the bottom of Figure 10 indicates that the data recorded from the 12/10/80 event have a dramatically different frequency dependence. In this case, the  $P_g$  phase dominates the broadband signal, with all the other phases having somewhat smaller, but comparable amplitudes. However, at high frequencies the  $P_g$  and  $L_g$  phases are essentially undetectable and the bandpass filter output is dominated by the  $P_n$  and  $S_n$  phases. Moreover, unlike the 10/26/73 event, the high frequency  $S/P$  ratio in this case is larger than 1.0, which is not generally considered to be characteristic of an explosive source.

Similar comparisons are shown in Figure 11 for two explosions in the 10.5 degree distance group. The results for the 4/19/87 event are shown at the top of this figure, where it can be seen that both the low frequency and high frequency filter outputs are quite different from the broadband signal, with the low frequency output being dominated by  $L_g$  and the high frequency output by  $P_n$ . In contrast to this, the 7/21/84 event recording shown at the bottom of this figure has a nearly frequency

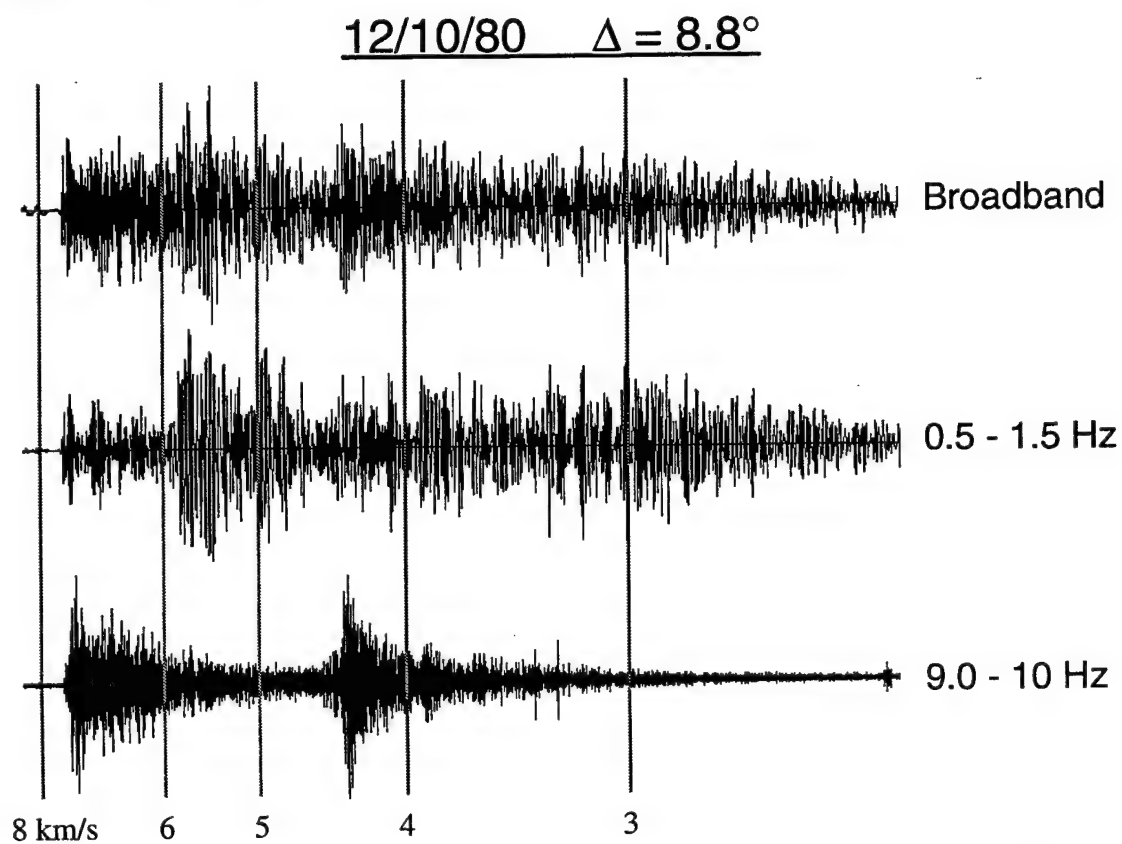
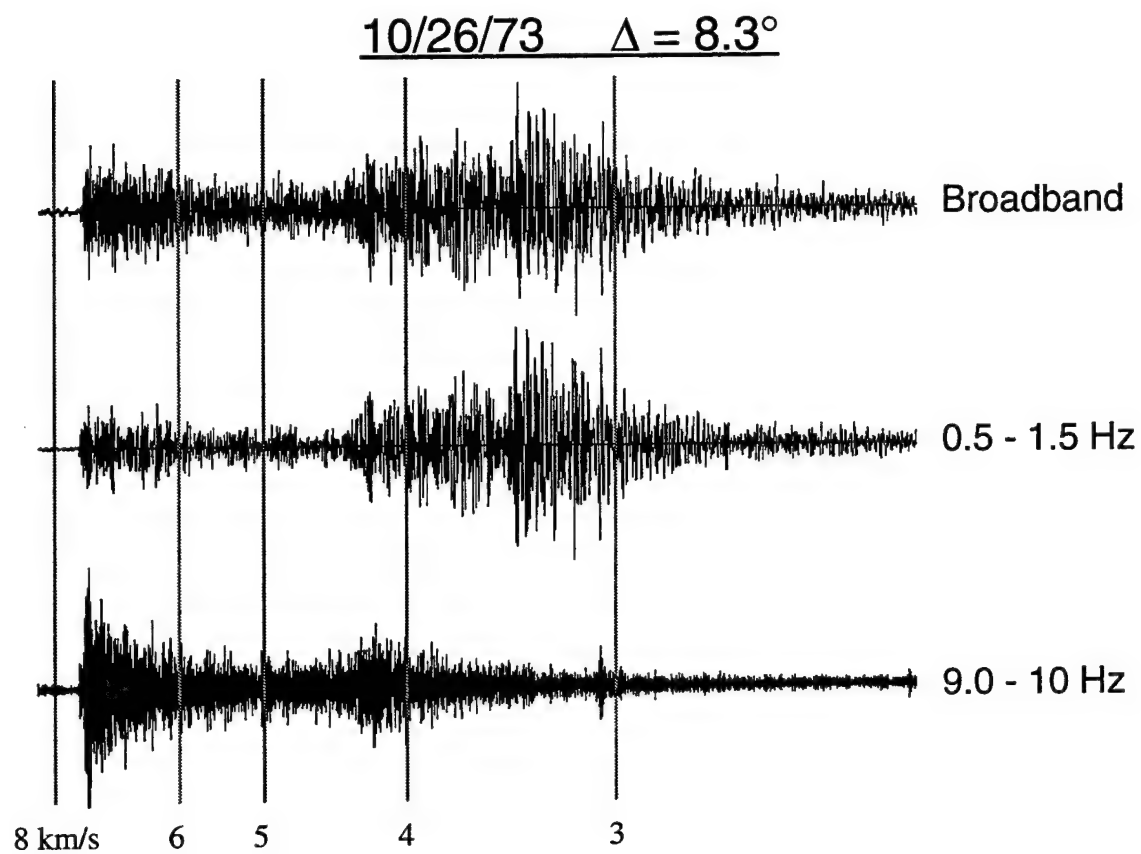


Figure 10. Comparison of the broadband vertical component recordings and associated bandpass filter outputs for two of the PNE events from the 8 degree distance group.

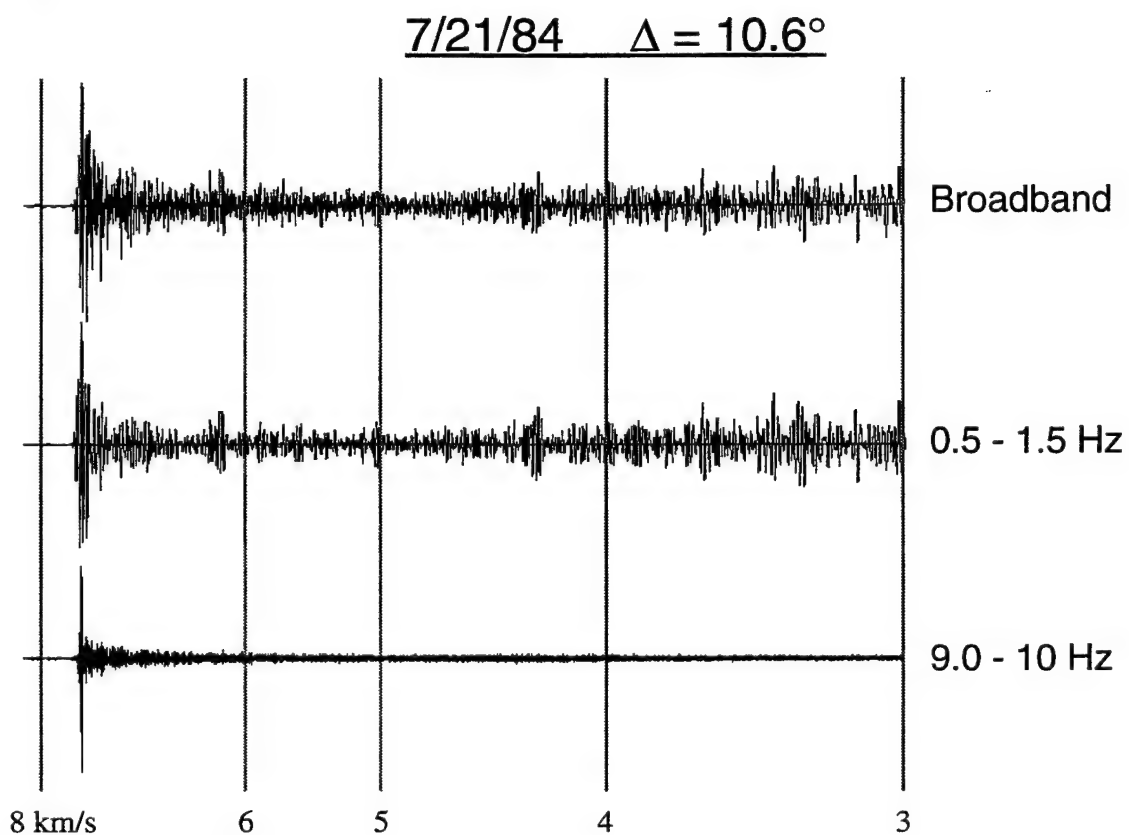
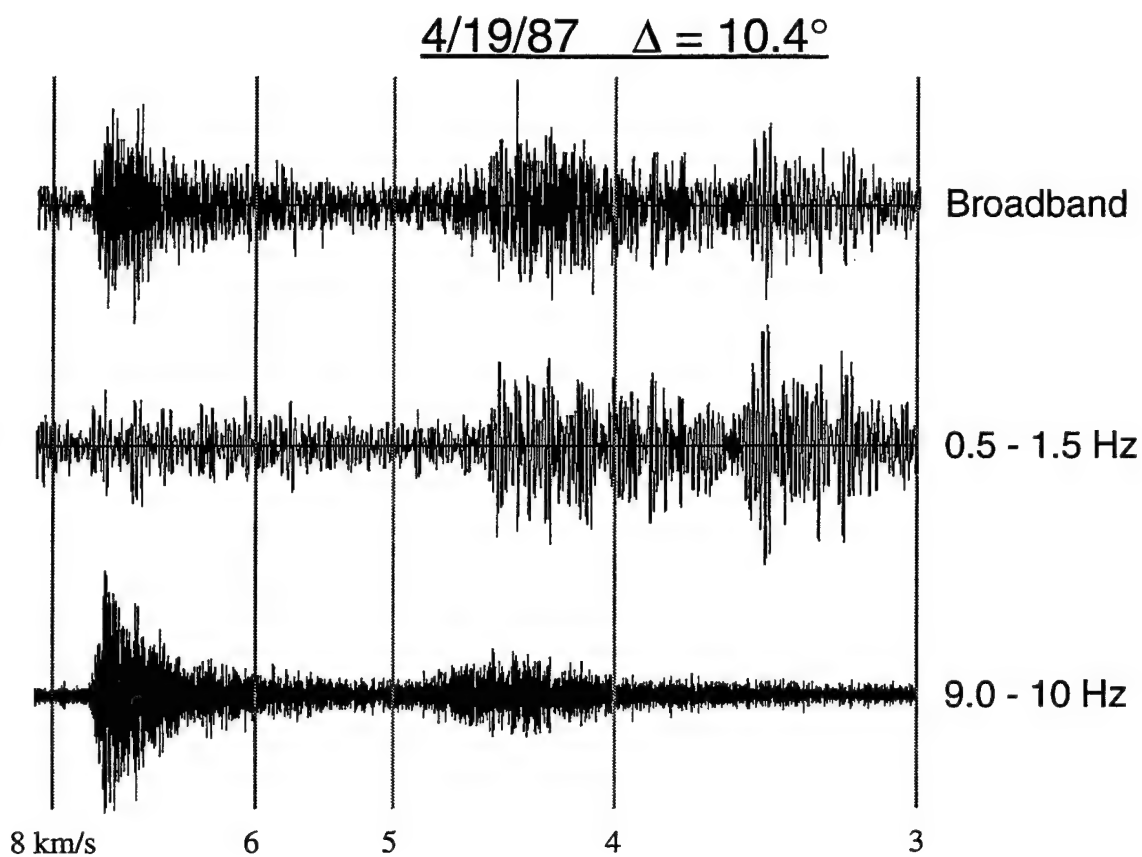


Figure 11. Comparison of the broadband vertical component recordings and associated bandpass filter outputs for two of the PNE events from the 10.5 degree distance group.

independent character to the extent that both the low and high frequency filter outputs are fairly comparable to the broadband signal with regard to relative phase amplitude levels. In both these cases, the high frequency  $L_g/P$  and  $S/P$  ratios are consistent with those expected from explosion sources. These examples clearly indicate that the regional phase characteristics for this data set are strongly dependent on frequency, as well as the source and propagation path variables, and this dependence needs to be explicitly accounted for in the discrimination analysis.

While the displays of Figures 8 and 9 provide good visualizations of the variations in relative regional phase excitation levels between the different explosions in these two distance groups, they do not illustrate the corresponding variations in absolute amplitude level. This information is represented in Figures 12 and 13 where the seismograms of Figures 8 and 9 have been approximately normalized for yield differences and replotted at the same absolute amplitude scale. For these purposes, the broadband amplitude levels were roughly normalized to a common average yield of 10 kt by assuming that they are directly proportional to yield. It can be seen that at both distance ranges, the normalized broadband signal amplitude levels vary quite considerably, but do not seem to show the same simple correlation with azimuth evidenced by the corresponding relative regional phase excitation levels. This presumably reflects the fact that the effects of varying propagation path characteristics on the amplitude levels are being modulated by the effects of variations in seismic source coupling efficiency between these explosions detonated at different scaled depths in different source media.

An obvious question which arises with regard to the amplitude variability shown in Figures 12 and 13 concerns the reliability of the Borovoye calibration data. While this issue is difficult to directly address without having access to periodic calibration data, the consistency of these Borovoye data has been addressed in an approximate fashion through an analysis of pre-signal spectral noise estimates obtained for each of the 12 selected PNE events in the 8 and 10.5 degree distance groups. These individual estimates were corrected for instrument response and logarithmically averaged to obtain the Borovoye station frequency

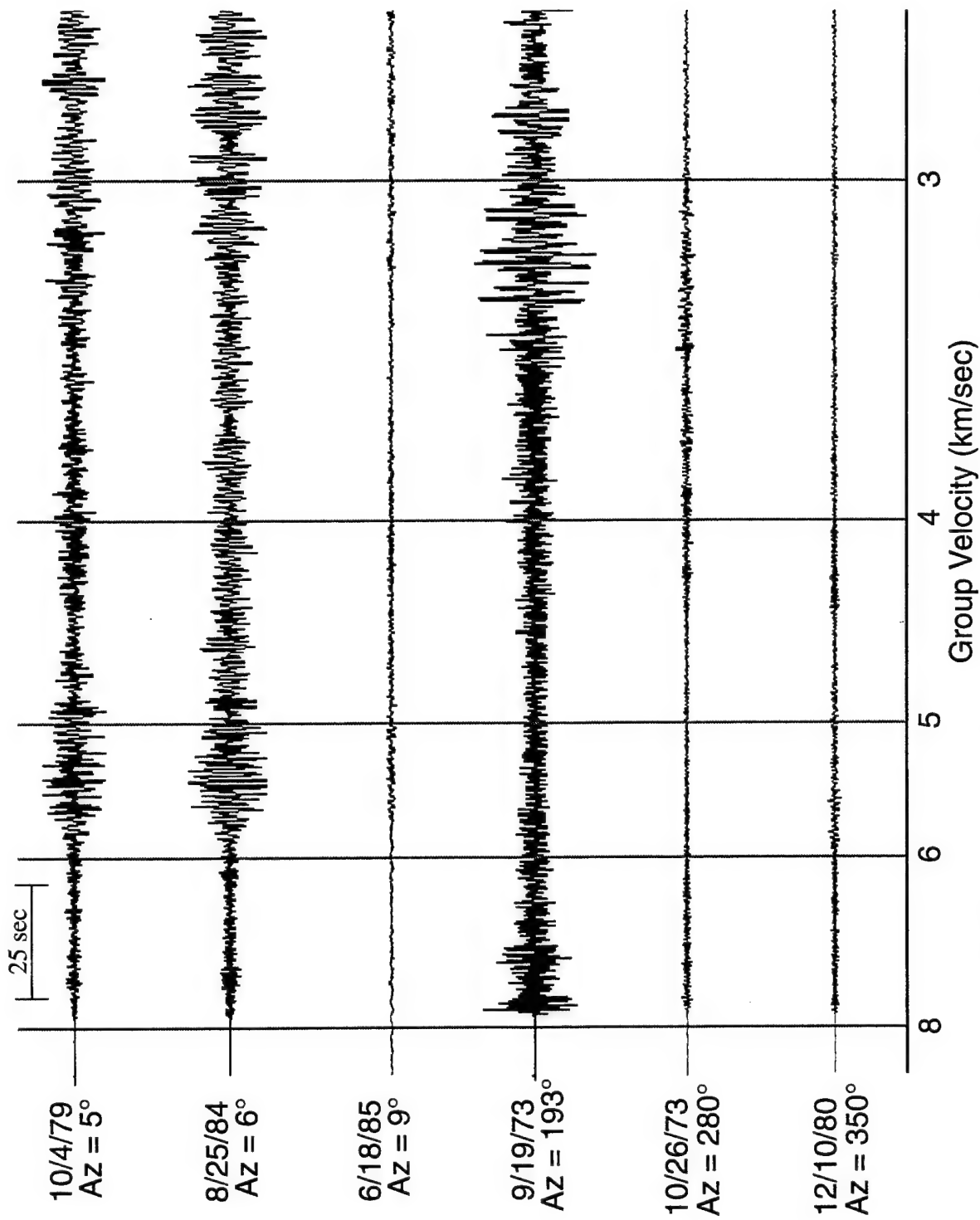


Figure 12. Vertical component regional signals recorded at Borovoye from six Soviet PNE events located at a common epicentral distance of about  $8^\circ$ . Here the data have been approximately normalized to a common yield of 10 kt and plotted at a fixed absolute amplitude scale.

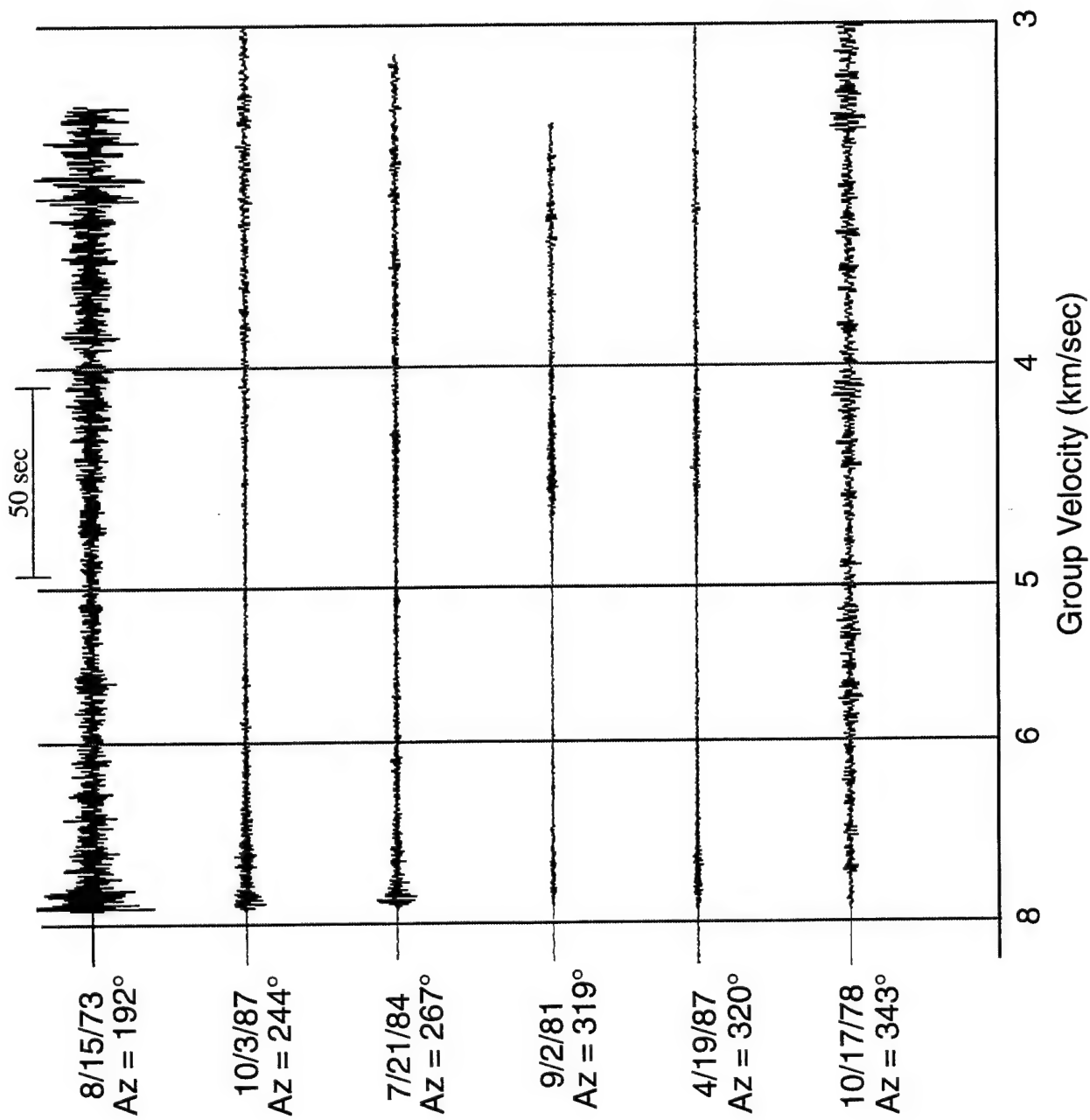


Figure 13. Vertical component regional signals recorded at Borovoye from six Soviet PNE events located at a common epicentral distance of about 10.5°. Here the data have been approximately normalized to a common yield of 10 kt and plotted at a fixed absolute amplitude scale.

dependent noise estimate shown as a solid line in Figure 14. The dashed lines in this figure denote the  $\pm 1\sigma$  levels about the mean which are associated with this sample of data. These  $\sigma$  values average to about a factor of 1.5 over this frequency band, which indicates that the background noise levels are quite stable at this site, and also suggest that the quoted system calibration factors must be quite accurate, at least in the short-period band below about 5 Hz where the specified instrument responses are reasonably flat. Above 5 Hz, the documented instrument responses all decrease fairly rapidly with increasing frequency and show significant variability between events. Application of the specified instrument correction factors in this frequency band was found to lead to a significant increase in data scatter and some rather implausible looking spectral behavior at high frequencies. Therefore, instrument corrections were not applied above 5 Hz in determining the noise estimates leading to Figure 14 and they are not applied in any of the subsequent spectral analyses described in this report. In the meantime, we are continuing to work with the IDG to resolve this apparent discrepancy in the high frequency instrument response curves for the Borovoye station. However, the consistency of the results shown in Figure 14 strongly suggest that the high frequency responses of the system must, in fact, have been fairly constant over the time intervals in which these selected PNE tests were conducted.

Thus, it is tentatively concluded that the variability in amplitude levels shown in Figures 12 and 13 is real and is not simply due to calibration problems. It then remains to determine if this variability is associated primarily with source or propagation path effects. If source effects are dominant, then these same relative differences should be evident in the results obtained by averaging the data recorded on large networks of stations from these explosions. However, the only regional network data which are currently available for these explosions are the parametric data published in the Soviet Bulletins. Selected excerpts from these bulletins are presented for the first time for these 12 explosions in Appendix A, and Figure 15 shows a plot of the reported maximum P wave amplitudes as a function of distance for one of these explosions (i.e., 7/21/84). It can be seen from this figure that these data are widely scattered about the nominal Veith/Clawson distance attenuation curve and, with reference to Appendix

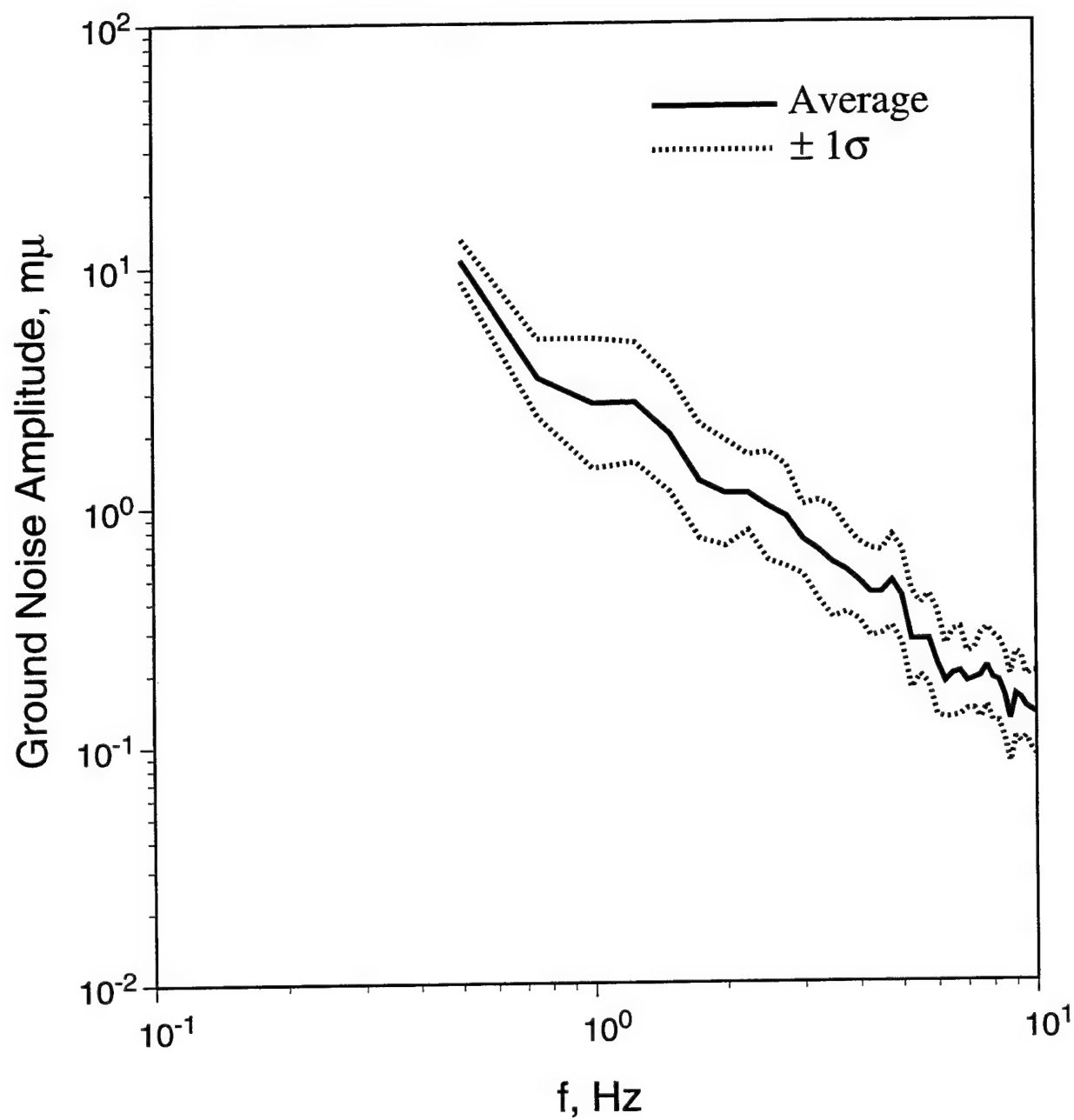


Figure 14. Noise levels as a function of frequency at the Borovoye station estimated from the pre-signal noise samples for the 12 selected Soviet PNE tests in the distance ranges of 8 and 10.5 degrees.

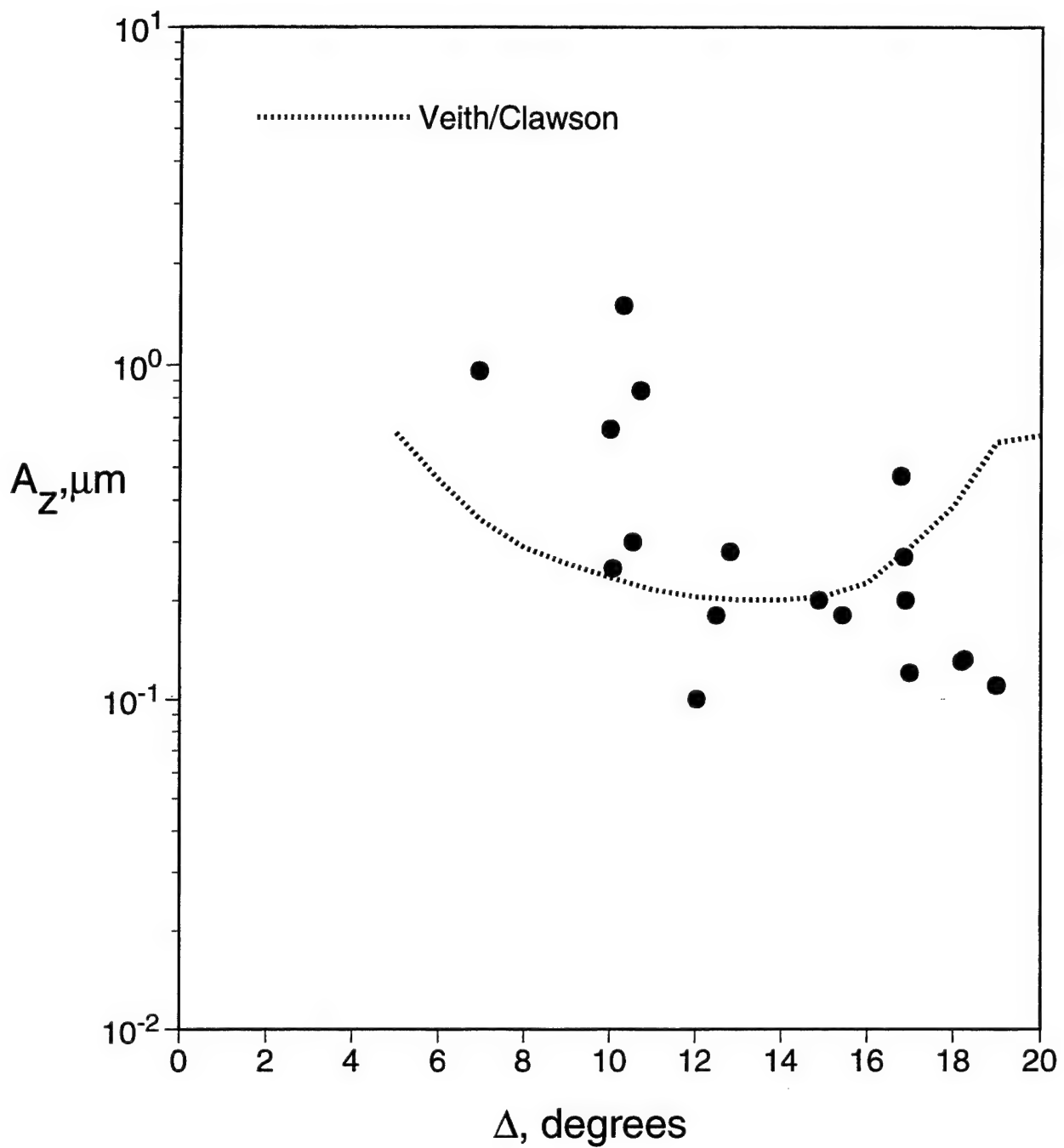


Figure 15. Maximum P wave amplitudes as a function of distance for the 7/21/84 PNE test. These amplitude data were taken from the Soviet Bulletin data for this event which is listed in Appendix A.

A, it is evident that the reporting network varies quite considerably between events. Thus, while valuable for characterization purposes, these data are not precise or consistent enough to be used to distinguish source from propagation path effects in the data of Figures 12 and 13.

An alternate approach to this question is to directly test how well the observed amplitude data correlate with the known source properties of these 12 tests. Thus, for example, Figure 16 shows a plot of the broadband peak amplitude values for the 12 selected PNE events plotted as a function of the corresponding explosion yields from Table 1. It can be seen that these data are widely scattered and appear to show an anomalously strong yield dependence (i.e.,  $A_p \sim W^{1.5}$ ). Moreover, it can be seen that there are no obvious correlations with the different source media, which are designated by different symbols on this plot. Thus, variations in yield or source medium alone cannot explain the observed variability in peak amplitude levels for this data set. Another source variable of potential interest is the source depth, which varies between 593 and 2859 m for this sample of explosions. In order to assess the joint dependence of the peak amplitudes on yield and depth, we postulate a functional dependence of the form

$$A_p = k W^n h^m \quad (1)$$

and estimate the parameters  $k$ ,  $n$  and  $m$  through a multivariable least squares analysis of the linearized form

$$\log A_p = \log k + n \log W + m \log h \quad (2)$$

The results of this analysis are summarized in Figure 17 where the normalized peak amplitude data at a fixed average source depth of 1000 m are plotted as a function of yield (left) and versus depth at a fixed average yield of 10 kt (right), where the data normalizations have been carried out using the scaling relations obtained from the least squares analysis. It can be seen from this figure that this proposed multivariable dependence on yield and source depth appears to explain these data remarkably well, with little evidence of any residual dependence on source medium or

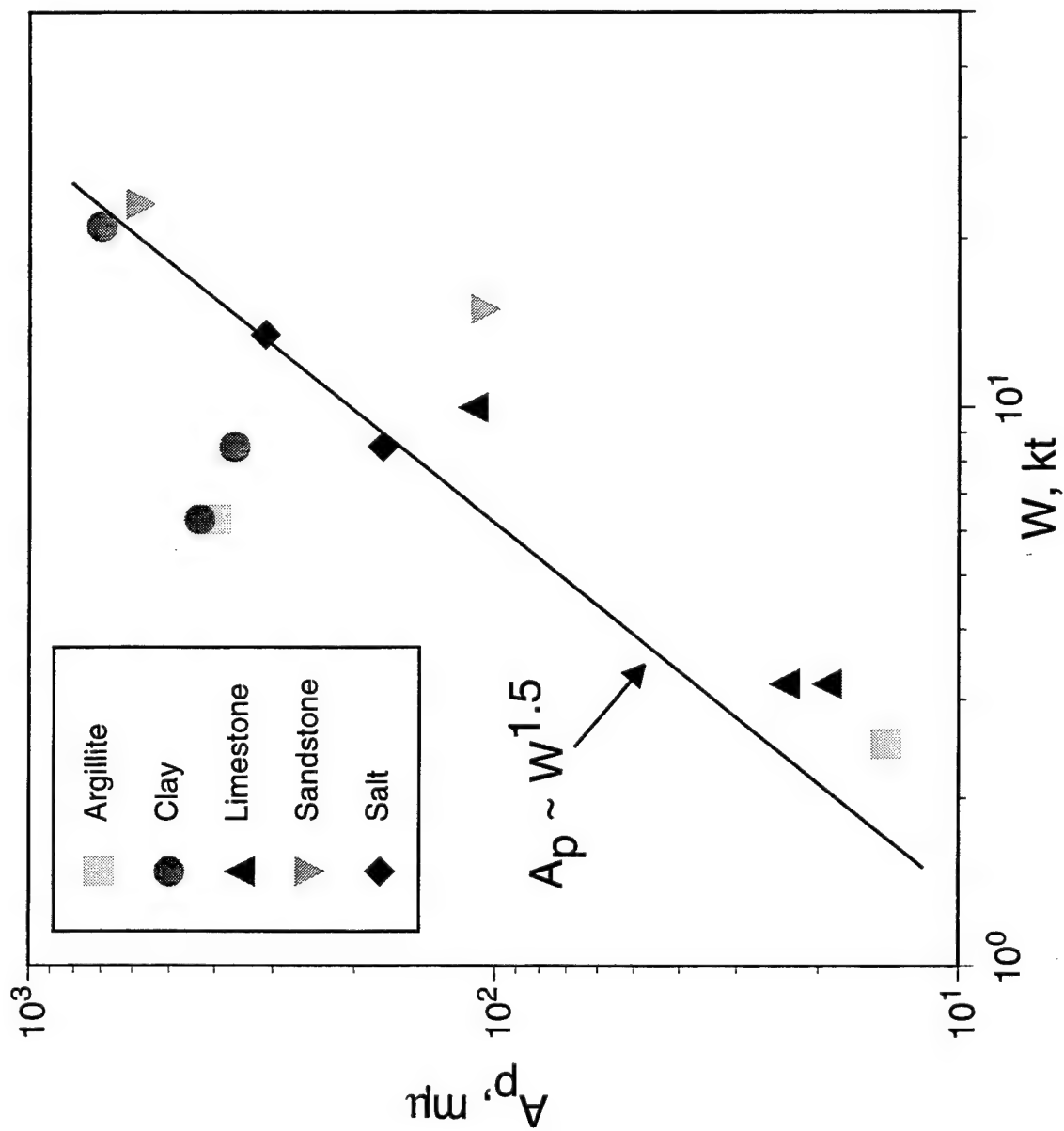


Figure 16. Borovoye broadband peak amplitudes as a function of yield for the selected Soviet PNE events.

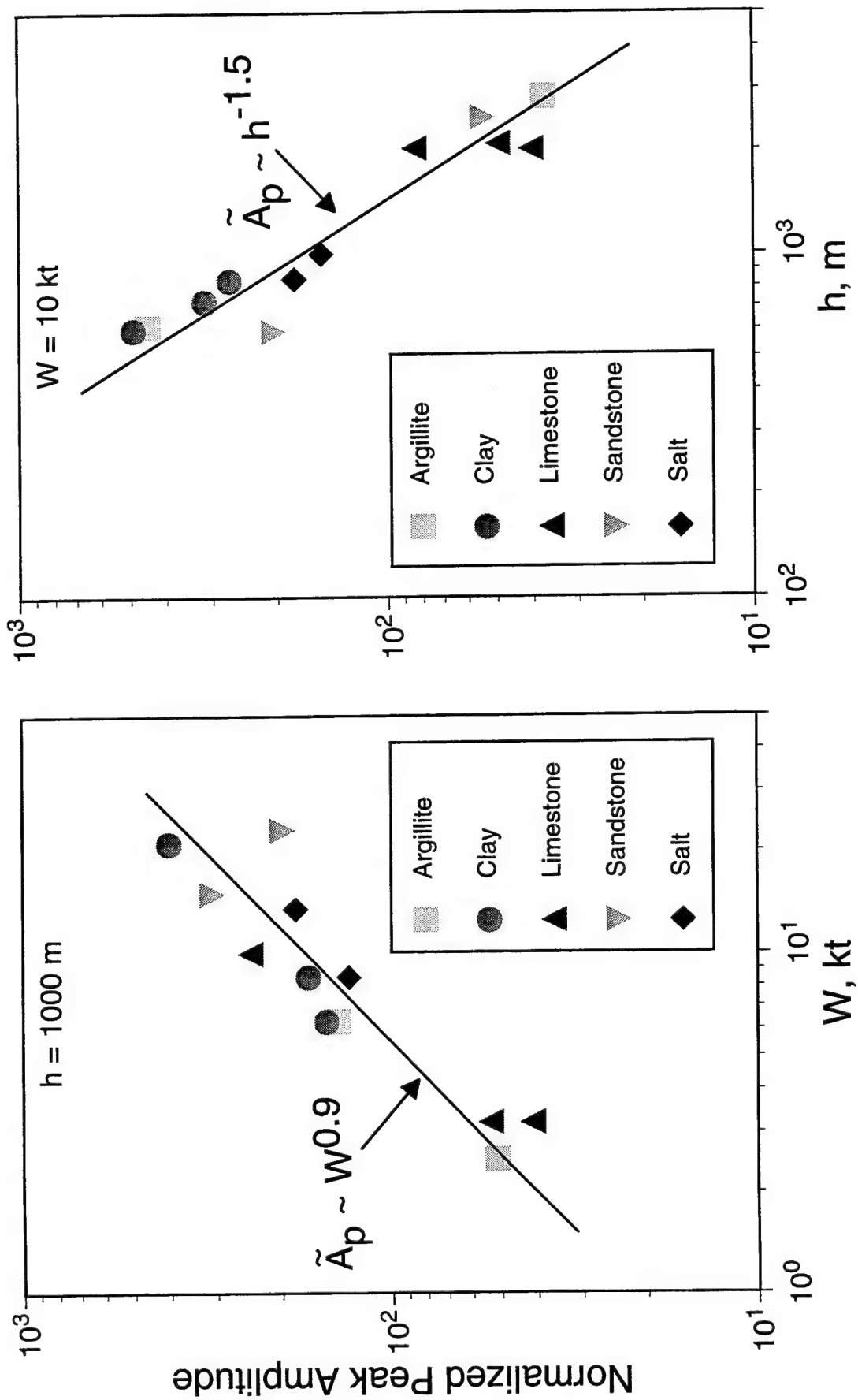


Figure 17. Normalized Borovoye PNE broadband peak amplitudes as a function of yield at a reference source depth of 1000 m (left) and as a function of source depth at a reference yield of 10 kt (right).

propagation path. Furthermore, the yield dependence obtained from this multivariable analysis is reduced to a more physically plausible value (i.e.,  $A_p \sim W^{0.9}$ ), although the associated inferred dependence on source depth is surprisingly strong (i.e.,  $A_p \sim h^{-1.5}$ ). However, these results need to be interpreted cautiously in that these broadband peaks may represent different regional phases and different dominant frequencies on the recordings of these various explosions, and this could lead to bias in the results for this relatively small sample of data. This issue of source scaling will be revisited in more detail in the following section where the analysis will be repeated for individual phases and frequency bands.

### 3. REGIONAL PHASE SPECTRA AND DISCRIMINATION

Much research has been conducted over the past several decades in attempts to characterize the regional seismic signals observed from underground nuclear explosions and earthquakes. Because of data availability limitations, most of the initial U.S. research in this area focused on analyses of data recorded from explosions at the Nevada Test Site (Blandford and Klouda, 1980; Blandford, 1981; Murphy and Bennett, 1982; Chael, 1988; Taylor *et al.*, 1988; Bennett and Murphy, 1986). These investigations were generally productive and led to rough characterizations of the different seismic phases observed in this particular region, as well as the identification of some diagnostic differences in the spectral composition of the  $L_g$  phases observed from earthquakes and explosions (Murphy and Bennett, 1982; Taylor *et al.*, 1988) which formed the basis for the definition of discriminants (i.e.,  $L_g$  spectral ratio,  $L_g/P$  spectral ratio) which have proved to be applicable in a number of other testing environments. However, in general, the applicability of many of the results of these empirical characterization studies to other testing environments has been viewed with caution, due to the rather unique source and propagation path features of the Basin and Range Province of the Western U.S. In more recent years, some regional data have started to become available from underground nuclear explosions at the principal Soviet test sites at Semipalatinsk and Novaya Zemlya and at the Chinese test

site at Lop Nor, and these data have been extensively processed and analyzed in attempts to assess their utility for event identification purposes (Ringdal and Hokland, 1987; Bennett *et al.*, 1993; Baumgardt, 1990; Taylor and Denny, 1991). These studies documented differences in the excitation of regional signals for different source types in Eurasia, but they also showed that propagation effects sometimes made the effects ambiguous or difficult to observe. In particular, it has been noted that there are some significant differences in the relative phase amplitudes and spectral composition of the signals observed from explosions at the different test sites and this has increased the level of concern regarding the transportability of simple empirical discriminants to new testing regimes.

Coincident with the empirical studies referenced above, extensive research has been on-going in attempts to define robust theoretical models which can be used to quantitatively explain the observed characteristics of these regional signals (McLaughlin *et al.*, 1993; Stump and Reinke, 1991; Taylor and Randall, 1989; Barker *et al.*, 1990). Although much progress has been made as a result of these theoretical investigations, the problem has proved to be complex and there are still important features of the observed regional waveforms which are only roughly and incompletely accounted for by existing simulation models. For example, it has proved to be very difficult to theoretically account for observed variations of S and  $L_g$  excitation levels and spectral composition for explosions in different environments and such variations can effect the performance of a number of proposed regional discriminants. Thus, it is not possible at the present time to confidently predict, either empirically or theoretically, how nuclear explosion regional seismic signals can be expected to vary over the range of source and propagation path conditions of potential interest in global test monitoring. Data recorded at regional distances from the extensive Soviet PNE test program provide the best available resource for evaluating such variability in regional discriminant performance.

As was noted in Section 2, observed variations in the regional seismic signal characteristics used for discrimination purposes clearly depend on both frequency and the specific regional phase under investigation. Therefore, the Borovoye data recorded from the selected

PNE events in the 8 and 10.5 degree distance groupings have been processed to obtain estimates of the different regional phase spectra for each event. In the first step of this processing, the data and pre-signal noise windows for each event were bandpass filtered using a Gaussian comb of filters spaced at intervals of 0.25 Hz between 0.5 and 10 Hz, where each filter is characterized by a  $Q$  value of  $6 f_c$ , with  $f_c$  the filter center frequency. Filters of this type have been used by us and a number of other investigators in previous studies (e.g., Murphy *et al.*, 1989) and have been found to provide spectral estimates which are useful for purposes of seismic analysis. These filter outputs were next sorted into seven distinct time windows and the spectral amplitudes at each center frequency were estimated by computing RMS values from the instrument-corrected filter outputs in each of the designated windows. In the interests of simplicity and consistency, these regional phase time windows were defined in terms of apparent group velocity intervals as follows: (1)  $V_g > 8$  km/sec, (2)  $8 > V_g > 7$  km/sec, (3)  $7 > V_g > 6$  km/sec, (4)  $6 > V_g > 5$  km/sec, (5)  $5 > V_g > 4$  km/sec, (6)  $4 > V_g > 3$  km/sec and (7)  $3 > V_g > 2.5$  km/sec. For purposes of subsequent discussion, these seven time windows will be identified as pre-signal noise,  $P_n$ ,  $P_{coda}$ ,  $P_g$ ,  $S_n$ ,  $L_g$  and  $L_{gcoda}$ , respectively. Although there are individual cases in which refined time windows could be specified which would precisely isolate particular regional phases of interest, this simple windowing procedure was employed throughout as a test of its potential utility for routine seismic discrimination purposes.

On the basis of the data quality review described in Section 2, one of the 12 explosions (i.e., 9/19/73) was eliminated from the spectral analysis because of questionable data quality and, in several other cases, specific time windows were not processed in order to avoid segments with unresolved data problems. In addition, the data for some of the events in the 10.5 degree distance grouping did not extend beyond the 3 km/sec group arrival time and, consequently,  $L_{gcoda}$  spectra could not be estimated in those cases. In general, however, usable spectral estimates were obtained for all phases for most events.

Complete spectral data for all regional phases recorded from the remaining sample of 11 PNE events are presented in Appendix B, and only

selected examples will be presented here to illustrate some of the more prominent features of these spectral estimates. As a first example, the regional phase spectra derived from the Borovoye recordings of the explosions of 10/04/79 and 12/10/80 from the 8 degree distance group are shown plotted at the same scale in Figure 18 for comparison purposes. With reference to Table 1, the 10/04/79 event had a yield of 21 kt and was detonated at a depth of 837 m in clay, while the 12/10/80 event had a yield of 15 kt and was detonated at a depth of 2485 m in sandstone. It can be seen from Figure 18 that although the yields of these two explosions differ by only a factor of 1.4, the amplitude levels of the corresponding regional phase spectra differ by as much as a factor of 10 at low frequency and show very different corner frequencies for the same regional phases. Since these two explosions share essentially identical propagation paths to the Borovoye station (i.e., they both fall in the northern cluster of events shown in Figure 7), these results suggest that other source variables such as depth and medium must be having pronounced effects on the excitation of the different regional phases in this case.

A second example is presented in Figure 19 using data recorded from the 8/15/73 and 9/02/81 explosions of the 10.5 degree distance group. Again, with reference to Table 1, the 8/15/73 event had a yield of 6.3 kt and was detonated at a depth of 600 m in clay, while the 9/02/81 event had a yield of 3.2 kt and was detonated at a depth of 2088 m in limestone. As in the preceding example, it is evident that the common regional phase spectra for these two events show differences in amplitude levels and corner frequencies which are much larger than those which might be simply attributed to the factor of two difference in yield. The interpretation of these observed spectral differences is somewhat more ambiguous in this instance, since these two explosions do not share a common propagation path to the Borovoye station. However, these data do provide additional strong evidence that factors other than explosion yield are having profound effects on the observed, frequency dependent regional phase characteristics of these explosions.

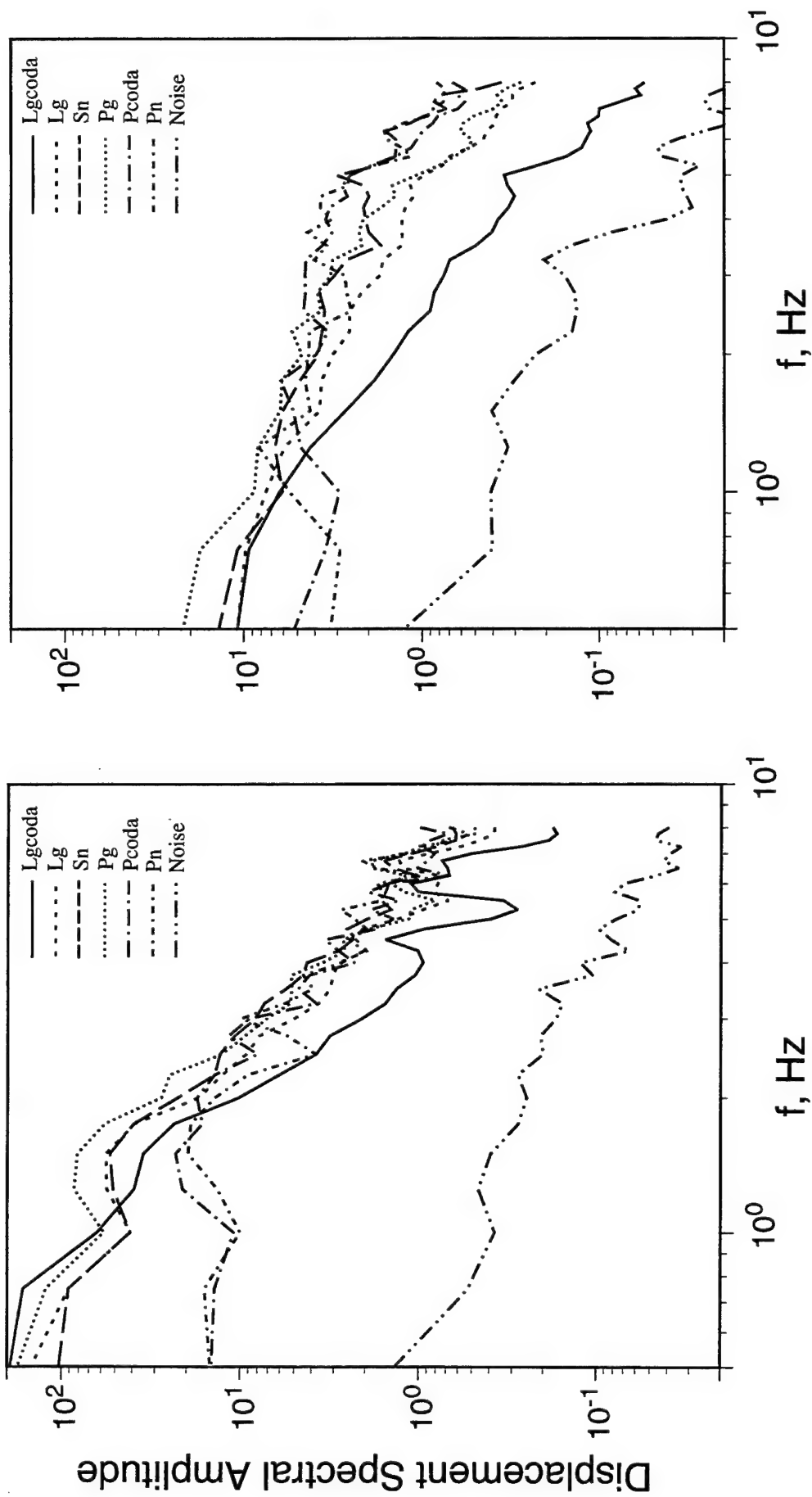


Figure 18. Borovoye regional phase spectra corresponding to the 10/04/79 (left) and 12/10/80 (right) PNE events from the 8° distance group.

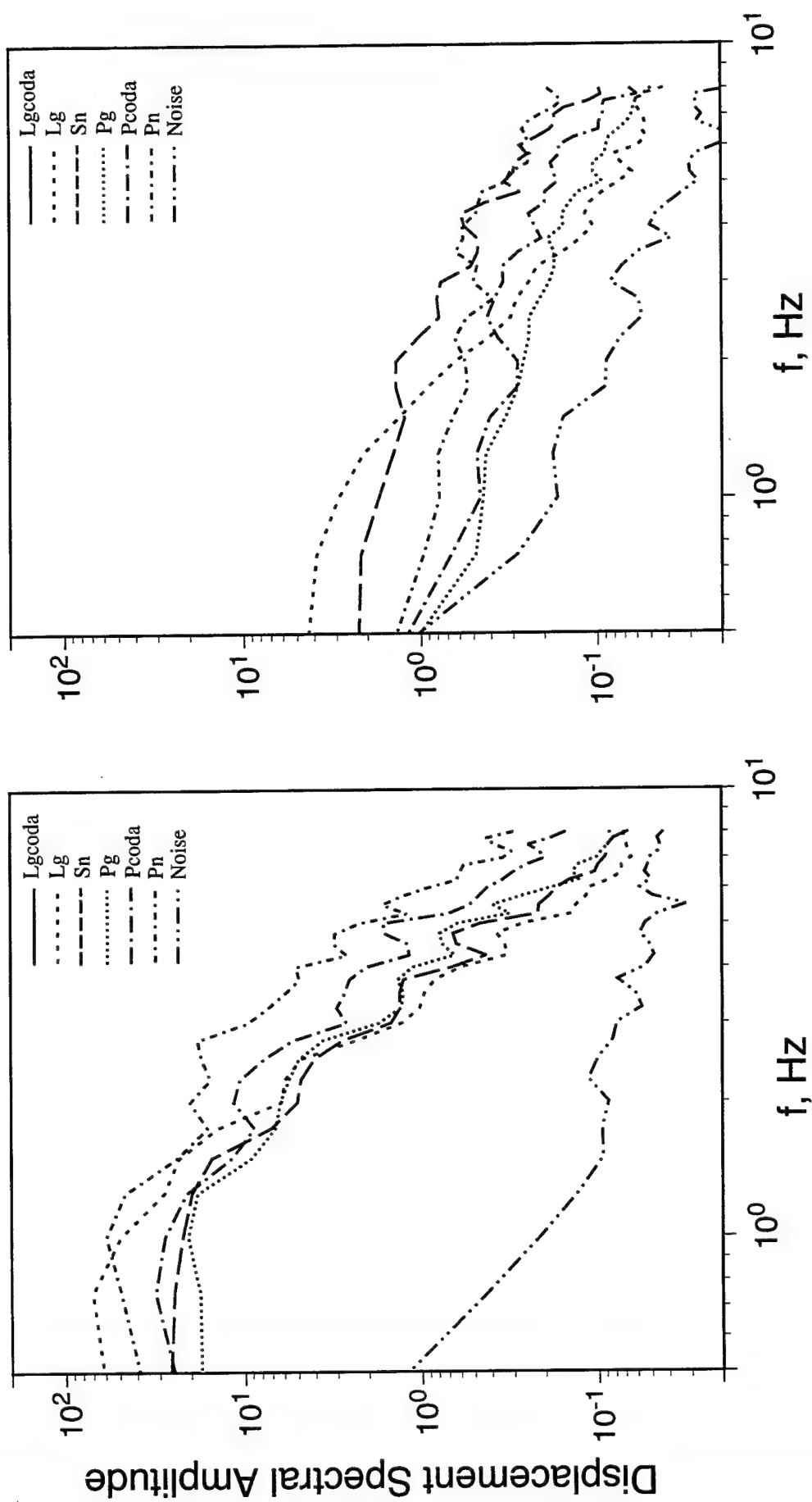


Figure 19. Borovoye regional phase spectra corresponding to the 8/15/73 (left) and 9/02/81 (right) PNE events from the  $10.5^\circ$  distance group.

An alternate way of examining the same spectral data is on a phase-by-phase basis. Thus, Figure 20 shows all the  $P_n$  (left) and  $L_g$  (right) phase spectra derived from the five events in the 8 degree distance group, again plotted at the same scale to facilitate comparisons. Here, all the effects of the source and propagation path differences between the events combine to produce the very large observed variability between the individual spectral estimates. It can be seen that the  $L_g$  spectral amplitude levels are typically larger than those for  $P_n$  at low frequencies, but that the  $L_g$  spectra have lower corner frequencies than the  $P_n$  spectra, leading to comparable or lower  $L_g$  spectral amplitude levels at high frequencies, which is consistent with previous observations of explosion spectra (e.g., Murphy and Bennett, 1982). It is also interesting to note from this figure that spectral differences between events can be quite different for the  $P_n$  versus  $L_g$  phases. Thus, for example, the differences between the  $P_n$  spectra for the 6/18/85 and 8/25/84 explosions are much larger than those observed for the corresponding  $L_g$  spectra, with neither difference showing any simple correlation with the factor of 3.4 difference in yields between these two events.

A second example is presented in Figure 21 where the  $P_n$  (left) and  $L_g$  (right) phase spectra derived from the six events in the 10.5 degree distance group are compared. Note that both the  $P_n$  and  $L_g$  spectra for the 4/19/87 and 9/02/81 explosions are quite similar over the entire frequency band extending from 0.5 to 10 Hz. This is reassuring, since in this case both explosions were detonated in limestone, have the same yield (i.e., 3.2 kt), nearly the same depths (i.e., 2015 versus 2088 m) and share nearly identical propagation paths to Borovoye. Thus, small changes in source and propagation path conditions lead to only small changes in the corresponding regional phase spectra and, therefore, it should be possible to quantify the effects of these different variables on the characteristics of the regional phases used for discrimination purposes.

As a first step in this process, the frequency dependent yield and depth scaling coefficients of each regional phase have been estimated by fitting the spectral amplitude data for the 11 PNE events to the power law functional form of Equation (1) on a frequency-by-frequency basis. Note

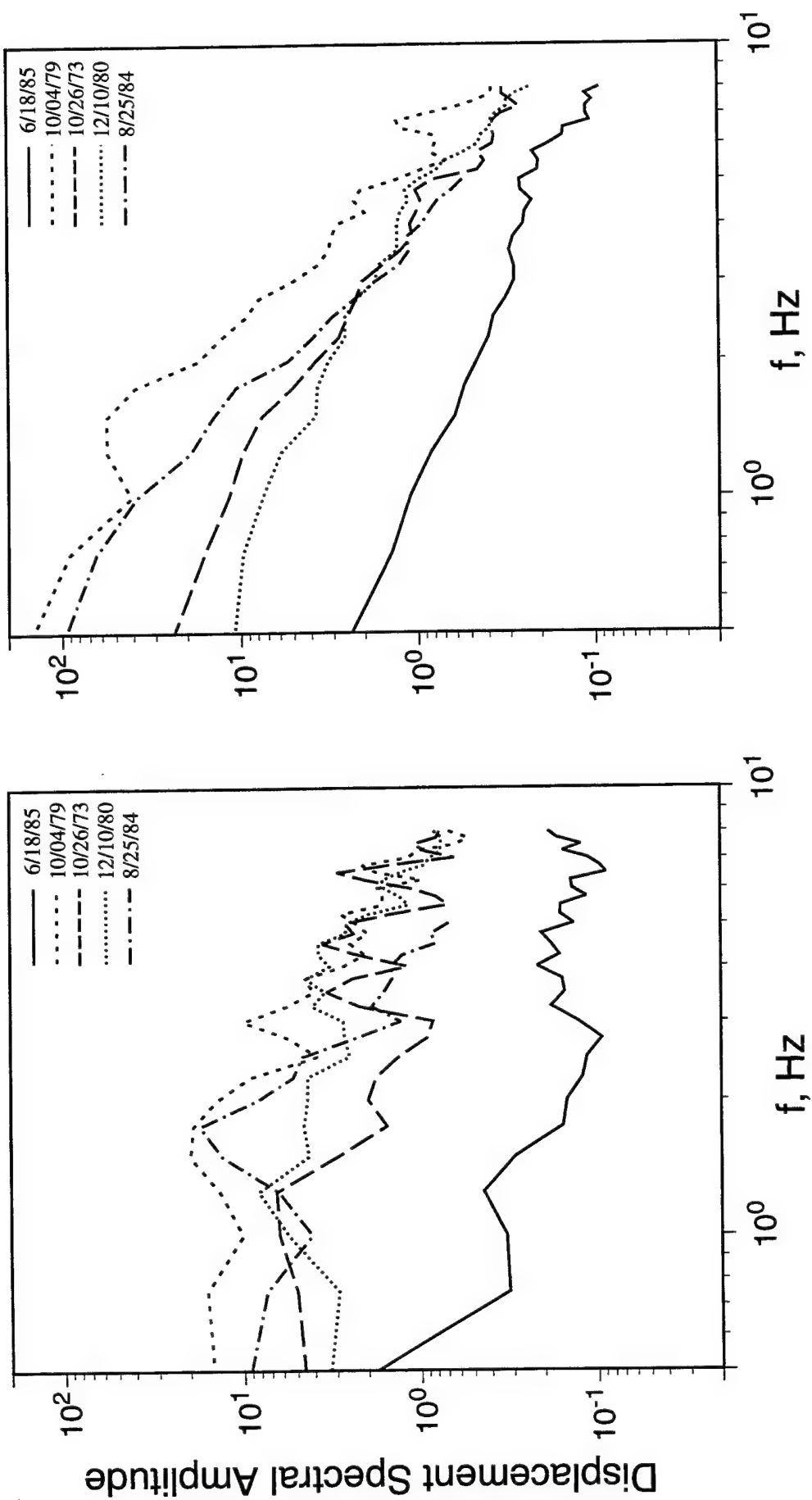


Figure 20. Comparison of Borovoye  $P_n$  (left) and  $L_g$  (right) spectra for the selected PNE events in the  $8^\circ$  distance group.

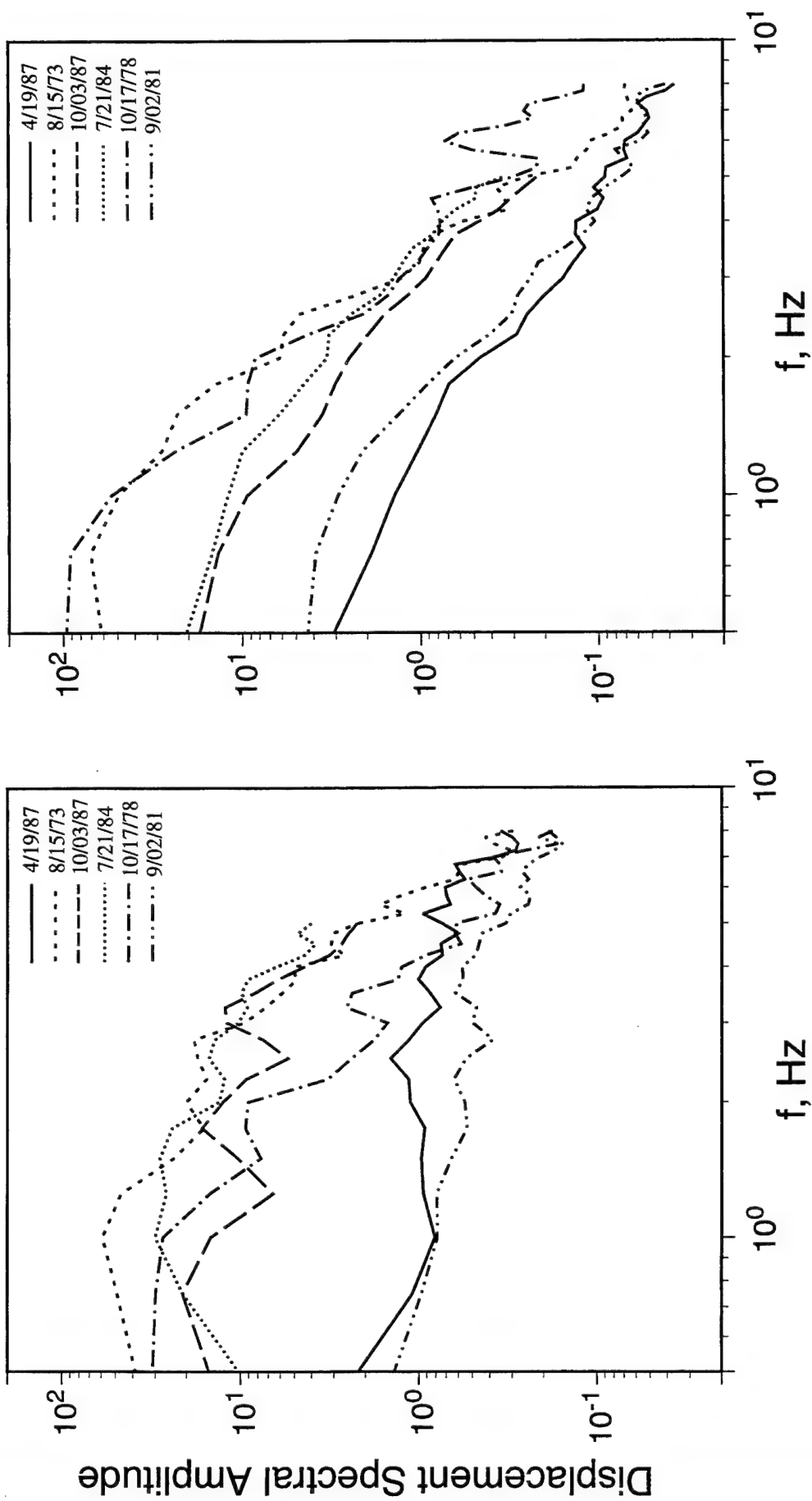


Figure 21. Comparison of Borovoye  $P_n$  (left) and  $L_g$  (right) spectra for the selected PNE events in the  $10.5^\circ$  distance group.

that, for the purposes of this analysis, the 8 and 10.5 degree groups of events have been combined in view of the fact that both the predicted and observed attenuation effects due to this difference in distance appear to be rather small. The results of this analysis are summarized in Figure 22 where the derived yield and depth scaling exponents as a function of frequency are plotted for each of the six regional phases analyzed. It can be seen from this figure that the frequency dependencies of both exponents are quite similar for all the phases except the  $L_{gcoda}$ , which shows physically unreasonable negative yield scaling exponents at low frequency. It was noted previously that  $L_{gcoda}$  spectra could not be determined for all the events due to data length limitations and, in fact, data from only 7 of the 11 PNE events were included in the analysis leading to the exponent estimates shown for this phase. However, these results do provide a cautionary reminder regarding the large uncertainties associated with small sample statistics.

The frequency dependent scaling exponents determined for the other five phases are plotted together in Figure 23 for both the yield (top) and source depth (bottom) variables. It can be seen from these plots that the frequency dependencies of these two sets of exponents are indeed remarkably similar for the five regional phases, which is consistent with the hypothesis that, to first order, all of these phases are produced from a single explosion P wave source function through linear conversion processes. Thus, as has been noted previously (Murphy, 1977), the entire regional waveform, including both P and S wave phases, can be approximately scaled for yield and depth effects using scaling laws derived from a spherically symmetric P wave source approximation. It can be seen from Figure 23 that, over the yield and depth ranges encompassed by this sample of explosions, the derived yield scaling exponents are roughly independent of frequency and average to a value of about 1.0, while the corresponding depth scaling exponents exhibit a pronounced frequency dependence, ranging from about -1.5 at low frequencies to +0.5 at high frequencies. Thus, the inferred low frequency depth scaling exponents are quite large, and are roughly consistent with the corresponding peak amplitude depth scaling exponent derived in Section 2.

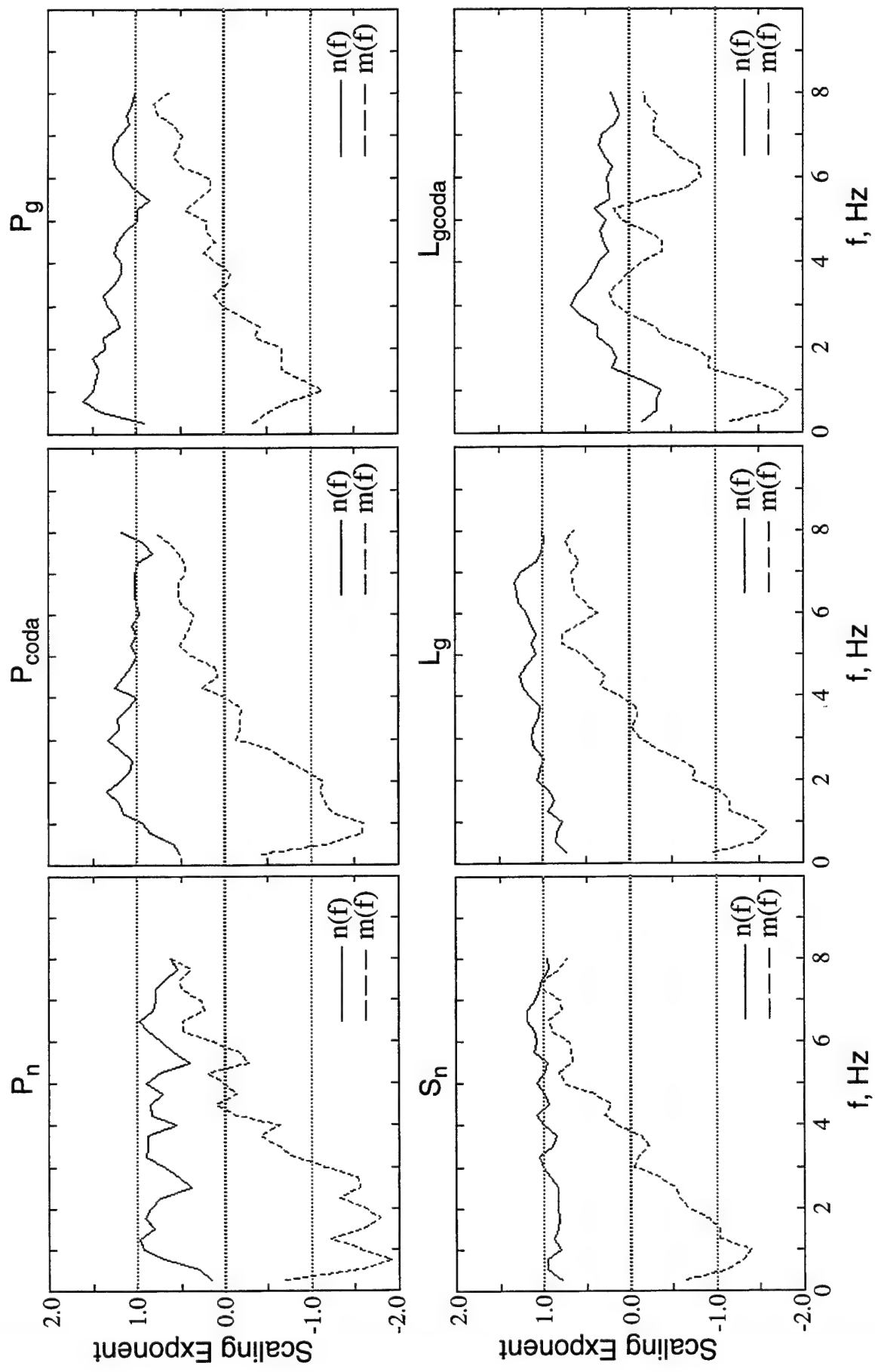


Figure 22. Comparison of yield (n) and depth (m) scaling exponents as a function of frequency for the different regional phases determined from least-squares analysis of the selected Borovoye data.

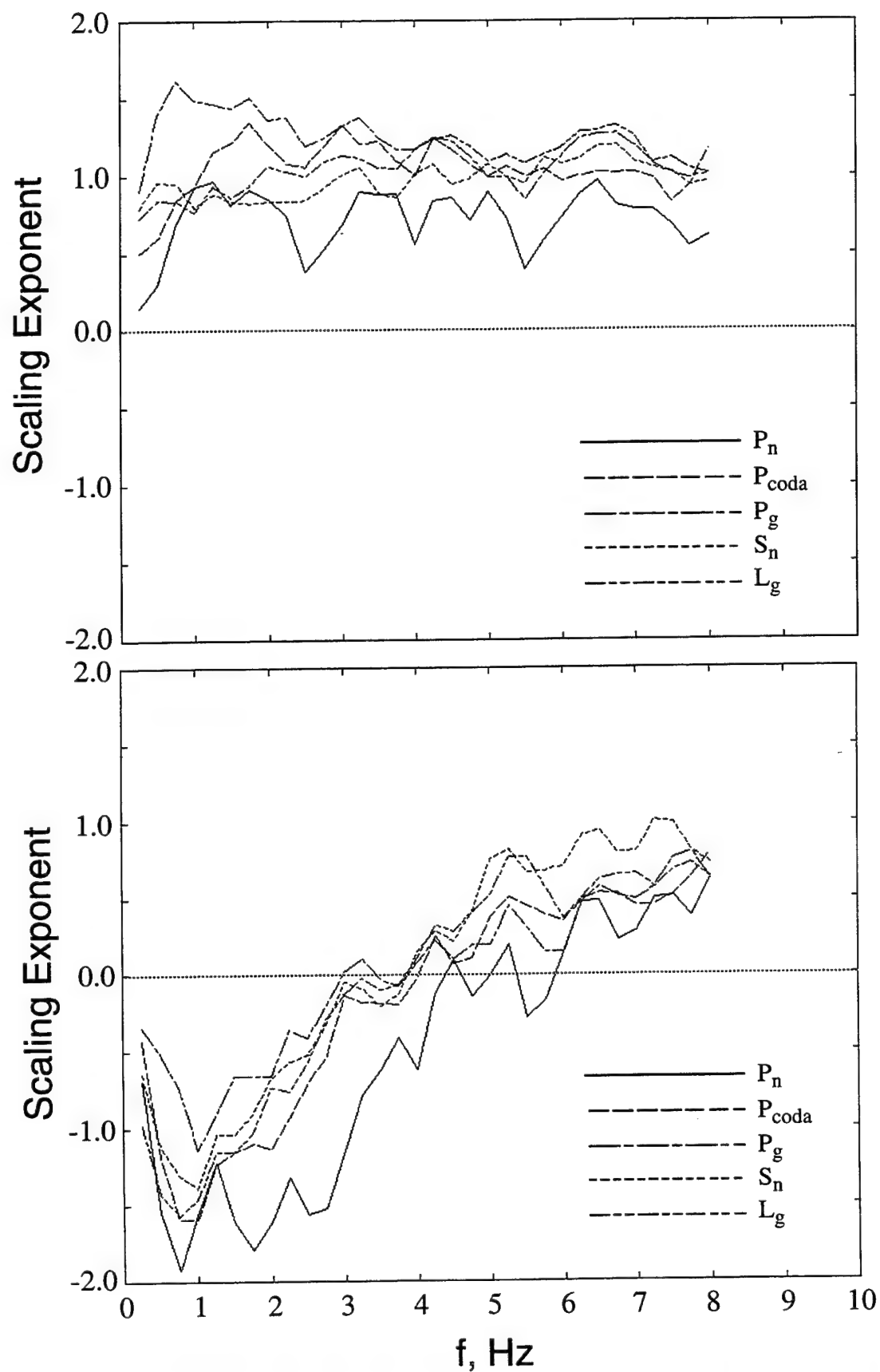


Figure 23. Comparison of yield (top) and depth (bottom) frequency dependent scaling exponents determined for the different regional phases recorded at Borovoye from the selected PNE events.

In an attempt to derive an improved, quantitative understanding of the derived scaling exponents, theoretical Mueller/Murphy (1971) source spectra were predicted for each of the 11 PNE events and the resulting spectral amplitudes were then statistically analyzed using the same procedures which were applied to the observed data. The resulting theoretical yield and depth scaling exponents are plotted as a function of frequency in Figure 24, where they are compared with the upper and lower bounds on the experimental exponents from Figure 23. It can be seen that the theoretical Mueller/Murphy scaling exponents are reasonably consistent with the observed regional phase spectral behavior in that the theoretical yield exponents are also essentially independent of frequency over this range, while the theoretical depth exponents change from negative to positive values with increasing frequency. The only notable discrepancy is that the theoretical depth scaling exponent has a value of about -0.7 at low frequency, while the experimental exponents are generally larger, ranging from about -1.0 to -1.5 in this frequency band. More data will have to be analyzed before it can be determined whether this apparent discrepancy is actually significant enough to warrant modification of the simple scaling model for applications to scaling of regional seismic data. In any case, the simple model is at least qualitatively consistent with the observations and provides a physical basis for understanding the observed frequency dependencies of the explosion yield and depth scaling exponents.

A remaining question concerns the extent to which the derived scaling laws based on the source yield and depth variables alone can account for the observed variability in the regional phase spectra. One approach to assessing this goodness of fit is to use the derived empirical scaling laws to predict the regional phase spectra for each event and to then compare the predicted and observed spectra on a phase-by-phase and event-by-event basis. A complete set of such comparisons is presented in Appendix C, and several typical examples are shown in Figures 25 and 26 for the  $P_n$  and  $L_g$  phase data corresponding to the five explosions in the 8 degree distance group. It can be seen from these figures that the agreement between these predicted and observed spectra is reasonably good, with differences generally being less than about a factor of 2 over the analyzed frequency band extending from 0.5 to 8.0 Hz. Examination of the other

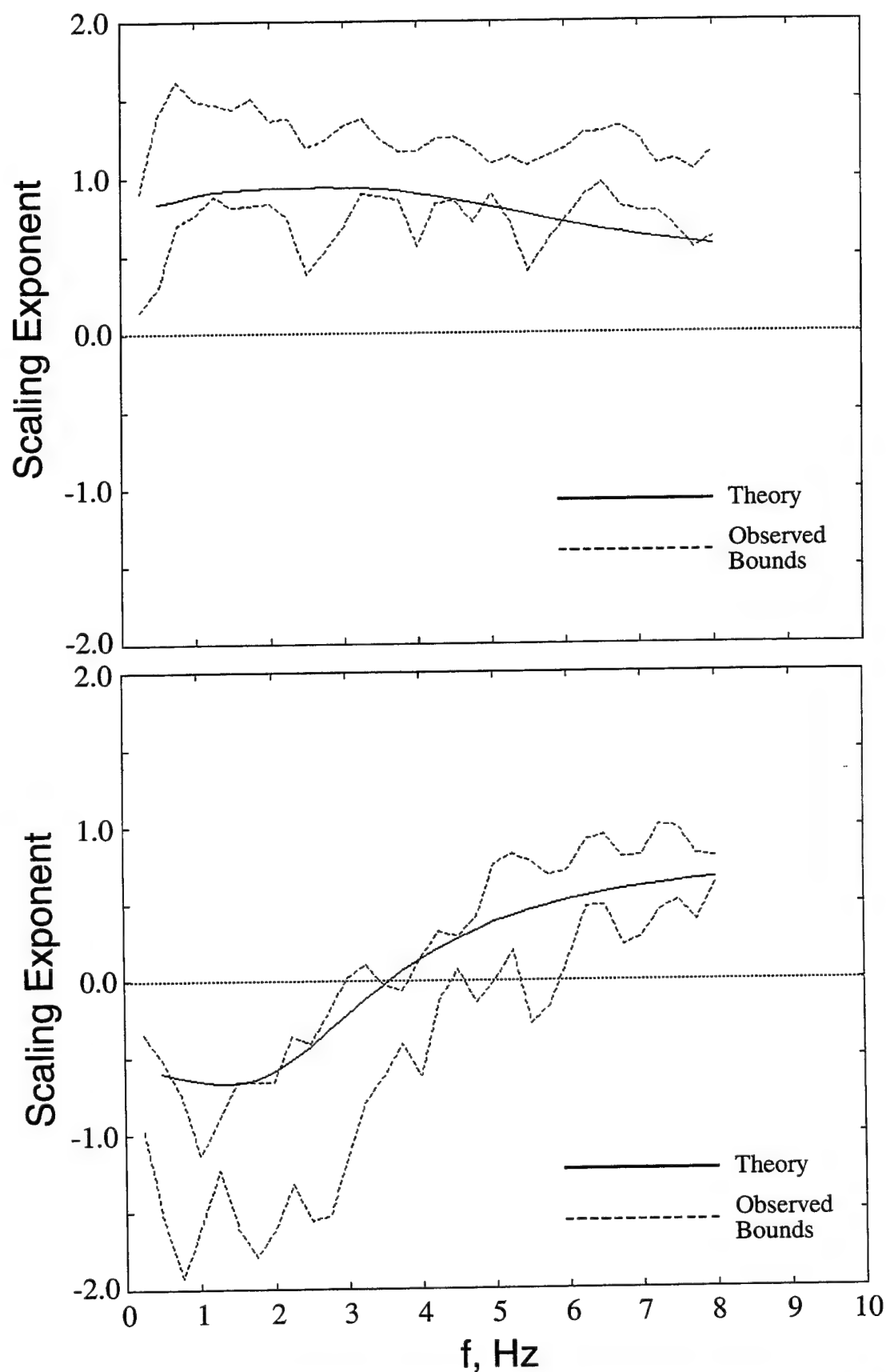


Figure 24. Comparison of theoretical (Mueller/Murphy) and observed bounds on the yield (top) and depth (bottom) frequency dependent scaling exponents determined for the regional phases for selected PNE events.

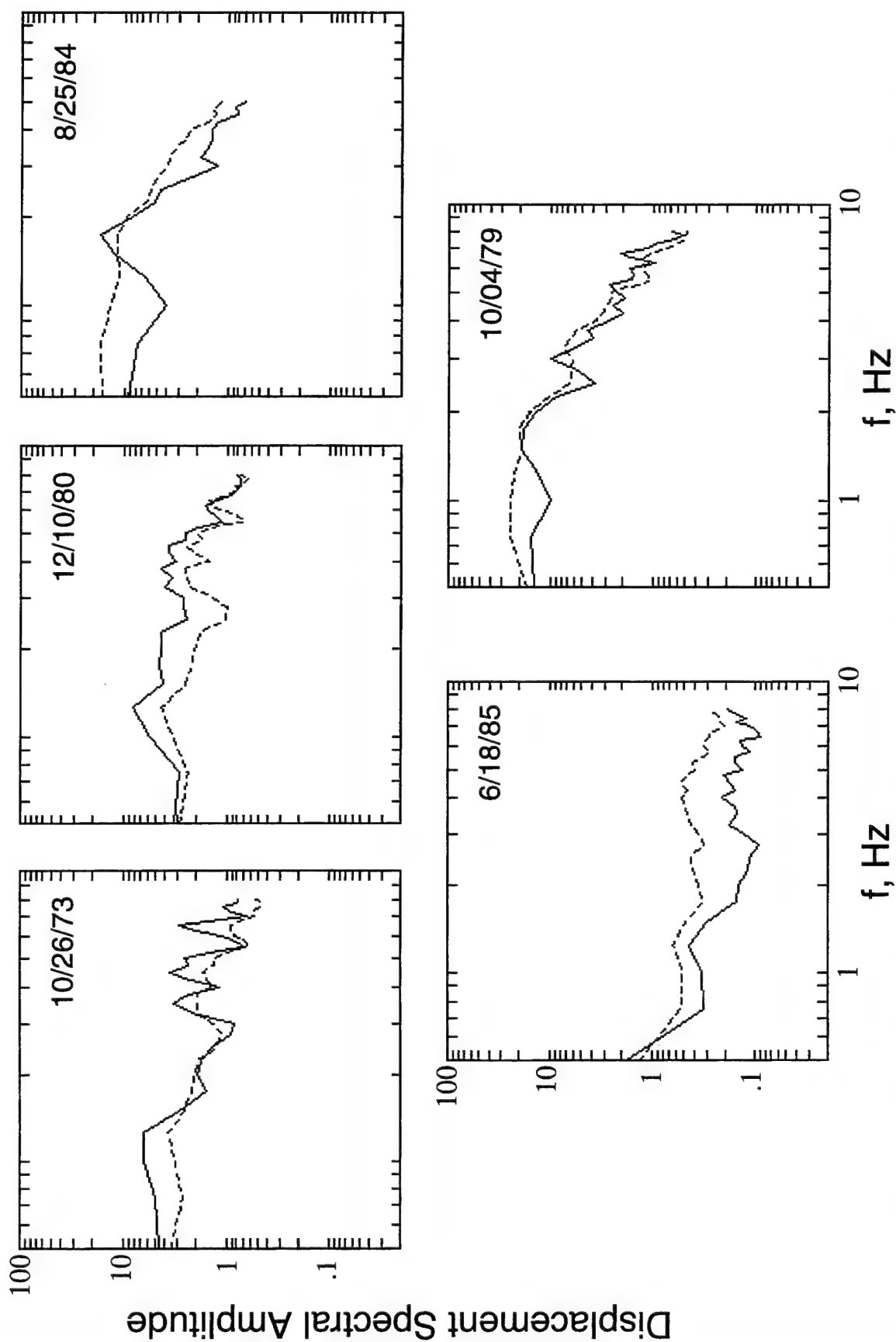


Figure 25. Comparison of predicted (dashed) and observed (solid) Borovoye  $P_n$  amplitude spectra for the selected PNE events in the  $8^\circ$  distance range.

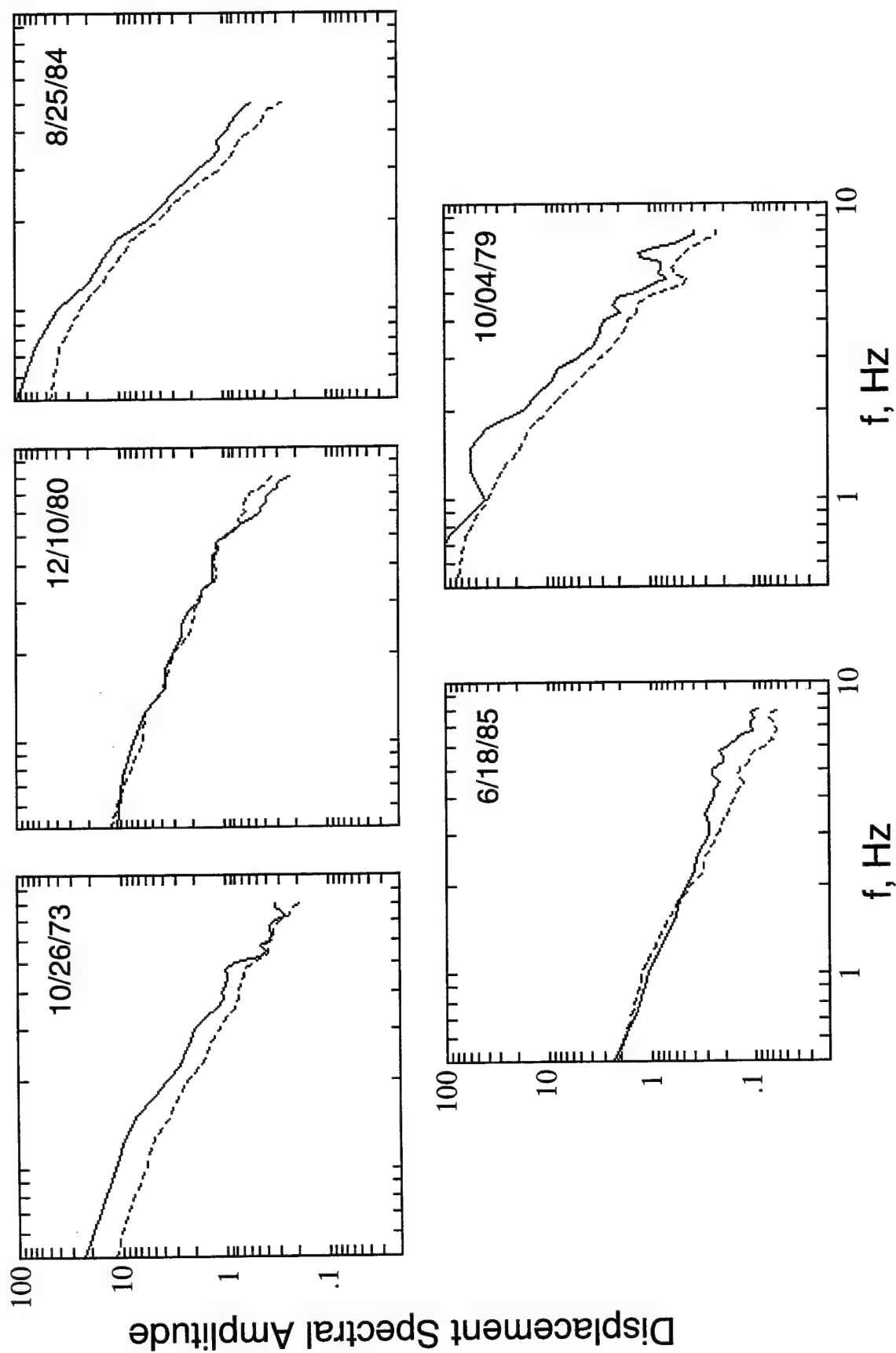


Figure 26. Comparison of predicted (dashed) and observed (solid) Borovoye  $L_g$  amplitude spectra for the selected PNE events in the  $8^\circ$  distance range.

comparisons in Appendix C indicates that these results are fairly typical, which suggests that the effects of other variables, such as source medium and propagation path, may be of second order importance with respect to those associated with yield and depth of burial, at least over the range of those variables represented in the sample of explosions under investigation here. More quantitative analysis of a larger data set will be required in order to fully test the generality of this preliminary conclusion.

Given that the derived scaling laws provide reasonably good descriptions of the variations in these observed regional phase spectra, it is of interest to examine the predicted, systematic dependencies on yield and source depth for the different regional phases which are used for discrimination purposes. Note first from Figure 23 that the derived yield exponents are fairly constant over the frequency range from 0.5 to 8.0 Hz. Thus, to first order, the shapes of the predicted regional phase spectra are independent of yield over the sampled yield range, and it is only necessary to examine the frequency dependent effects due to the inferred source depth dependence. Therefore, the predicted spectra corresponding to selected regional phases have been evaluated over the sample source depth range extending from about 500 to 2500 m at the average sample yield of 10 kt. The results for the  $P_n$  and  $P_g$  phases are shown in Figure 27, while those for the  $S_n$  and  $L_g$  phases are shown in Figure 28. It can be seen that all these spectra show a strong decrease in low frequency spectral amplitude level with increasing depth and a corresponding increase in high frequency spectral amplitude level with increasing depth, with the crossover occurring in the 3-4 Hz band for these ranges of yield and source depth. Note also that the  $P_g$  phase shows significantly less dependence on source depth than the other three phases, again consistent with the range of depth exponents shown in Figure 23. Comparisons of the spectra of Figures 27 and 28 reveal that the predicted  $S_n$  and  $L_g$  spectra decrease more rapidly with increasing frequency than do the predicted  $P_n$  and  $P_g$  spectra, which is consistent with previous observations for explosions in other areas (e.g., Murphy and Bennett, 1982).

The implications of these preliminary Borovoye data analysis results with respect to the transportability of regional discriminants are illustrated

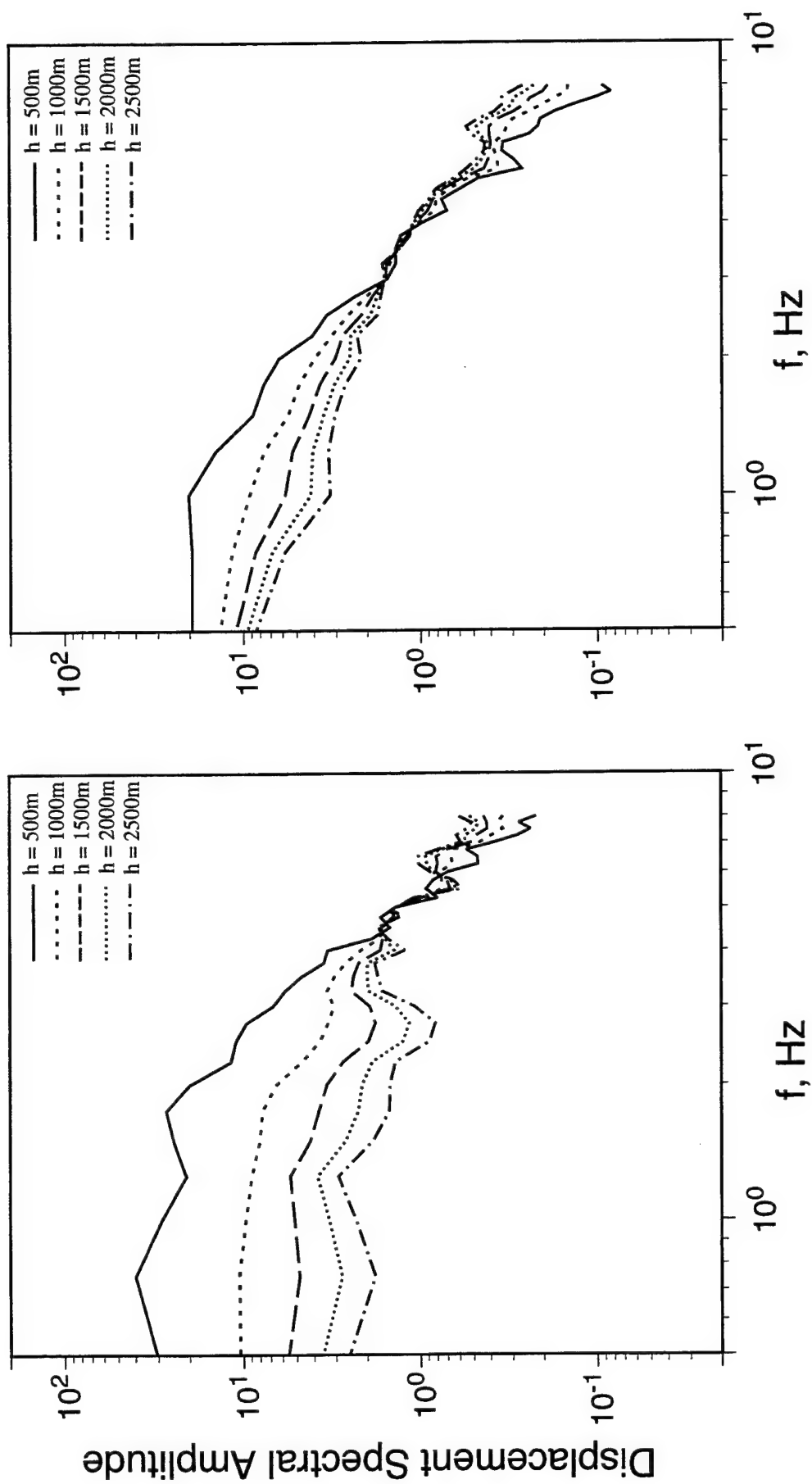


Figure 27. Comparison of predicted spectra as a function of source depth for the  $P_n$  (left) and  $P_g$  (right) regional phases at Borovoye,  $W = 10$  kt.

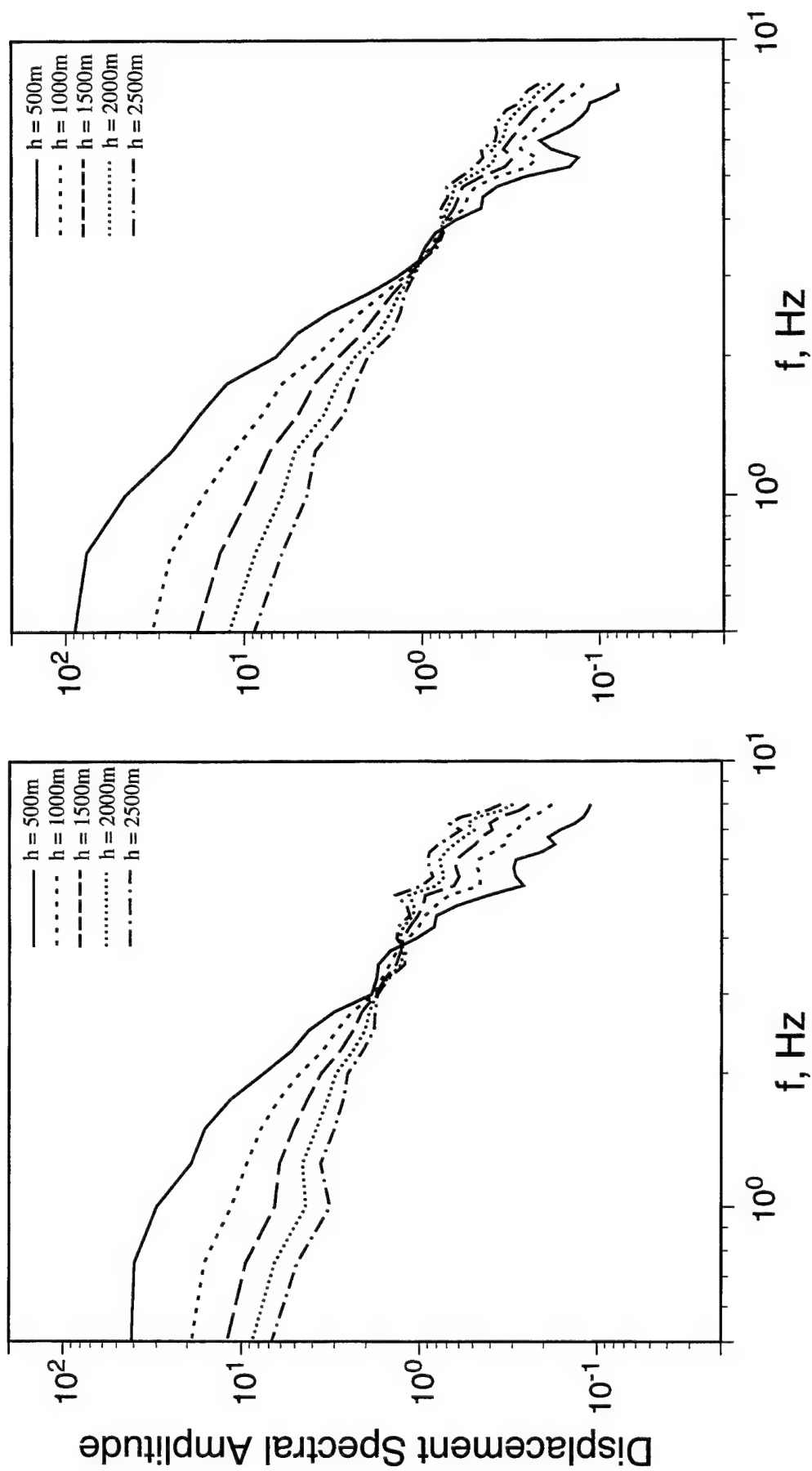


Figure 28. Comparison of predicted spectra as a function of source depth for the  $S_n$  (left) and  $L_g$  (right) regional phases at Borovoye,  $W = 10$  kt.

in Figures 29 and 30 which show the  $L_g$  to P ( $P_n$  and  $P_g$ ) and  $S_n$  to P spectral ratios, respectively, derived from the Borovoye recordings of the 11 PNE events selected for initial analysis. It can be seen that, although there is considerable scatter in the data, all of the spectral ratios trend to average values of about 1 or less at high frequency ( $> 4$  Hz), consistent with previous observations for explosion sources. Note from both Figures 29 and 30 that the spectral ratios computed with respect to the  $P_g$  phase show much less scatter than those computed with respect to the  $P_n$  phase, in agreement with the differences in inferred depth dependence shown in Figure 27. However, it is also evident that these  $P_g$  ratios show significantly less frequency dependence than the corresponding  $P_n$  ratios. Thus, although the ratios computed with respect to  $P_g$  may be more stable, they may also be less diagnostic for discrimination purposes.

The corresponding ratios predicted by the statistical scaling laws over the depth range from 500 to 2500 m for the sample average yield of 10 kt are shown in Figures 31 and 32. These sample average spectral ratios confirm the above observation that the  $L_g$  and  $S_n$  ratios computed with respect to  $P_g$  show less frequency dependence than the corresponding ratios computed with respect to the  $P_n$  phase. Thus, for example, the predicted  $S_n/P_g$  spectral ratios shown in Figure 32 are essentially independent of frequency over the entire band extending from 0.5 to 8.0 Hz. In all cases, the deeper events are predicted to have the largest high frequency spectral ratio levels, indicating that they would be the most difficult to identify using regional phase spectral ratio discriminants. It is also evident in comparing the predicted spectral ratios of Figures 31 and 32 with the corresponding observed spectral ratios of Figures 29 and 30 that, although the predicted ratios reproduce the average frequency dependencies of the observed ratios remarkably well, the observed data show considerably more variability than do the predictions. That is, the predicted variations with source depth at a fixed average yield can not fully account for all the observed variability, which indicates that other, unaccounted for variables, such as source medium and propagation path, are having an influence on the observed regional phase spectral ratios which are most commonly used for discrimination purposes. However, these preliminary results are encouraging and suggest that it should be

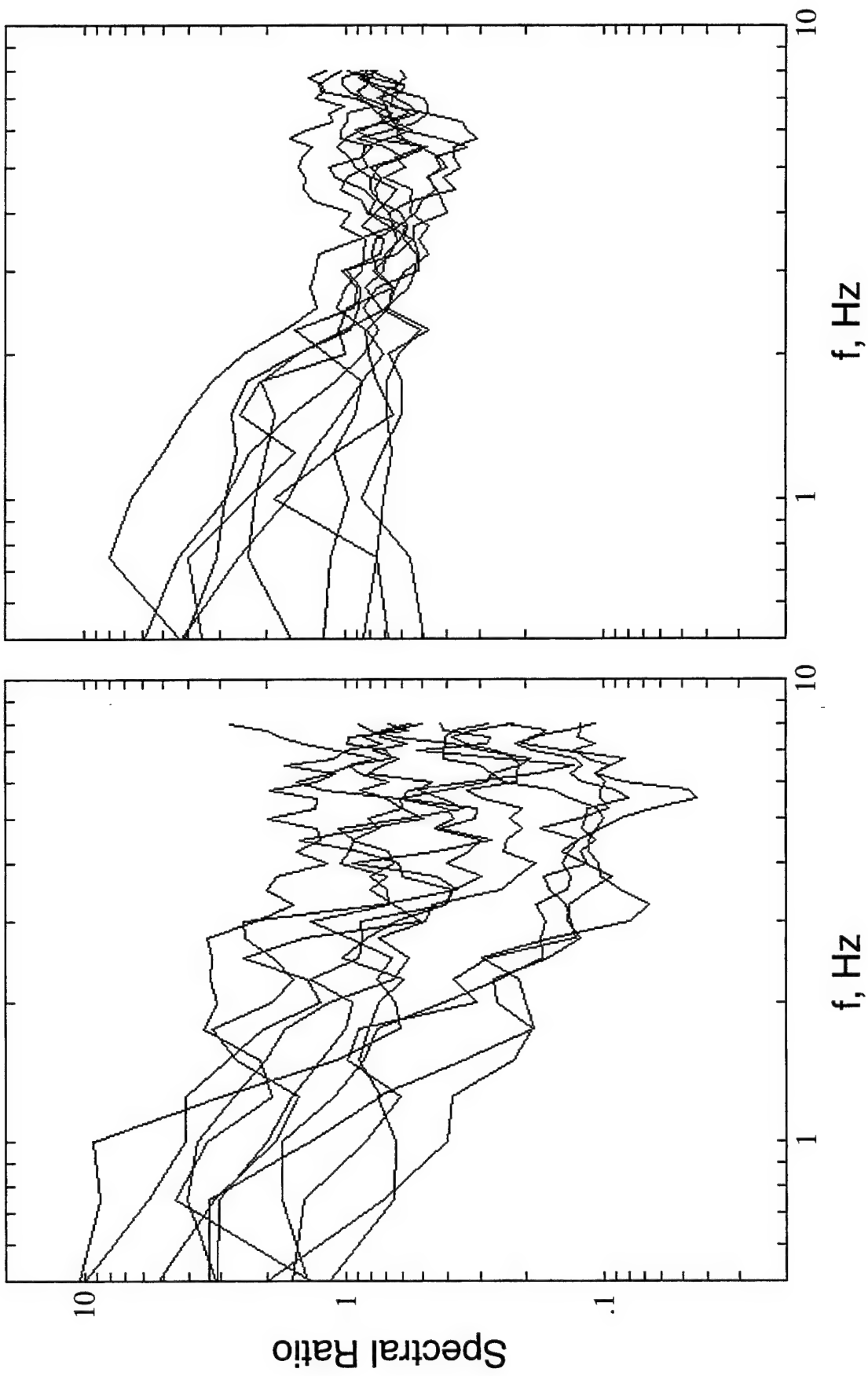


Figure 29. Observed Borovoye  $L_g$  spectral ratios with respect to  $P_n$  (left) and  $P_g$  (right).

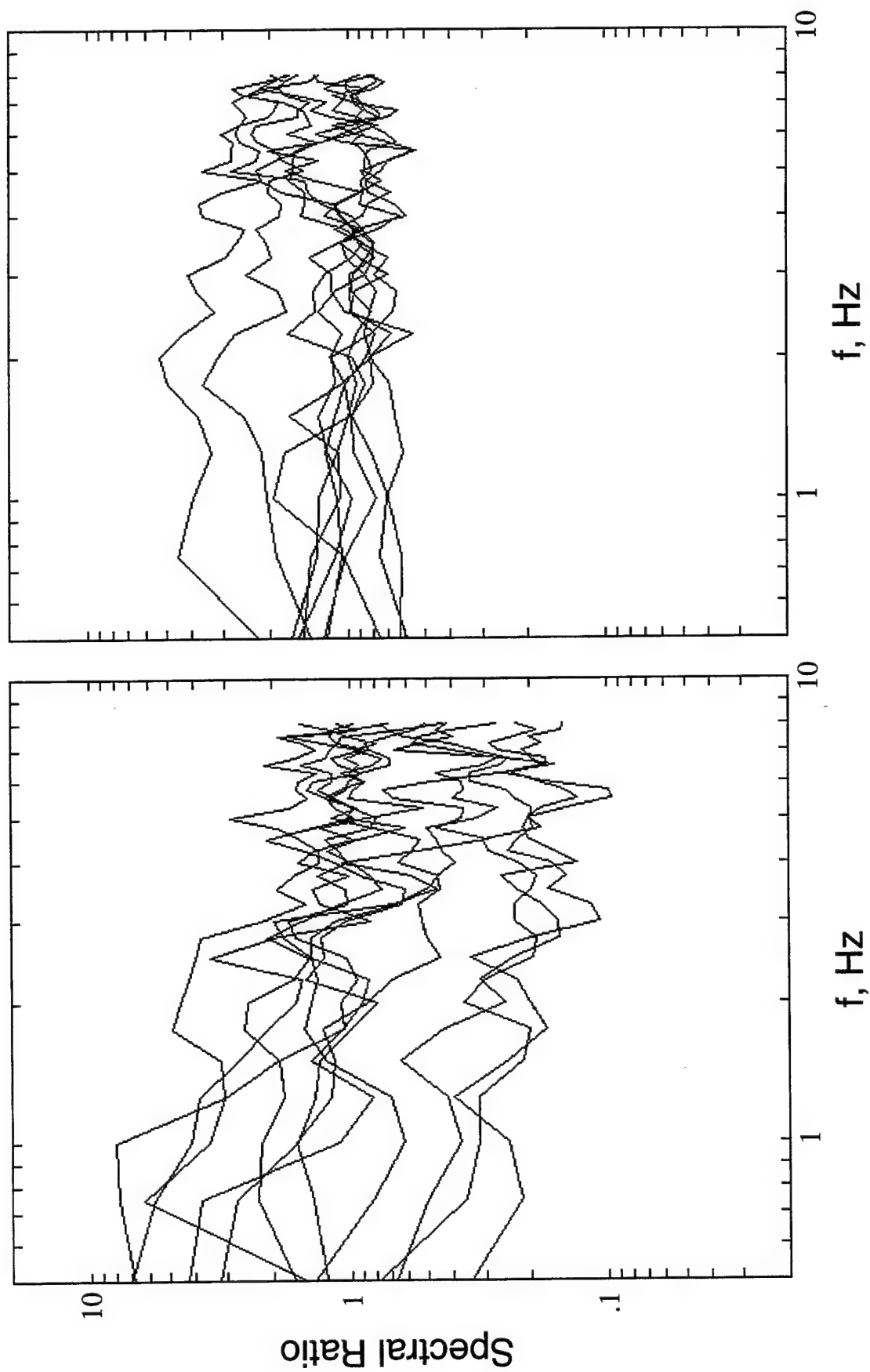


Figure 30. Observed Borovoye  $S_n$  spectral ratios with respect to  $P_n$  (left) and  $P_g$  (right).

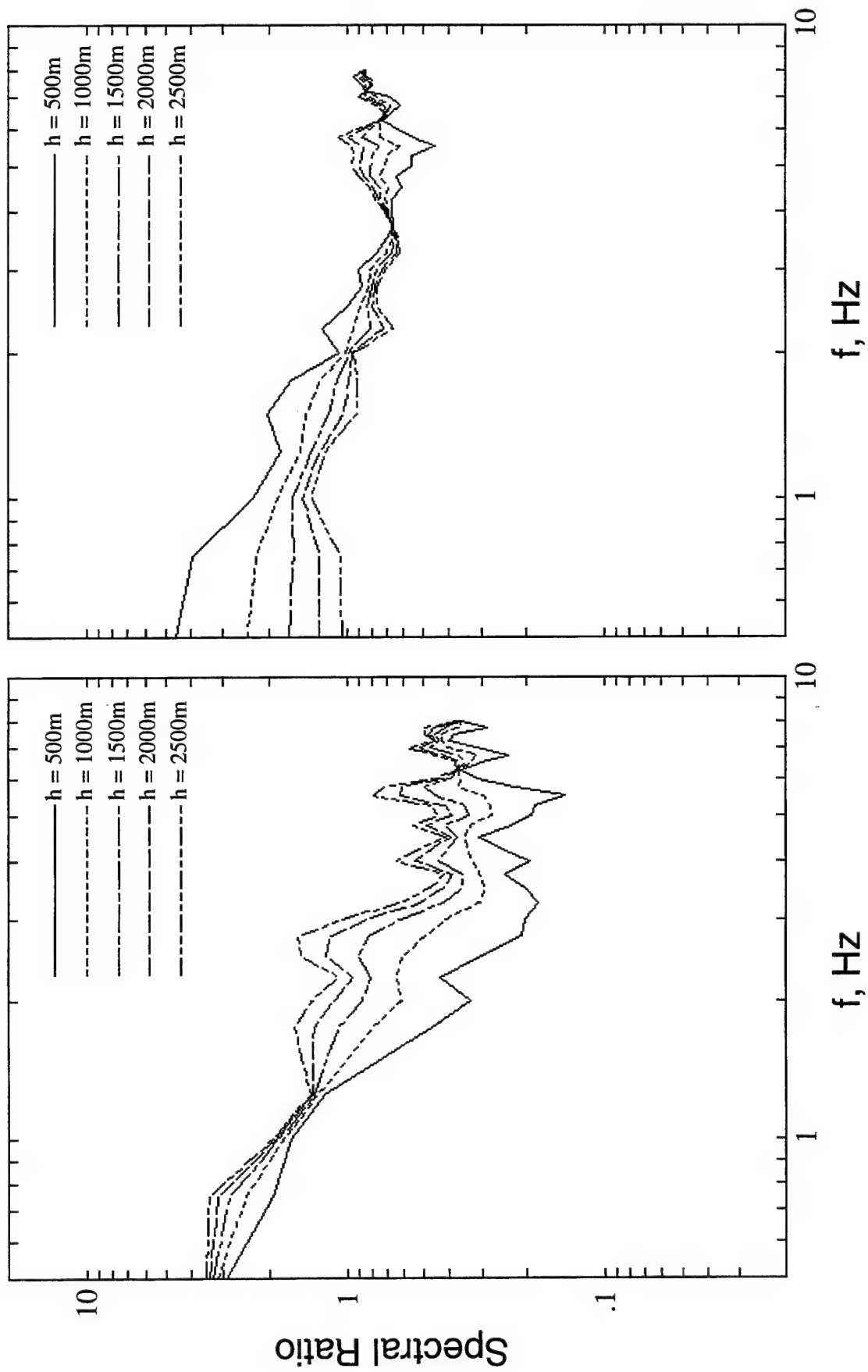


Figure 31. Predicted Borovoye  $L_g$  spectral ratios as functions of source depth computed with respect to  $P_n$  (left) and  $P_g$  (right).

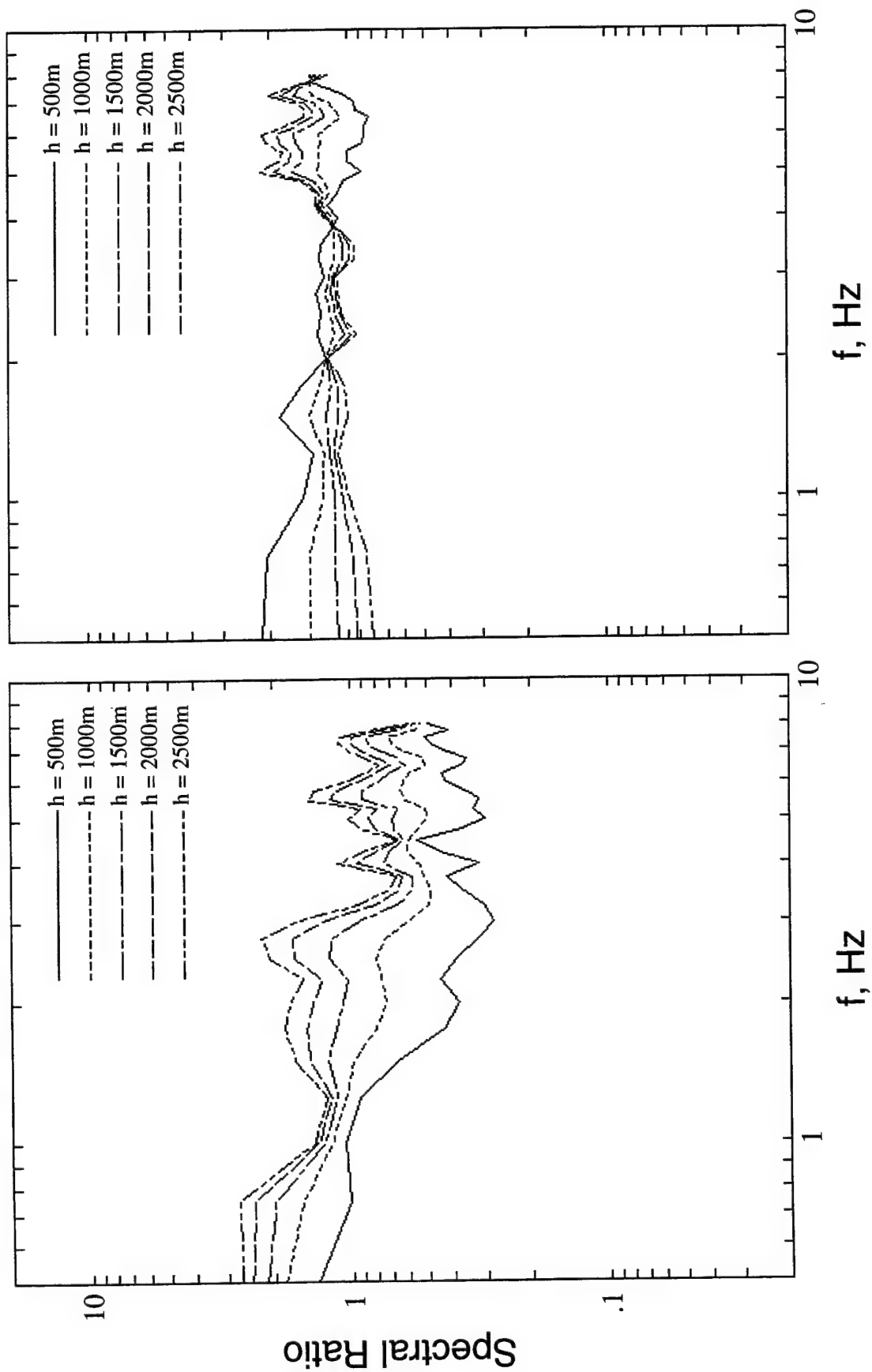


Figure 32. Predicted Borovoye  $S_n$  spectral ratios as functions of source depth computed with respect to  $P_n$  (left) and  $P_g$  (right).

possible to separate and quantify the effects of all the important variables, and then use the results to derive improved bounds on the transportability of various regional discriminants.

## **4. SUMMARY AND CONCLUSIONS**

### **4.1 Summary**

This report has provided an overview of the initial results of an on-going research program in which scientists from Maxwell Technologies, Inc. and the Russian Institute for Dynamics of the Geospheres (IDG) are working together in an attempt to derive improved, quantitative constraints on the transportability of various regional seismic discriminants as they apply to the identification of underground nuclear explosions under the CTBT. In particular, regional seismic data recorded at the Borovoye Geophysical Observatory in Central Asia from selected Soviet PNE tests have been collected and analyzed in order to better define the ranges of seismic signal characteristics which could be expected from underground nuclear explosions which might be conducted under the wide variety of source and propagation path conditions which must be considered in global test monitoring.

The characteristics of the 46 selected Soviet PNE tests were described in Section 2, where the regional seismic data recorded at the Borovoye station were also reviewed and analyzed. It was noted there that these explosions encompass wide ranges in source medium (argillite, clay, dolomite, sandstone, limestone and salt), yield (2.1-103 kt) and source depth (131-2859 m) and, therefore, that they can provide valuable insight into the effects of explosion source conditions on seismic discrimination capability. Waveform data from a selected subset of these explosions located in a narrow distance band extending from 7.2 to 11 degrees from the Borovoye station were also analyzed in some detail and it was demonstrated that they show some significant and consistent dependencies on both source conditions and source to station azimuth, confirming the

fact that both source and propagation path variability can strongly affect the regional seismic signal characteristics of underground nuclear explosions.

The spectral characteristics of the selected subsample of Borovoye data were analyzed in Section 3 where these data were bandpass filtered through a Gaussian comb of filters spaced at intervals of 0.25 Hz between 0.5 and 10 Hz. These filter outputs were then used to estimate the spectral composition of the recorded signals in group velocity time windows corresponding to six different regional phases (i.e.,  $P_n$ ,  $P_{coda}$ ,  $P_g$ ,  $S_n$ ,  $L_g$ ,  $L_{gcoda}$ ), and these spectral data were then statistically analyzed to define their functional dependencies on source yield and depth and to evaluate the implications of these inferred dependencies for the transportability of some proposed regional discriminants.

## 4.2 Conclusions

The research summarized above supports the following preliminary conclusions regarding the variability of regional seismic signals observed at the Borovoye station from Soviet PNE tests.

- 1) The observed broadband excitation levels of the different regional phases observed at the Borovoye station from Soviet PNE events show complex dependencies on epicentral distance and source to station azimuth. Such variability will have to be explicitly accounted for in calibrating regional stations for use in seismic monitoring.
- 2) Even for PNE events at a nearly constant distance from the Borovoye station, the observed, broadband regional seismic signal amplitudes show order of magnitude variability as functions of source and propagation path differences between the events.
- 3) Multivariate statistical analysis of the spectral amplitude data determined from the Borovoye recordings of the 11 selected PNE

events for the regional phases  $P_n$ ,  $P_{\text{coda}}$ ,  $P_g$ ,  $S_n$  and  $L_g$  indicate that they all show very similar dependencies on yield and source depth. This observation is consistent with the hypothesis that, to first order, all of these phases are produced from a single explosion P wave source function through linear conversion processes.

- 4) The inferred frequency dependencies of the observed Borovoye regional phase amplitude spectra on explosion yield and depth are generally consistent with the predictions of the Mueller/Murphy source model in that the depth scaling exponents change from negative to positive values with increasing frequency. However, the estimated degree of dependence of the observed low frequency amplitude level on source depth is somewhat greater than predicted and this apparent discrepancy merits further investigation.
- 5) Comparisons of the observed Borovoye regional phase spectra with corresponding spectra predicted using the statistically derived scaling laws indicate that the effects of other variables, such as source medium and propagation path, may be of second order importance with respect to those associated with explosion yield and depth of burial, at least over the ranges of those variables represented in the analyzed sample of PNE events. Data recorded over a wider variety of propagation paths will have to be analyzed in order to accurately bound the effects of these other variables on the spectral characteristics of the regional seismic phases produced by underground nuclear explosions.
- 6) Although the data show considerable scatter, the  $L_g/P$  and  $S_n/P$  spectral ratios determined from the observed Borovoye PNE data generally decline to average values of 1 or less at frequencies above about 4 Hz and, therefore, are typically explosion-like at high frequencies. Explosions with large depths of burial are found to pose the greatest challenges for the spectral ratio discriminants.

- 7) The preliminary Borovoye regional phase spectral analysis results are encouraging and suggest that it should be possible to separate and quantify the effects of all the variables which have an important influence on the transportability of regional discriminants applicable to underground nuclear explosion data.

## REFERENCES

- Adushkin, V. V. and V. A. An (1990), "Seismic Observations and Monitoring of Underground Nuclear Explosions at Borovoye Geophysical Observatory," *Izv. Acad. Sci. USSR, Phys. Solid Earth*, No. 12, 1023-1031.
- Barker, T. G., S. M. Day, K. L. McLaughlin, B. Shkoller, and J. L. Stevens (1990), "An Analysis of the Effects of Spall on Regional and Teleseismic Waveforms Using Two-Dimensional Numerical Modeling of Underground Explosions," GL-TR-90-0126, ADA226921.
- Baumgardt, D. R. (1990), "Investigation of Teleseismic  $L_g$  Blockage and Scattering Using Regional Arrays," *Bull. Seism. Soc. Am.*, 80, pp. 2261-2281.
- Bennett, T. J. and J. R. Murphy (1986), "Analysis of Seismic Discrimination Capabilities Using Regional Data From Western U.S. Events," *Bull. Seism. Soc. Am.*, 76, 1069-1086.
- Bennett, T. J., J. R. Murphy, M. E. Marshall and B. W. Barker (1993), "A Preliminary Regional Seismic Discrimination Analysis of the Novaya Zemlya Event of December 31, 1992," in *The Novaya Zemlya Event of 31 December 1992 and Seismic Identification Issues*, edited by A. S. Ryall, 15th Annual Seismic Research Symposium, PL-TR-93-2160, ADA271458.
- Blandford, R. and P. Klouda (1980), "Magnitude-Yield Results at the Tonto Forest Observatory," in *Studies of Seismic Wave Characteristics at Regional Distances*, Teledyne-Geotech Report AL-80-1, Teledyne-Geotech, Alexandria, Virginia.
- Blandford, R. R. (1981), "Seismic Discrimination Problems at Regional Distances, in *Identification of Seismic Sources - Earthquake or*

- Underground Explosion*, D. Reidel Publishing Company, Boston, Massachusetts.
- Chael, E. P. (1988), "Spectral Discrimination of NTS Explosions and Earthquakes in the Southwestern United States Using High-Frequency Regional Data," *Geophys. Res. Lett.*, 15, pp. 625-628.
- Kim, W-Y and G. Ekström (1996), "Instrument Responses of Digital Seismographs at Borovoye, Kazakhstan, by Inversion of Transient Calibration Pulses," *Bull. Seism. Soc. Am.*, 86, 191.
- Laushkin, V. A., S. I. Oreshin and V. M. Ovtchinnikov (1995), "Regional Analysis of Former Soviet Union Peaceful Nuclear Explosions Recorded in the Former Soviet Union," EOARD Report SPC-94-4065.
- McLaughlin, K. L., J. L. Stevens, T. G. Barker, S. M. Day, and B. Shkoller (1993), "2D and 3D Numerical Modeling of Seismic Waves from Explosion Sources," in *Proceedings of the Numerical Modeling for Underground Nuclear Test Monitoring Symposium*, Editors: S. R. Taylor, and J. R. Kamm, LANL Report LA-UR-93-3839.
- Mueller, R. A. and J. R. Murphy (1971), "Seismic Characteristics of Underground Nuclear Detonations. Part I. Seismic Spectrum Scaling," *Bull. Seism. Soc. Am.*, 61, 1975.
- Murphy, J. R. (1977), "Seismic Source Functions and Magnitude Determinations for Underground Nuclear Detonations," *Bull. Seism. Soc. Am.*, 67, 135-158.
- Murphy, J. R. and T. J. Bennett (1982), "A Discrimination Analysis of Short-Period Regional Seismic Data Recorded at Tonto Forest Observatory," *Bull. Seism. Soc. Am.*, 72, pp. 1351-1366.
- Murphy, J. R., B. W. Barker and A. O'Donnell (1989), "Network-Averaged Teleseismic P-Wave Spectra For Underground Explosions. Part I. Definitions and Examples," *Bull. Seism. Soc. Am.*, 79, 141-155.
- Murphy, J. R., I. O. Kitov, N. Rimer, D. D. Sultanov, B. W. Barker, J. L. Stevens, V. V. Adushkin and K. H. Lie (1996), "Further Studies of the Seismic Characteristics of Russian Explosions in Cavities: Implications For Cavity Decoupling of Underground Nuclear Explosions," PL-TR-96-2017, ADA305955.
- Ringdal, F. and B. K. Hokland (1987), "Magnitudes of Large Semipalatinsk Explosions Using P Coda and  $L_g$  Measurements at NORSAR," in *NORSAR Semiannual Technical Summary*, 1 April - 30 September 1987, Rept. 1-87/88.
- Stump, B. W. and R. E. Reinke (1991), "Free-field and Free Surface Ground Motions From Nuclear Explosions, Their Spatial Variations, and the Constraint of the Physical Source Mechanisms," in *Explosion*

- Source Phenomenology, Geophysical Monograph 65, AGU, Washington, DC.*
- Taylor, S. R., N. W. Sherman and M. D. Denny (1988), "Spectral Discrimination Between NTS Explosions and Western United States Earthquakes at Regional Distances," *Bull. Seism. Soc. Am.*, 78, pp. 1563-1579.
- Taylor, S. R. and G. E. Randall (1989), "The Effects of Spall on Regional Seismograms," *Geophys. Res. Lett.*, 16, 211-214.
- Taylor, S. R. and M. D. Denny (1991), "An Analysis of Spectral Differences Between Nevada Test Site and Shagan River Nuclear Explosions," *J. Geophys. Res.*, 96, pp. 6237-6245.



## **Appendix A**

### **Soviet Bulletin Data For Selected PNE Events**

In the following pages, the previously unpublished Soviet bulletin data for the 12 selected PNE events located at distances of 8 and 10.5 degrees from the Borovoye station are presented in chronological order. Only data recorded at stations within 20 degrees of the epicenter are included for purposes of the present regionalization study. In some cases, amplitude values have been reported for multiple phases, but only the P phase data have been included here since that is the only phase which is reported consistently enough to permit comparisons between events. The phase designation  $P_n$  generally denotes the first arriving P wave, while  $P_M$  denotes the maximum amplitude within about 10 seconds of P wave onset. Most frequently, the reported data were recorded on the SKM short-period seismic system.

August 15, 1973

Station	Distance, degrees	Phase	Arrival Time, UT	Az, $\mu$ m	Period, sec
TAS	2.02	PM	02:00:38.2	8.300	1.0
FRG	4.06	PM	02:01:04.8	1.000	1.0
ANR	4.22	PM	02:01:07.6	1.250	1.0
GAR	4.37	Pn	02:01:07.0	1.100	0.7
BRV	10.46	PM	02:02:29.5	0.690	0.8
SVE	14.70	PM	02:03:26.0	0.200	2.0
NVS	15.97	PM	02:03:43.9	0.105	1.1
CUR	16.16	PM	02:03:52.0	0.430	1.0
GRS	16.21	PM	02:03:50.2	0.160	1.2
ELT	16.35	Pn	02:03:46.1	0.160	1.0
BKR	17.71	PM	02:04:07.2	0.460	1.1

September 19, 1973

Station	Distance, degrees	Phase	Arrival Time, UT	Az, $\mu$ m	Period, sec
TAS	4.56	PM	03:01:11.5	0.500	1.2
ANR	6.00	PM	03:01:33.5	0.120	1.3
FRG	6.10	PM	03:01:33.3	0.080	0.4
AAB	7.26	Pn	03:01:45.0	0.050	0.6
NRN	7.34	Pn	03:01:51.0	0.360	0.6
BRV	7.47	PM	03:01:50.3	0.630	0.4
PRZ	8.28	PM	03:02:04.0	0.080	0.5
SVE	11.94	PM	03:02:49.0	0.280	1.0
ELT	14.11	PM	03:03:17.6	0.100	1.0
BKR	18.00	PM	03:04:13.8	0.130	1.0

October 26, 1973

Station	Distance, degrees	Phase	Arrival Time, UT	Az, $\mu$ m	Period, sec
BRV	8.99	Pn	06:02:07.6	0.046	0.8
MIK	10.34	Pn	06:02:28.2	0.069	0.4
OBN	11.01	PM	06:02:34.0	0.110	0.4
BKR	14.23	PM	06:03:30.5	0.040	1.1
TAS	15.46	PM	06:03:44.0	0.100	1.5
ASH	15.77	PM	06:03:42.0	0.200	1.0
NVS	16.39	PM	06:03:51.7	0.087	1.1
ANR	17.24	PM	06:04:02.0	0.100	0.7
ELT	18.41	PM	06:04:13.8	0.040	1.0
PRZ	18.94	PM	06:04:23.0	0.040	1.0

October 17, 1978

Station	Distance, degrees	Phase	Arrival Time, UT	Az, $\mu$ m	Period, sec
SVE	6.55	PM	14:01:	0.320	1.0
ARU	7.23	PM	14:01:	0.900	1.8
BRV	10.78	PM	14:02:	0.077	0.6
NRI	11.64	PM	14:02:	0.500	1.2
NVS	13.12	PM	14:03:	0.150	1.0
APA	13.20	PM	14:03:	0.260	1.2
MOS	15.00	PM	14:03:	0.310	1.5
MIK	15.46	PM	14:03:	0.234	0.9
ELT	15.52	PM	14:03:	0.202	1.0
OBN	15.82	PM	14:03:	0.200	1.0
UER	19.97	PM	14:04:	0.140	0.8

October 4, 1979

Station	Distance, degrees	Phase	Arrival Time, UT	Az, $\mu$ m	Period, sec
SVE	6.83	PM	16:01:41.8	1.500	1.0
ARU	7.97	PM	16:02:01.0	0.500	1.0
ELT	10.97	PM	16:02:34.8	0.459	0.8
UER	15.49	Pn	16:03:37.8	0.112	0.8
APA	17.75	PM	16:04:10.0	0.270	0.7
FRU	17.97	PM	16:04:08.8	0.360	1.6
AAB	18.04	PM	16:04:11.0	0.260	1.7
MOY	18.59	PM	16:04:18.0	0.110	1.6
PRZ	18.70	PM	16:04:21.7	0.360	0.8
OBN	19.15	PM	16:04:29.0	0.390	0.8
TAS	19.42	PM	16:04:31.0	0.450	2.0
NRN	19.47	PM	16:04:34.4	0.300	1.6
IRK	19.81	PM	16:04:34.7	0.197	1.4

December 10, 1980

Station	Distance, degrees	Phase	Arrival Time, UT	Az, $\mu$ m	Period, sec
BRV	8.95	Pn	07:02:05.4	0.050	0.8
ELT	13.37	PM	07:03:20.0	0.050	1.1
MIK	16.71	Pn	07:03:48.4	0.047	0.4
UER	17.90	PM	07:04:08.1	0.020	1.4
KHE	19.07	PM	07:04:26.5	0.100	1.7
AAB	19.78	PM	07:04:30.9	0.043	1.0

September 2, 1981

Station	Distance, degrees	Phase	Arrival Time, UT	Az, $\mu$ m	Period, sec
MIK	11.45	Pn	04:02:44.0	0.044	0.3
NVS	15.19	Pn	04:03:37.4	0.008	1.2

July 21, 1984

Station	Distance, degrees	Phase	Arrival Time, UT	Az, $\mu$ m	Period, sec
SVE	6.95	PM	03:01:42.0	0.960	0.5
MIK	10.01	PM	03:02:23.0	0.648	0.4
PYA	10.07	PM	03:02:22.0	0.250	1.0
MOS	10.31	PM	03:02:27.0	1.500	1.2
BRV	10.54	PM	03:02:29.2	0.300	1.1
OBV	10.71	PM	03:02:34.0	0.840	0.8
AKH	12.04	PM	03:02:50.4	0.100	0.6
ANN	12.50	PM	03:02:55.0	0.180	0.9
GRS	12.82	PM	03:03:01.0	0.280	1.0
TAS	14.88	PM	03:03:28.0	0.200	1.0
PUL	15.43	PM	03:03:35.0	0.180	0.8
FRU	16.78	PM	03:03:55.2	0.470	1.2
FRG	16.85	PM	03:03:59.7	0.270	0.8
ANR	16.89	PM	03:03:57.6	0.200	1.2
SEM	16.99	PM	03:03:54.8	0.120	0.9
AAB	18.20	PM	03:04:12.0	0.130	0.9
NVS	18.26	PM	03:04:16.7	0.132	1.2
APA	18.99	PM	03:04:28.5	0.110	0.6

August 25, 1984

Station	Distance, degrees	Phase	Arrival Time, UT	Az, $\mu$ m	Period, sec
SVE	7.78	PM	19:01:56.1	0.240	0.8
NVS	9.12	PM	19:02:12.0	0.960	0.6
NRI	9.97	PM	19:02:21.2	0.140	1.4
ELT	11.48	PM	19:02:43.6	0.433	1.0
UER	15.77	PM	19:03:55.8	0.200	1.3
APA	17.28	PM	19:04:05.0	0.280	0.7
MOY	18.64	PM	19:04:29.2	0.210	1.8
MOS	18.74	PM	19:04:23.0	0.410	1.6
FRU	19.14	PM	19:04:28.0	0.350	1.2
AAB	19.16	PM	19:04:26.2	0.158	1.2

June 18, 1985

Station	Distance, degrees	Phase	Arrival Time, UT	Az, $\mu$ m	Period, sec
USK	11.55	Pn	04:02:48.0	0.006	0.5
OBN	19.67	Pn	04:04:32.0	0.022	0.8

April 19, 1987

Station	Distance, degrees	Phase	Arrival Time, UT	Az, $\mu$ m	Period, sec
SVE	3.97	PM	04:06:03.0	0.040	1.1
BRV	10.22	Pn	04:07:25.2	0.015	0.3
MIK	11.76	Pn	04:07:44.0	0.035	0.3
NRI	15.07	PM	04:08:47.0	0.015	1.2

October 3, 1987

Station	Distance, degrees	Phase	Arrival Time, UT	Az, $\mu$ m	Period, sec
SVE	9.63	PM	15:17:20.0	0.220	1.1
KRV	9.90	PM	15:17:23.0	0.200	0.8
PYA	9.92	PM	15:17:24.5	0.100	1.0
BRV	10.46	PM	15:17:31.0	0.201	0.7
BKR	10.83	PM	15:17:37.5	0.050	1.0
GRS	10.84	PM	15:17:37.0	0.140	0.6
TAS	11.17	PM	15:17:40.0	0.230	1.0
GAR	13.29	PM	15:18:09.4	0.180	1.0
FRU	13.73	PM	15:18:26.0	0.090	0.4
MIK	13.74	PM	15:18:10.8	0.105	0.5
KUL	13.81	PM	15:18:16.9	0.300	1.2
OBN	14.44	PM	15:18:22.0	0.114	0.5
KHO	15.06	PM	15:18:35.2	0.080	1.2
AAB	15.29	PM	15:18:43.9	0.230	1.2
PRZ	16.41	PM	15:18:50.0	0.080	0.9
NVS	18.29	PM	15:19:13.0	0.056	1.4
USK	18.81	PM	15:19:22.5	0.092	0.6
ELT	19.81	PM	15:19:29.8	0.067	1.2



## **Appendix B**

### **Borovoye Regional Phase Spectra**

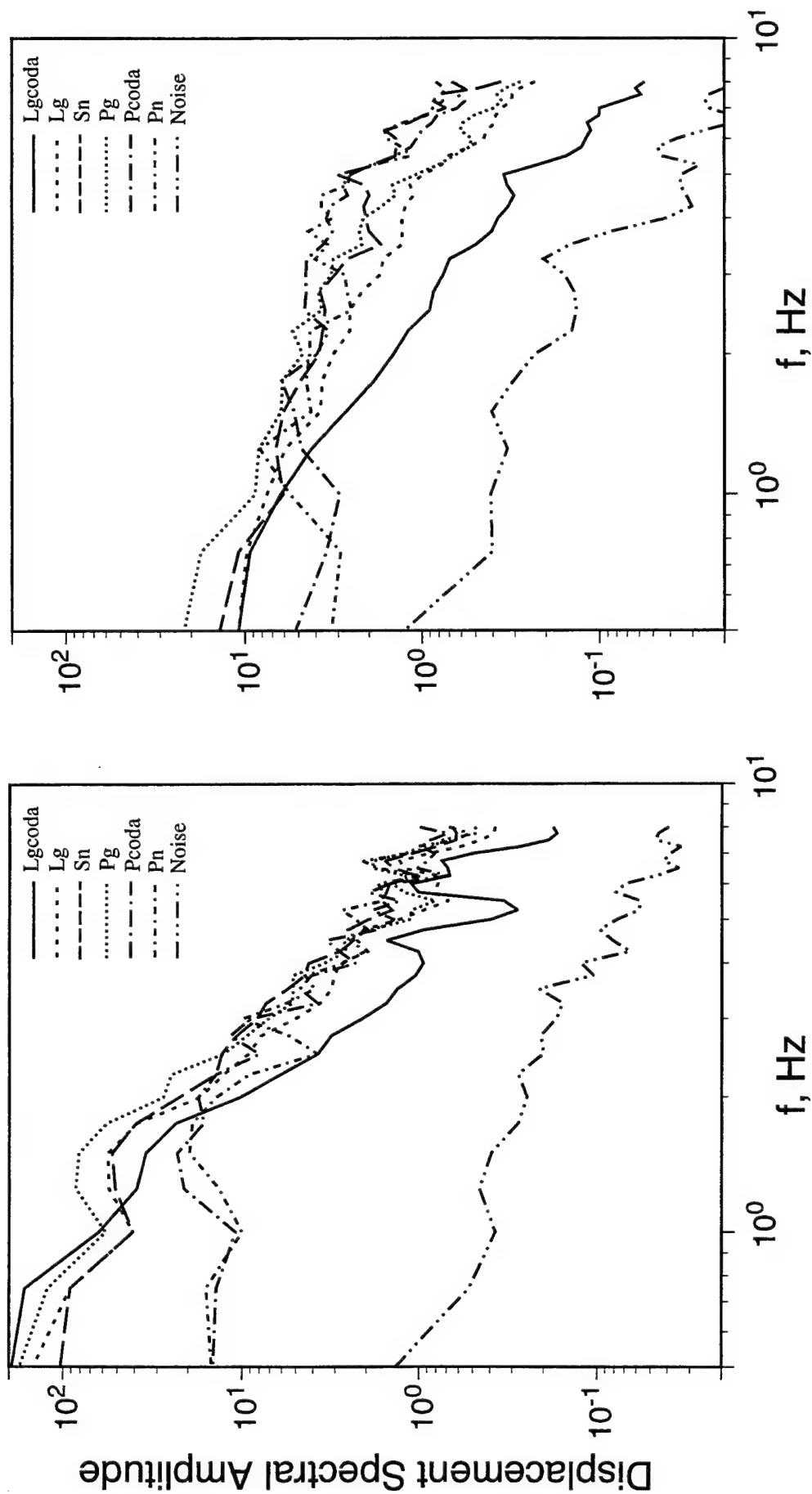


Figure B-1. Borovoye regional phase spectra corresponding to the 10/04/79 (left) and 12/10/80 (right) PNE events from the 8° distance group.

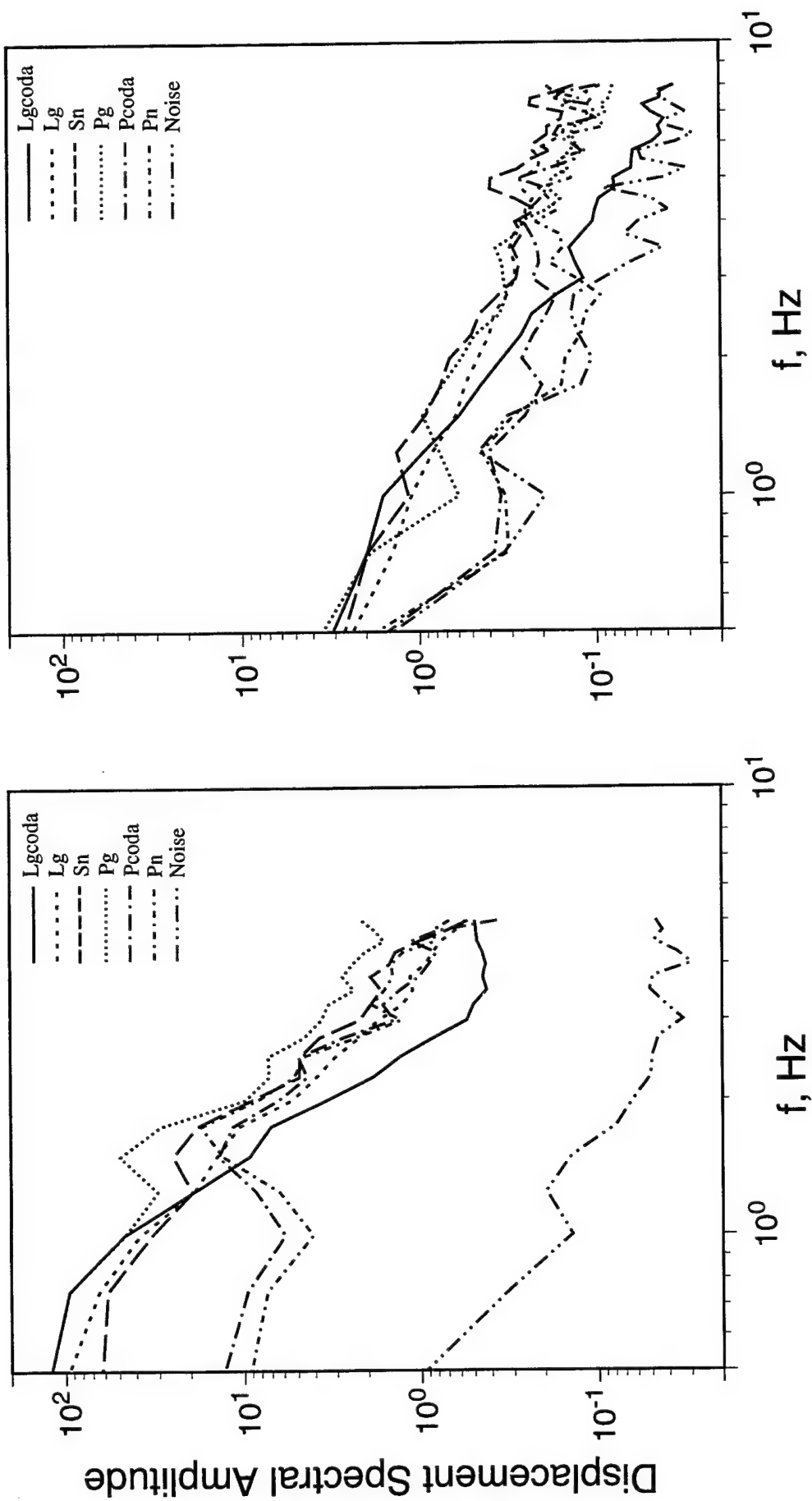


Figure B-2. Borovoye regional phase spectra corresponding to the 8/25/84 (left) and 6/18/85 (right) PNE events from the 8° distance group.

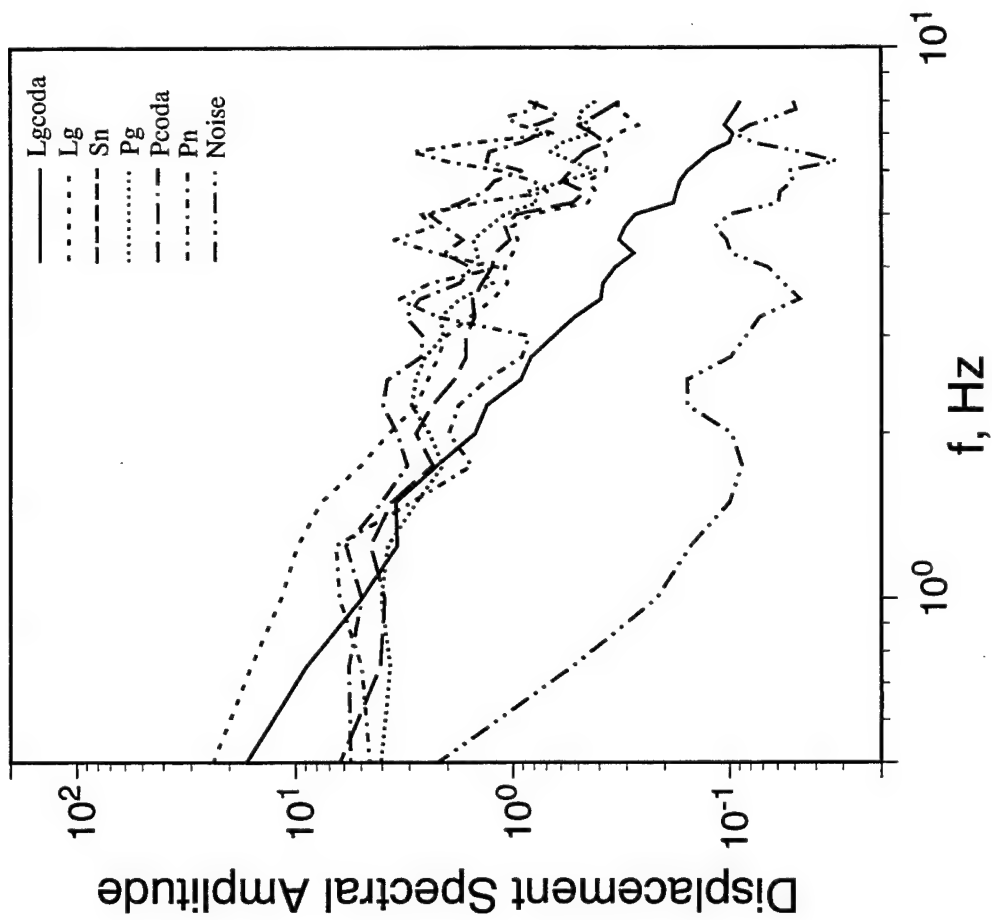


Figure B-3. Borovoye regional phase spectra corresponding to the 10/26/73 PNE event from the 8° distance group.

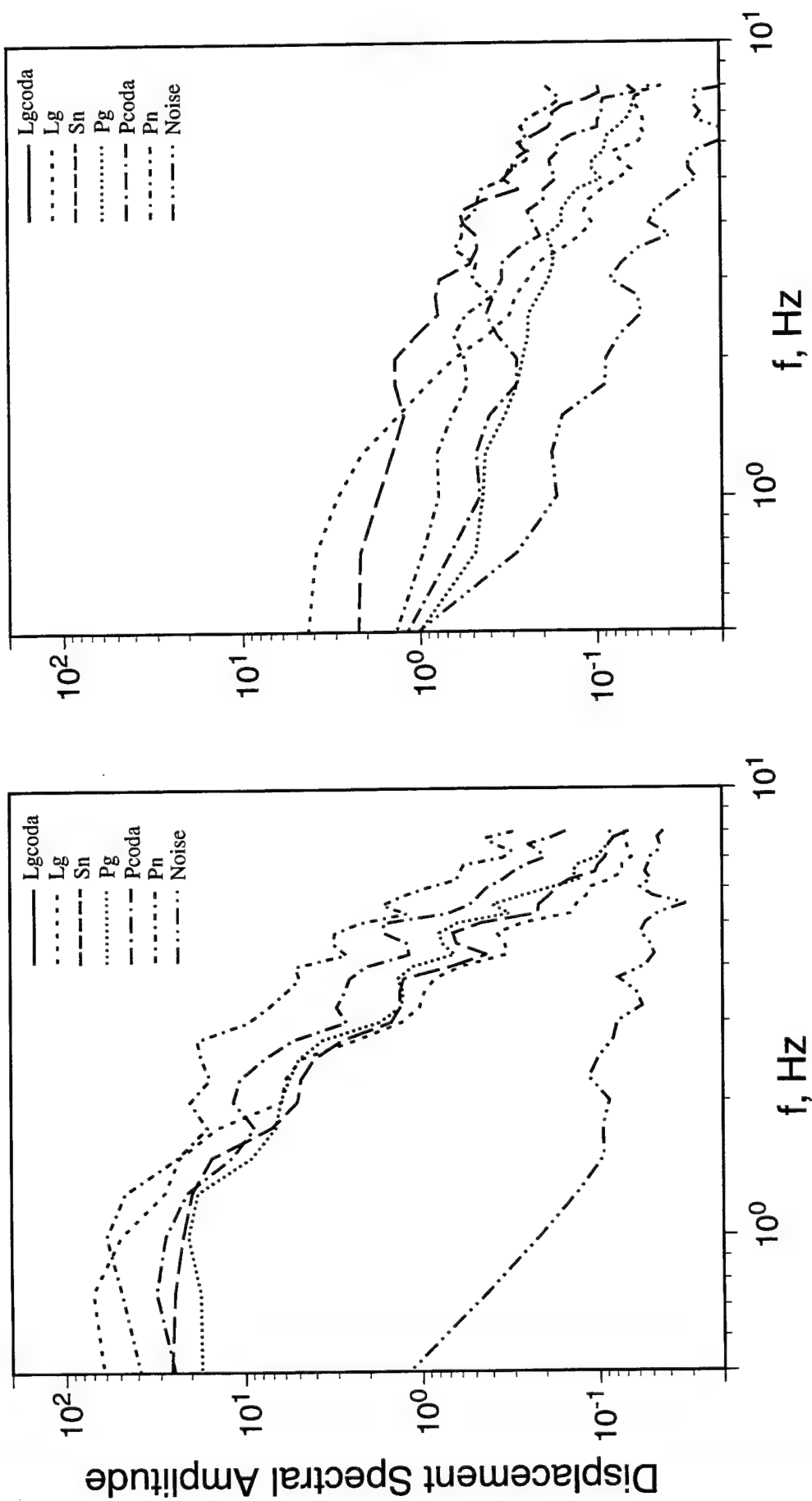


Figure B-4. Borovoye regional phase spectra corresponding to the 8/15/73 (left) and 9/02/81 (right) PNE events from the  $10.5^\circ$  distance group.

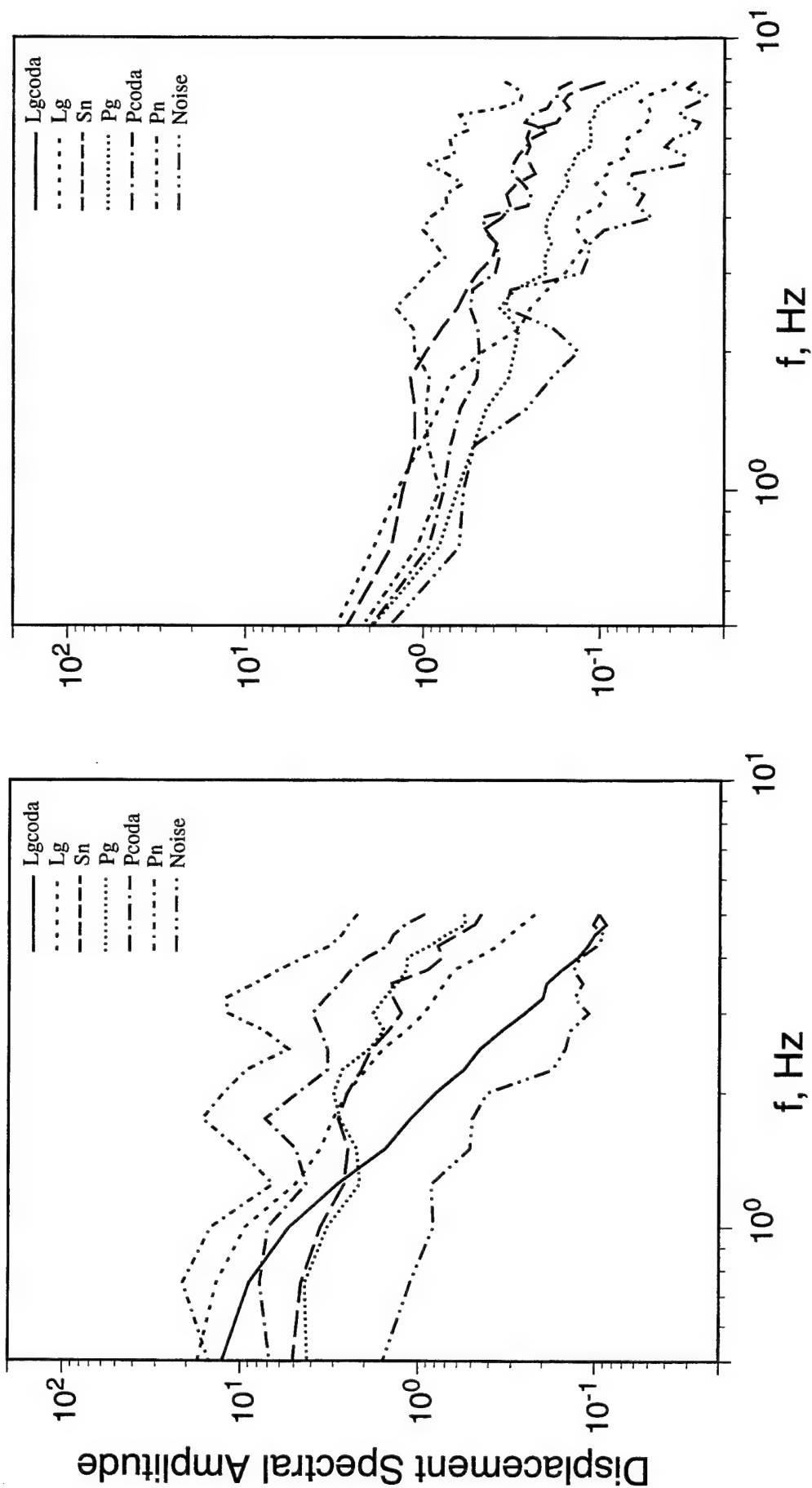


Figure B-5. Borovoye regional phase spectra corresponding to the 10/03/87 (left) and 4/19/87 (right) PNE events from the 10.5° distance group.

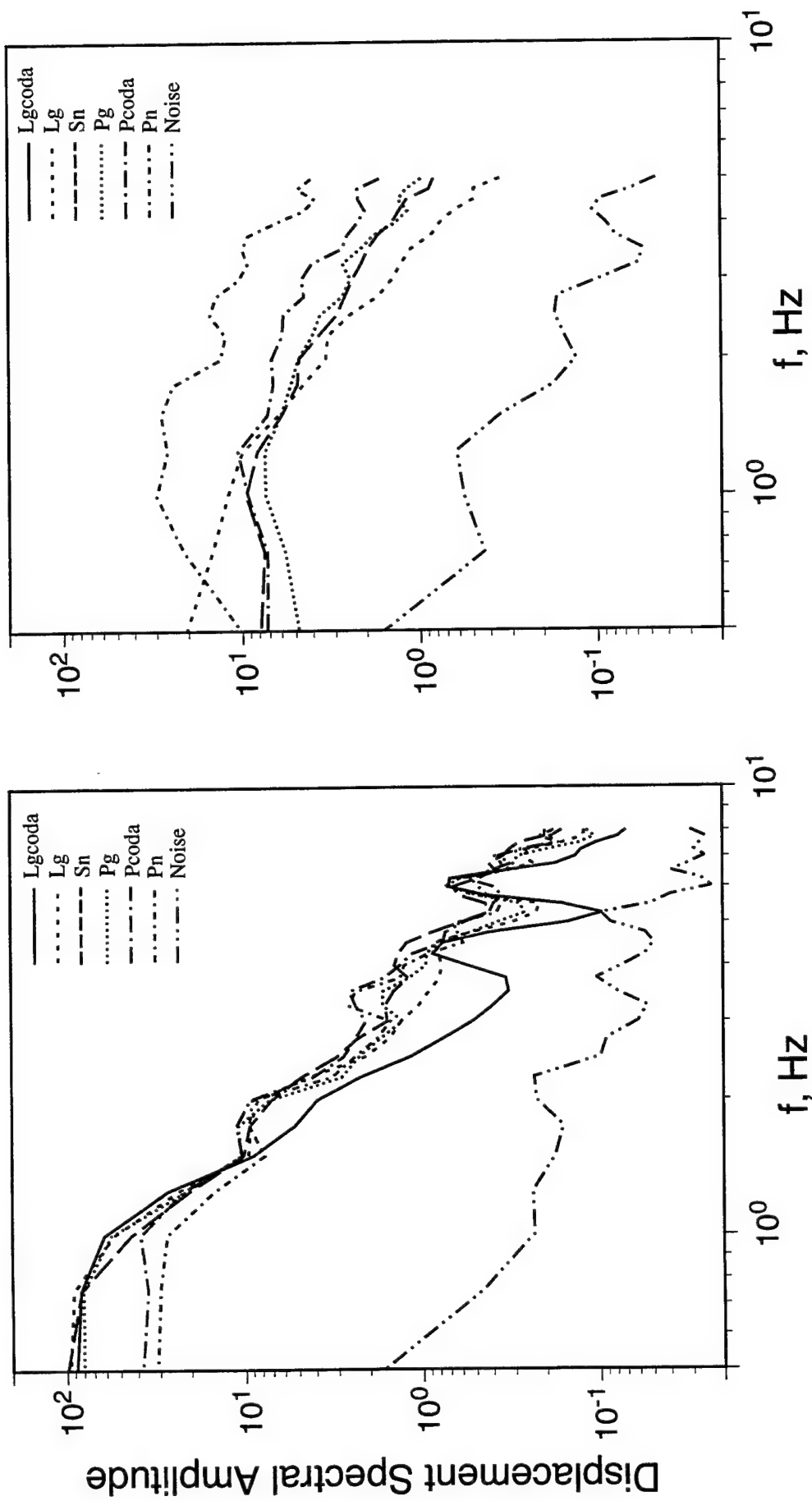


Figure B-6. Borovoye regional phase spectra corresponding to the 10/17/78 (left) and 7/21/84 (right) PNE events from the 10.5° distance group.

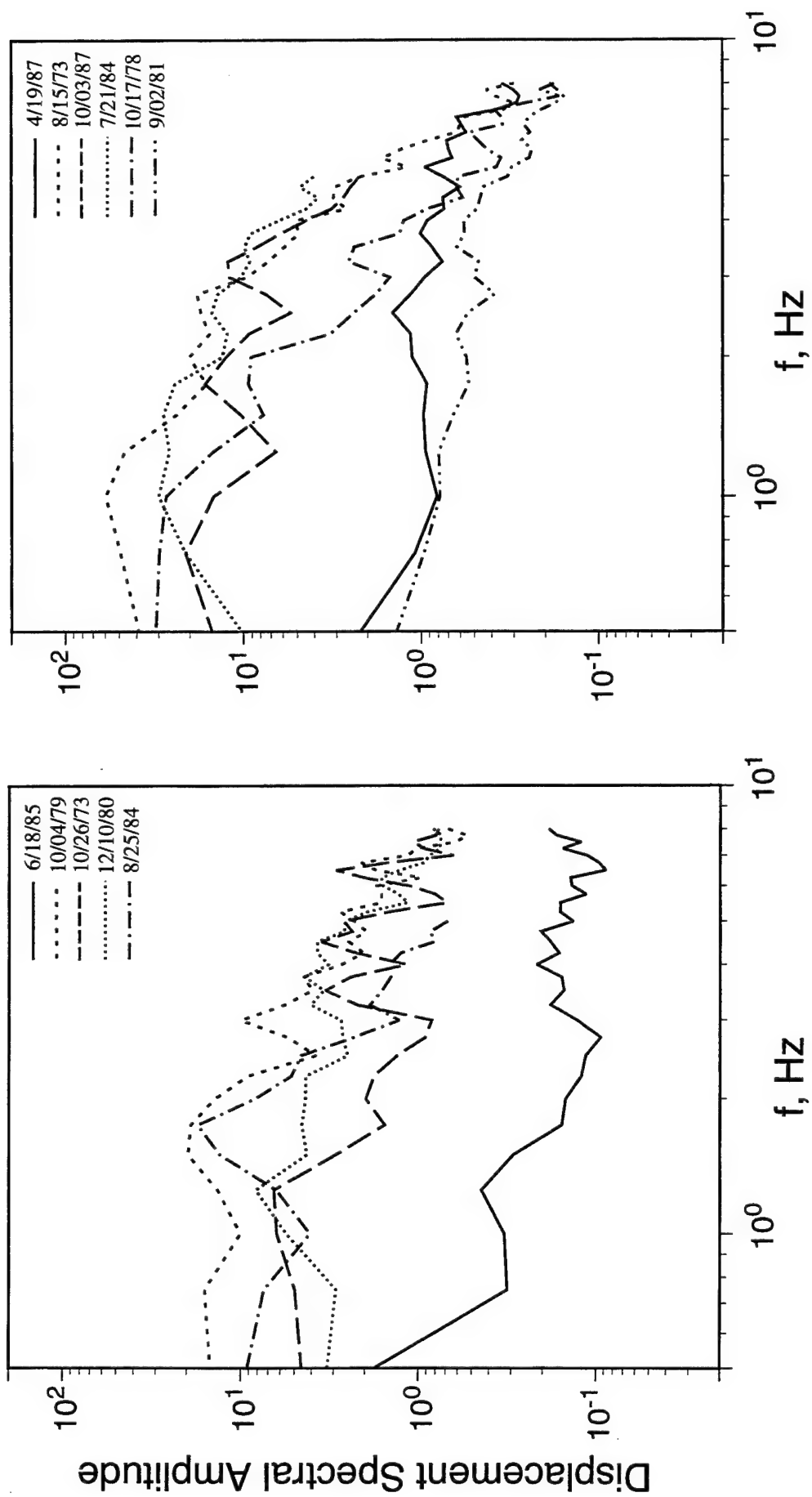


Figure B-7. Comparison of Borovoye  $P_n$  spectra for selected PNE events in the 8° (left) and 10.5° (right) distance groups.

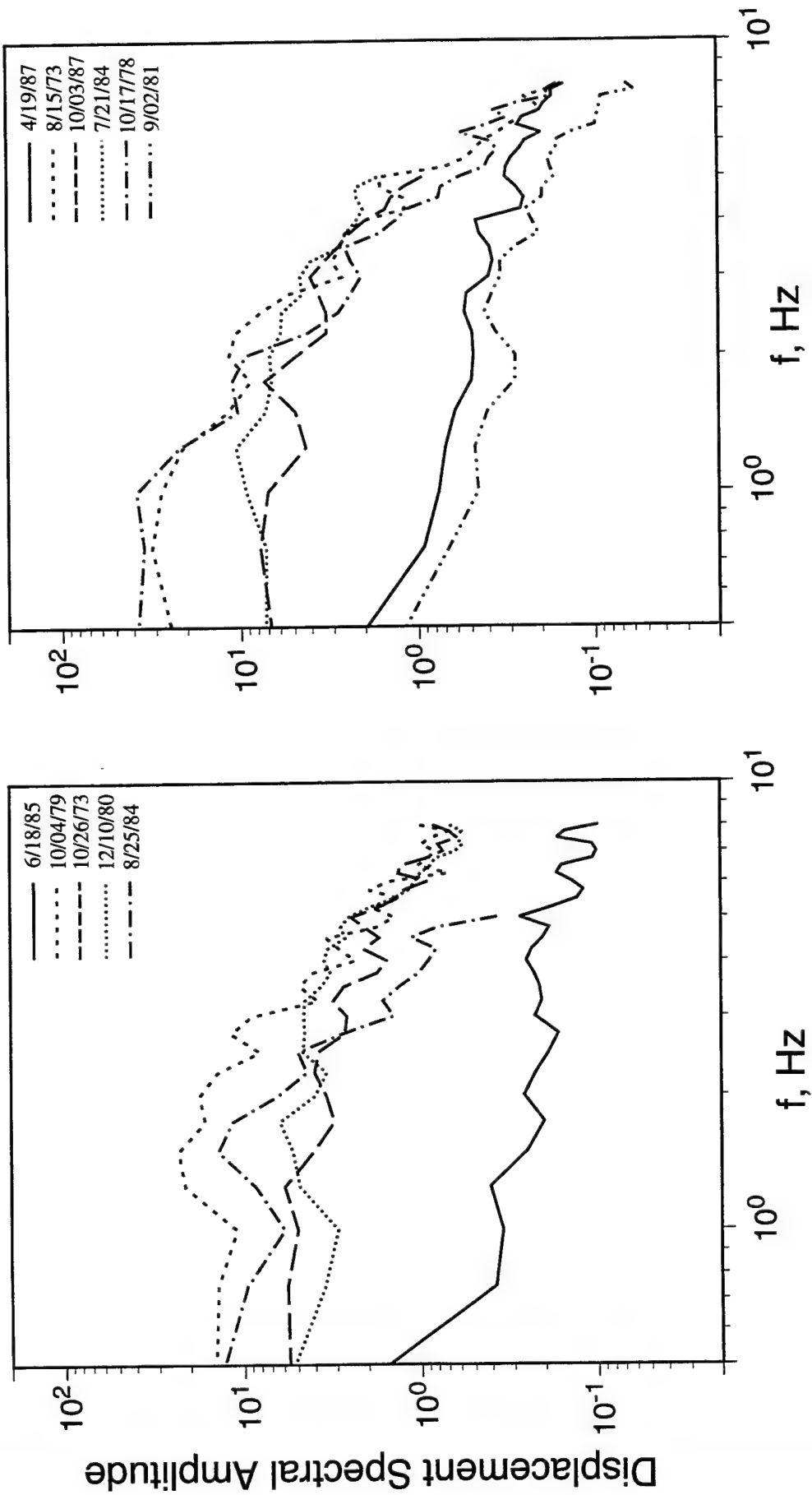


Figure B-8. Comparison of Borovoye  $P_{\text{coda}}$  spectra for selected PNE events in the  $8^\circ$  (left) and  $10.5^\circ$  (right) distance groups.

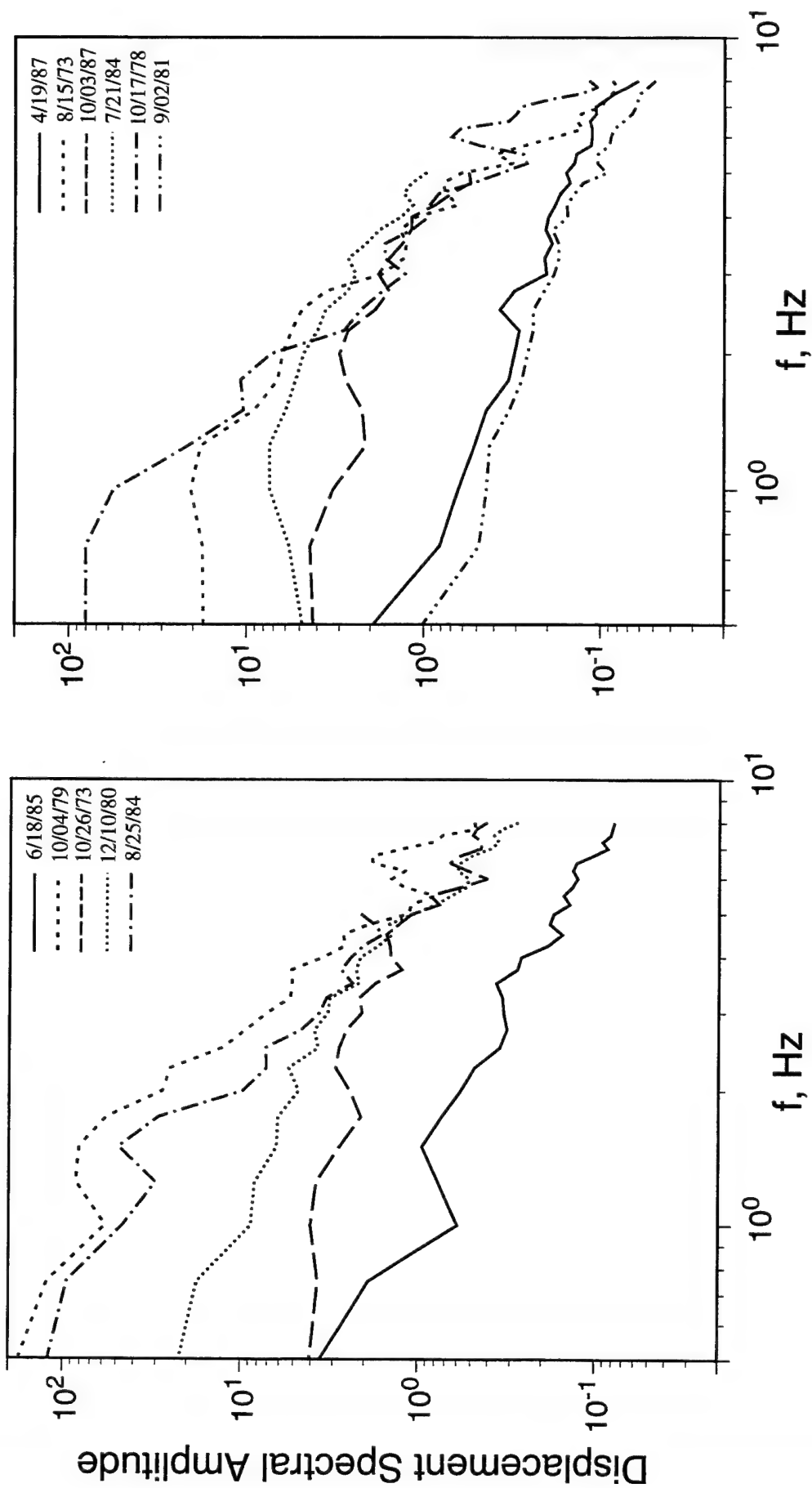


Figure B-9. Comparison of Borovoye  $P_g$  spectra for selected PNE events in the 8° (left) and 10.5° (right) distance groups.

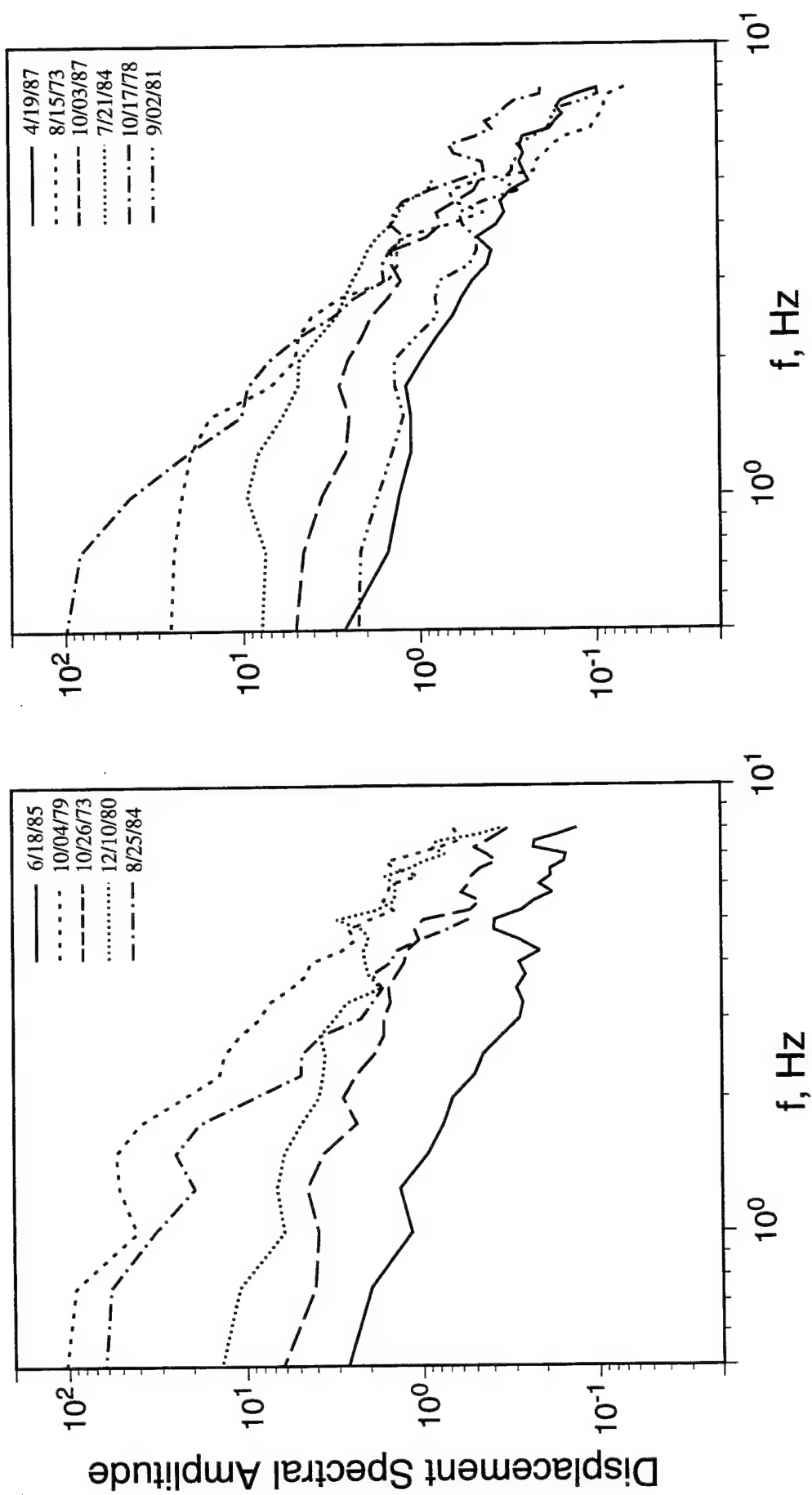


Figure B-10. Comparison of Borovoye  $S_n$  spectra for selected PNE events in the 8° (left) and 10.5° (right) distance groups.

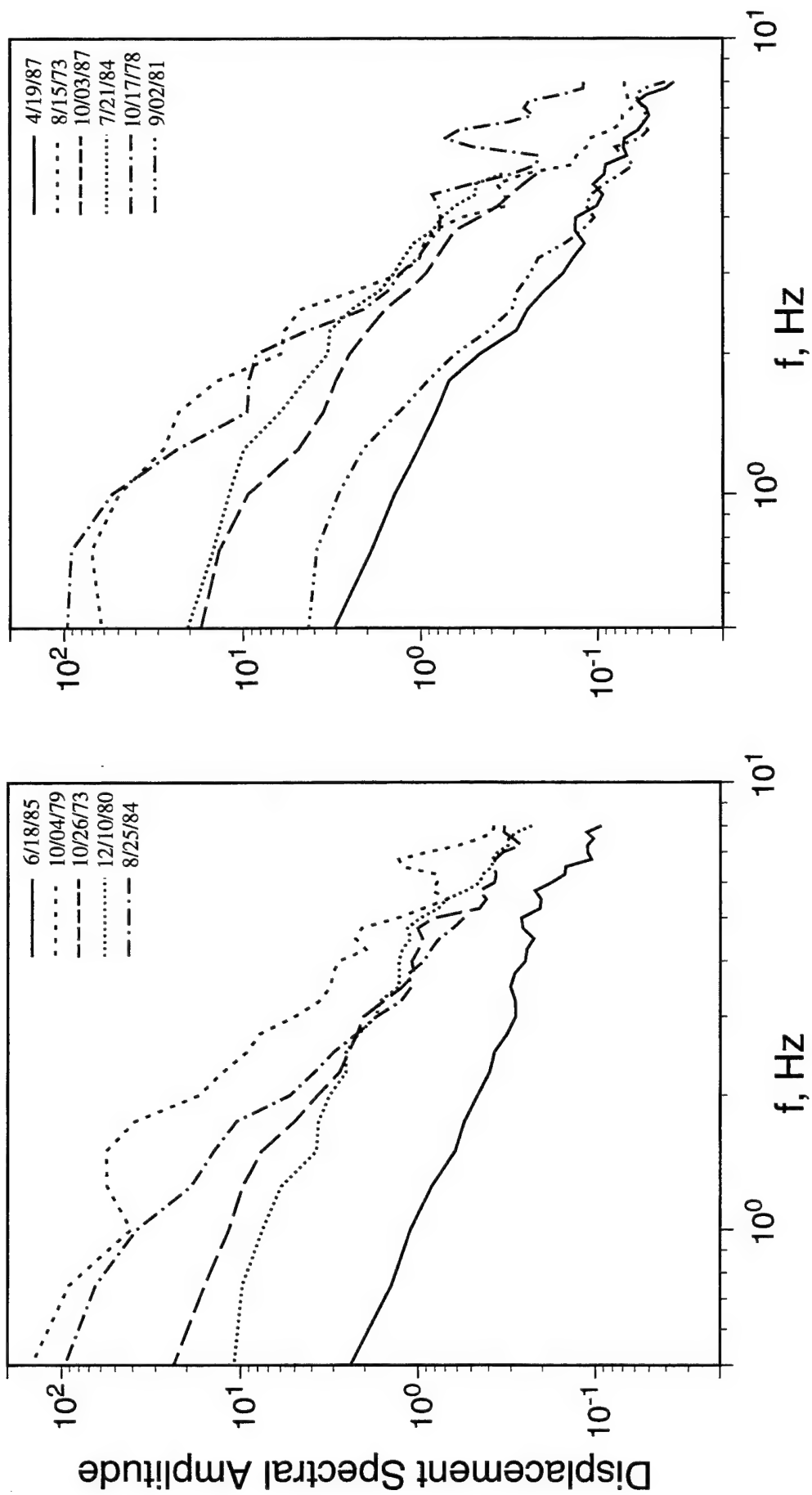


Figure B-11. Comparison of Borovoye  $L_g$  spectra for selected PNE events in the 8° (left) and 10.5° (right) distance groups.

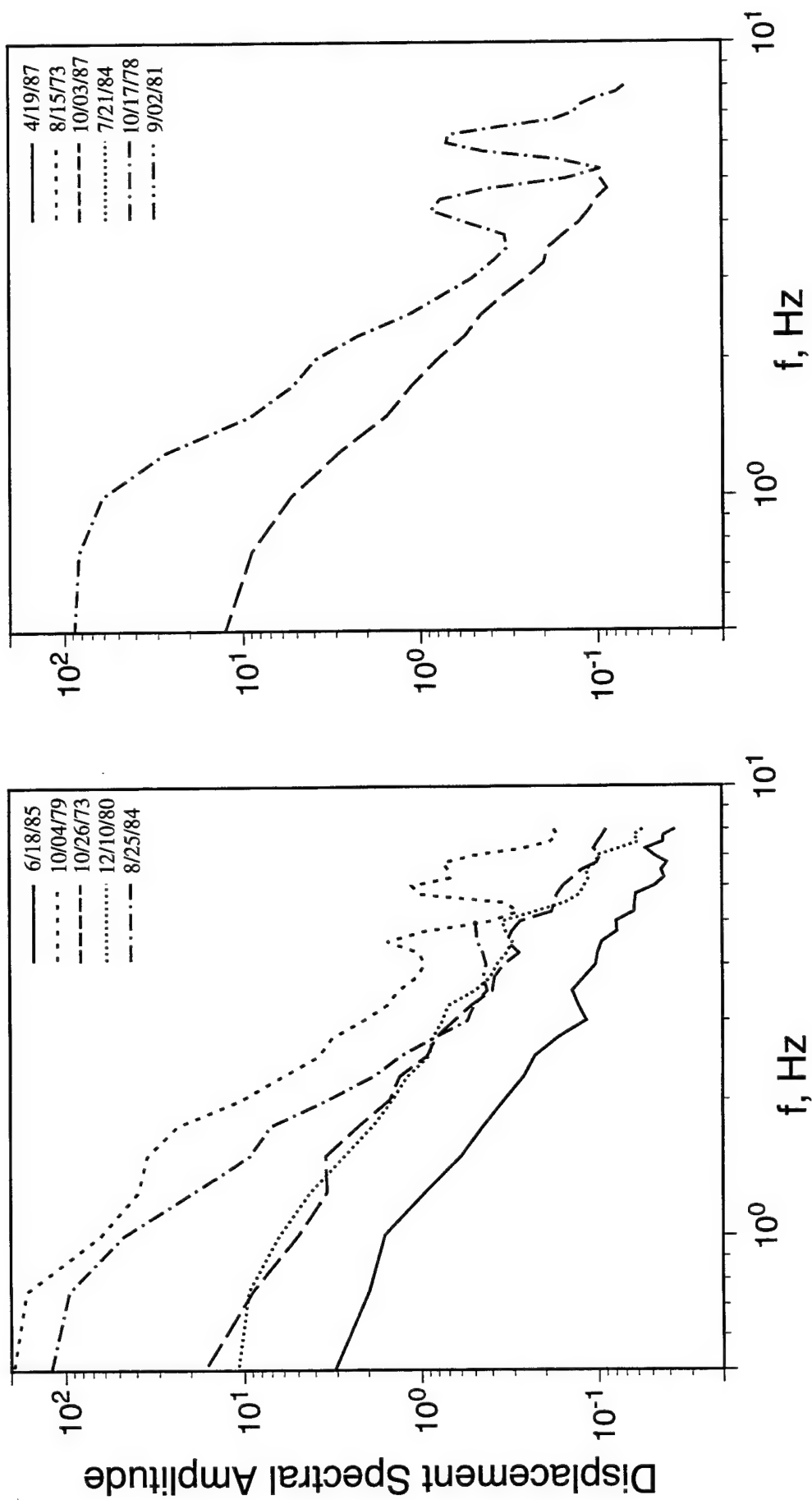


Figure B-12. Comparison of Borovoye  $L_{g\text{coda}}$  spectra for selected PNE events in the 8° (left) and 10.5° (right) distance groups.



## **Appendix C**

### **Comparison of Predicted and Observed Borovoye Regional Phase Spectra for the Selected PNE Events**

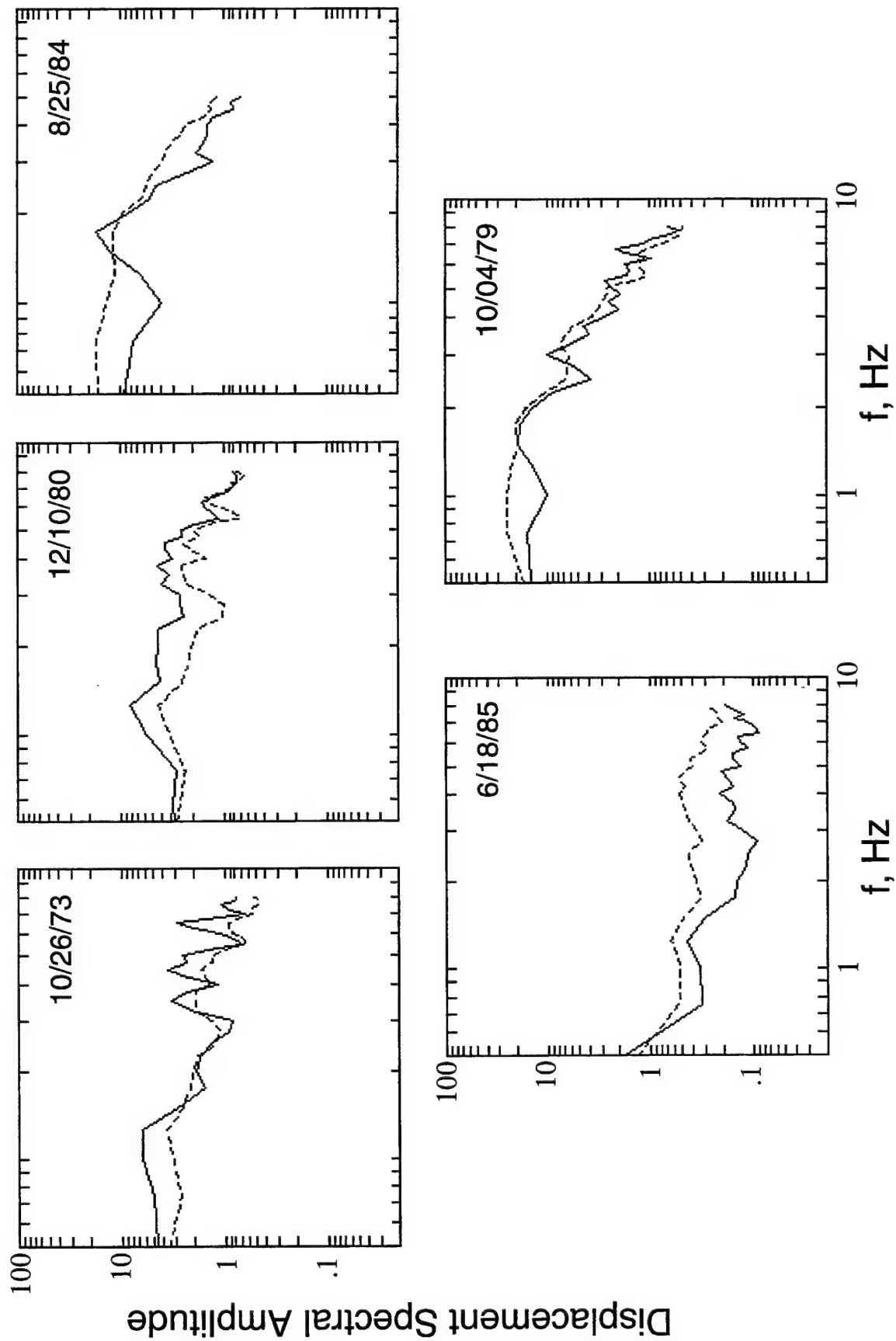


Figure C-1. Comparison of predicted (dashed) and observed (solid) Borovoye  $P_n$  amplitude spectra for the selected PNE events in the  $8^\circ$  distance range.

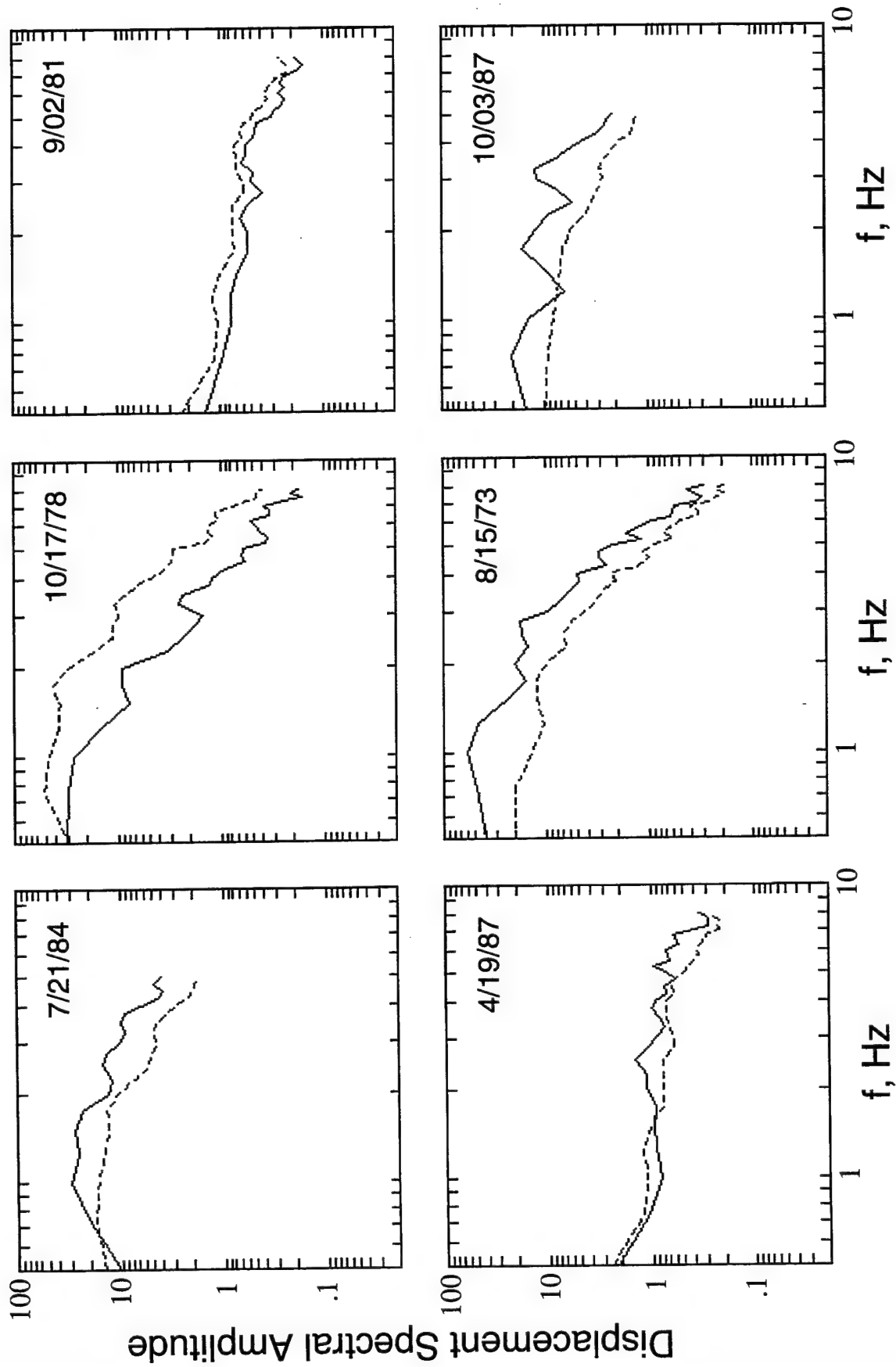


Figure C-2. Comparison of predicted (dashed) and observed (solid) Borovoye  $P_n$  amplitude spectra for the selected PNE events in the  $10.5^\circ$  distance range.

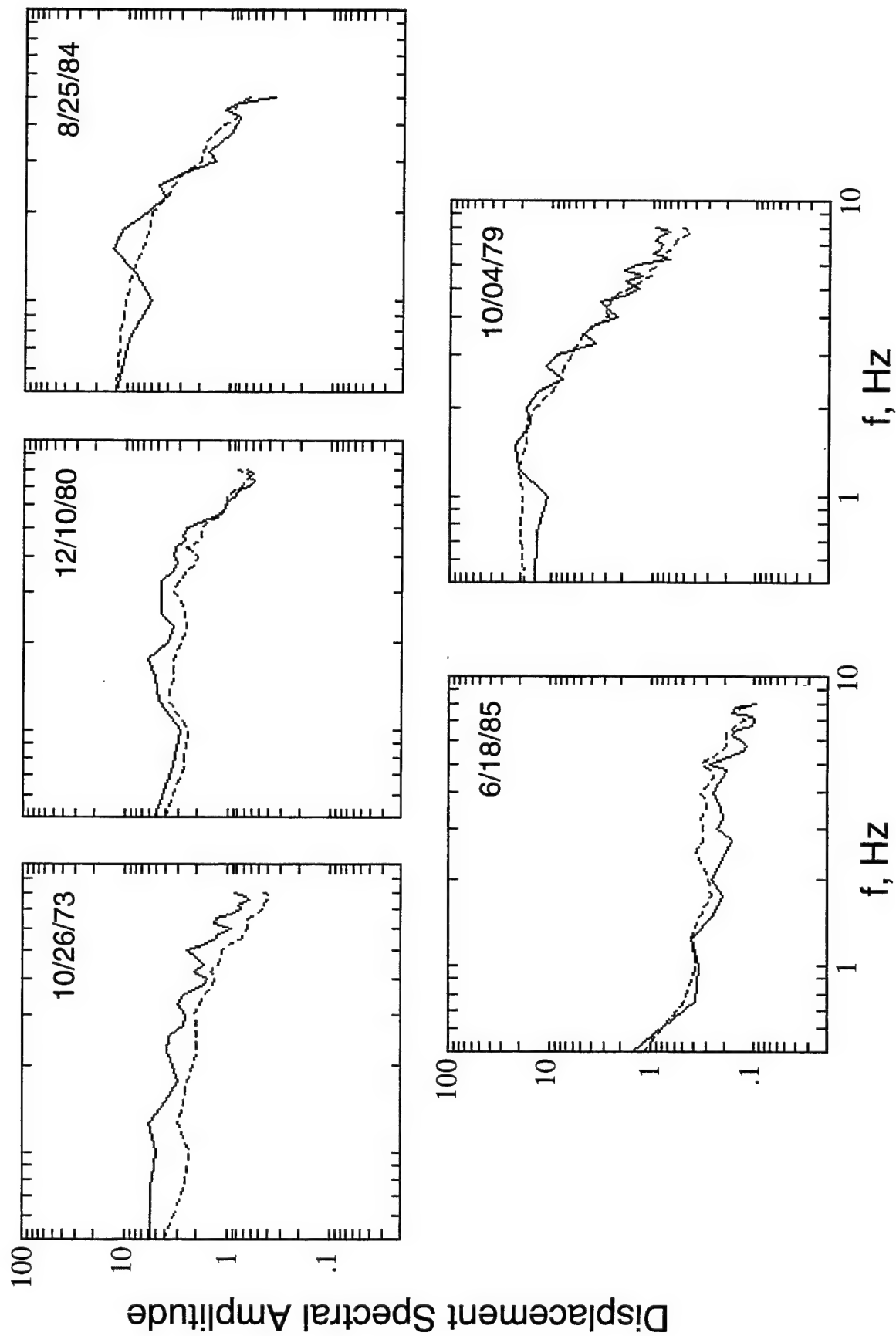


Figure C-3. Comparison of predicted (dashed) and observed (solid) Borovoye  $P_{\text{coda}}$  amplitude spectra for the selected PNE events in the  $8^\circ$  distance range.

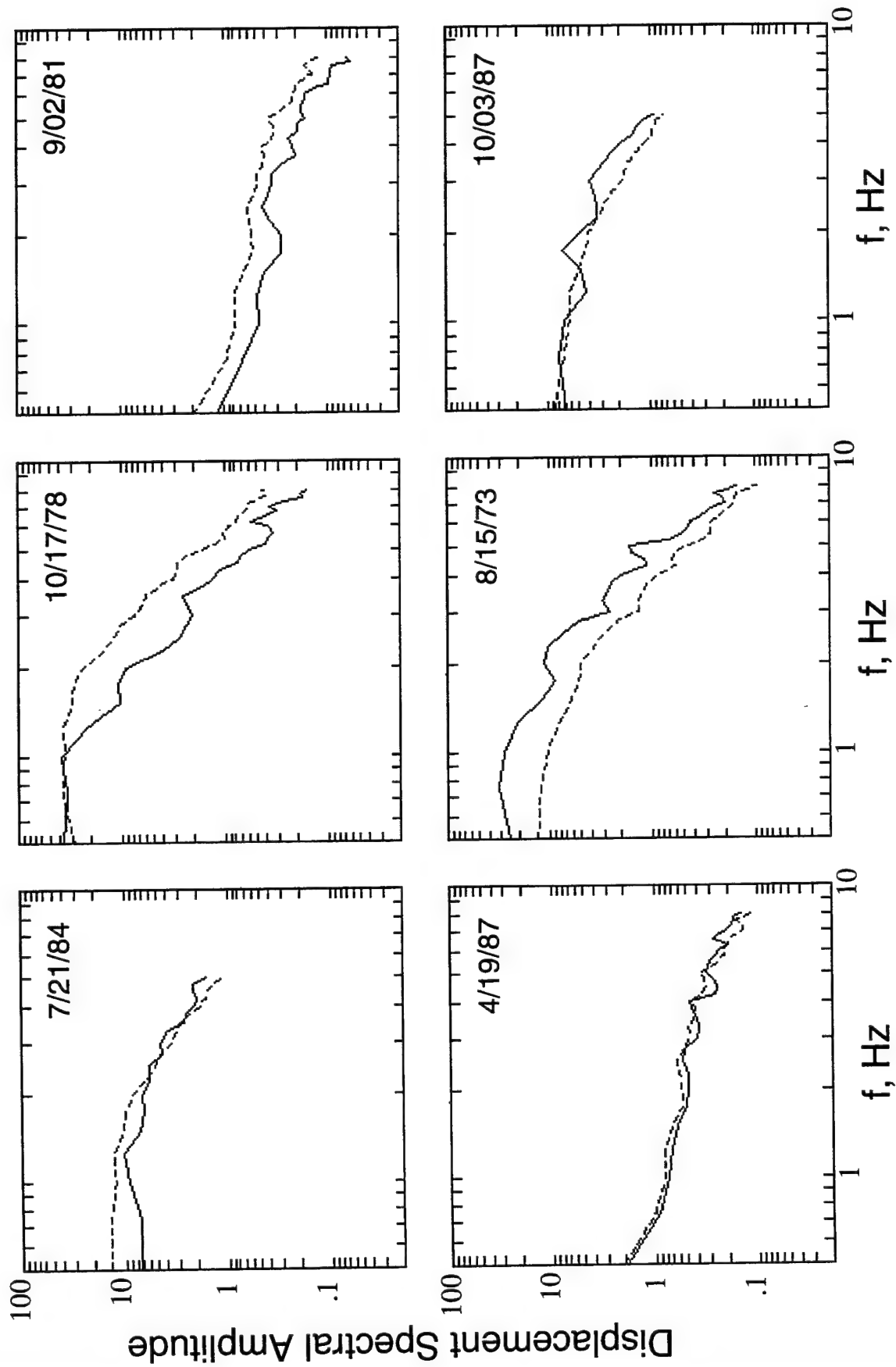


Figure C-4. Comparison of predicted (dashed) and observed (solid) Borovoye  $P_{\text{coda}}$  amplitude spectra for the selected PNE events in the  $10.5^\circ$  distance range.

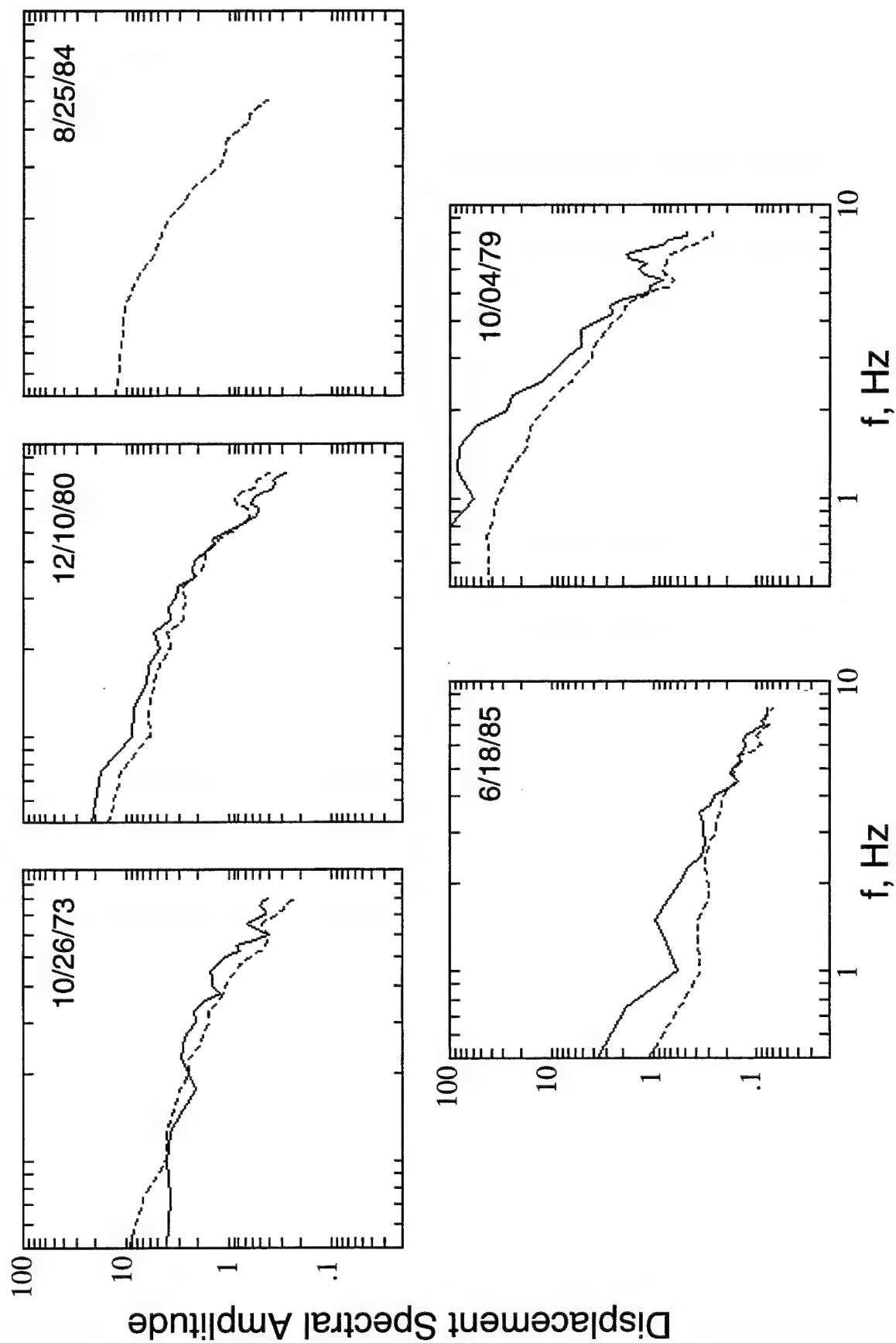


Figure C-5. Comparison of predicted (dashed) and observed (solid) Borovoye  $P_g$  amplitude spectra for the selected PNE events in the  $8^\circ$  distance range.

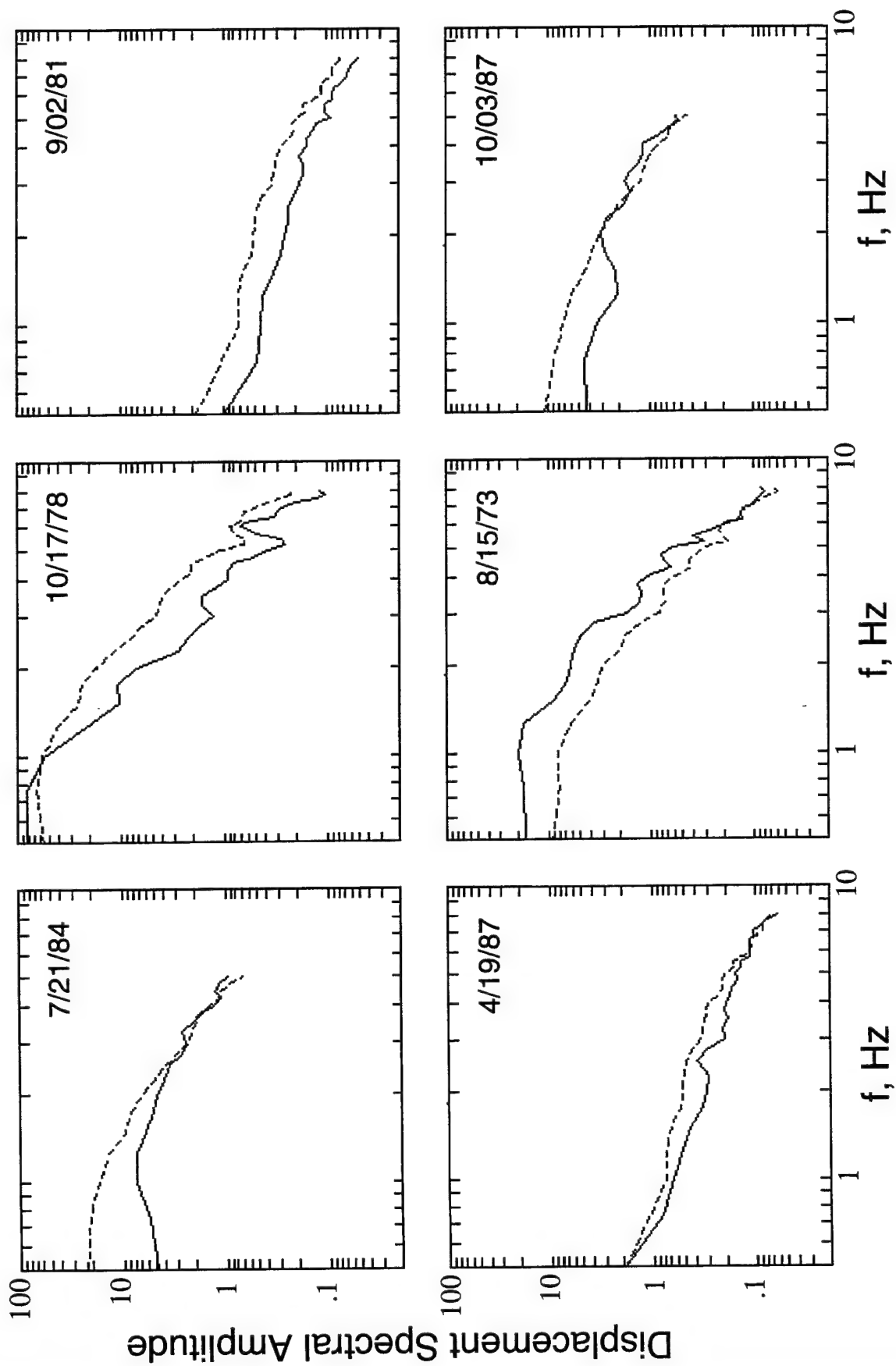


Figure C-6. Comparison of predicted (dashed) and observed (solid) Borovoye  $P_g$  amplitude spectra for the selected PNE events in the  $10.5^\circ$  distance range.

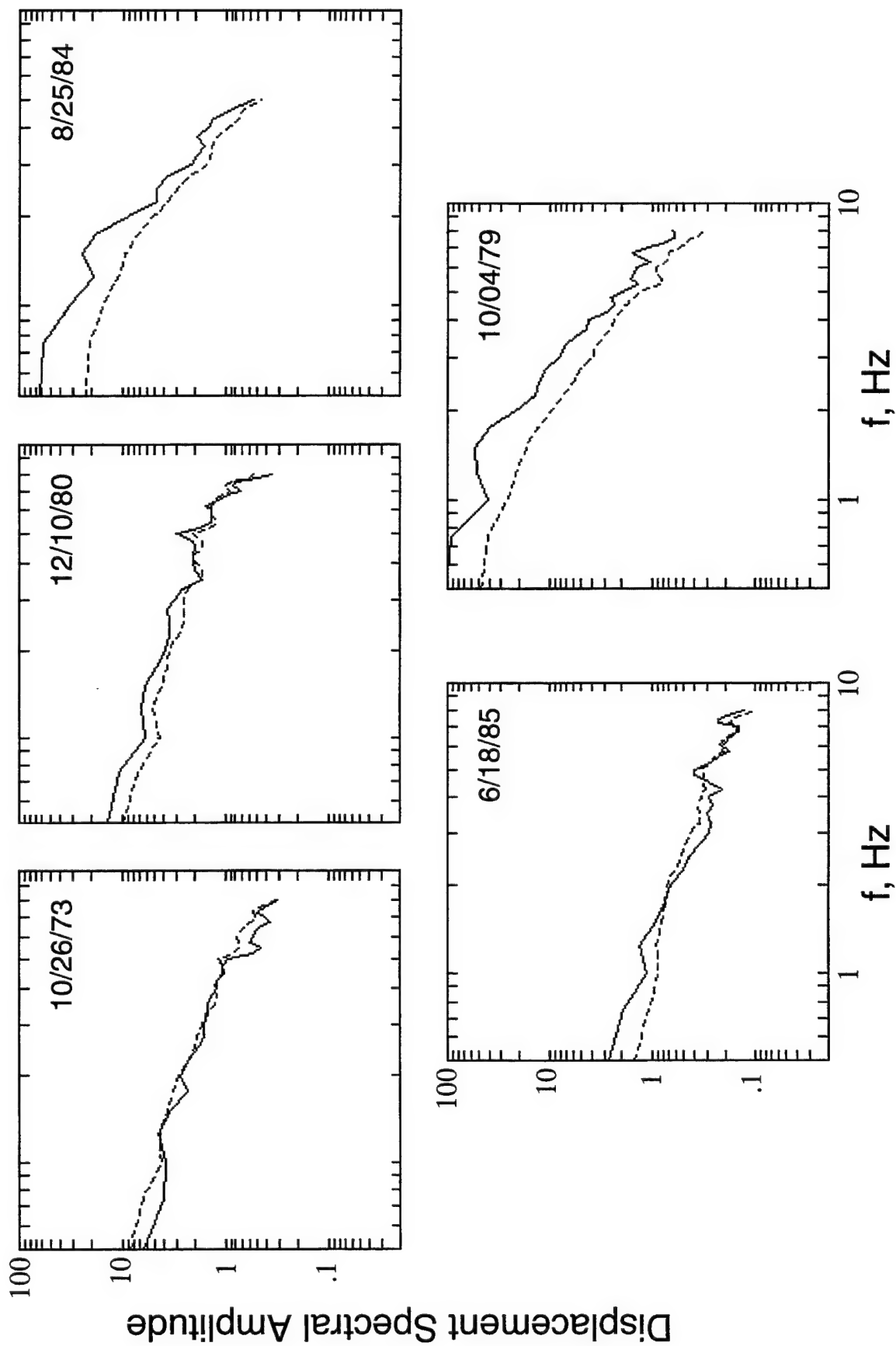


Figure C-7. Comparison of predicted (dashed) and observed (solid) Borovoye  $S_n$  amplitude spectra for the selected PNE events in the  $8^\circ$  distance range.

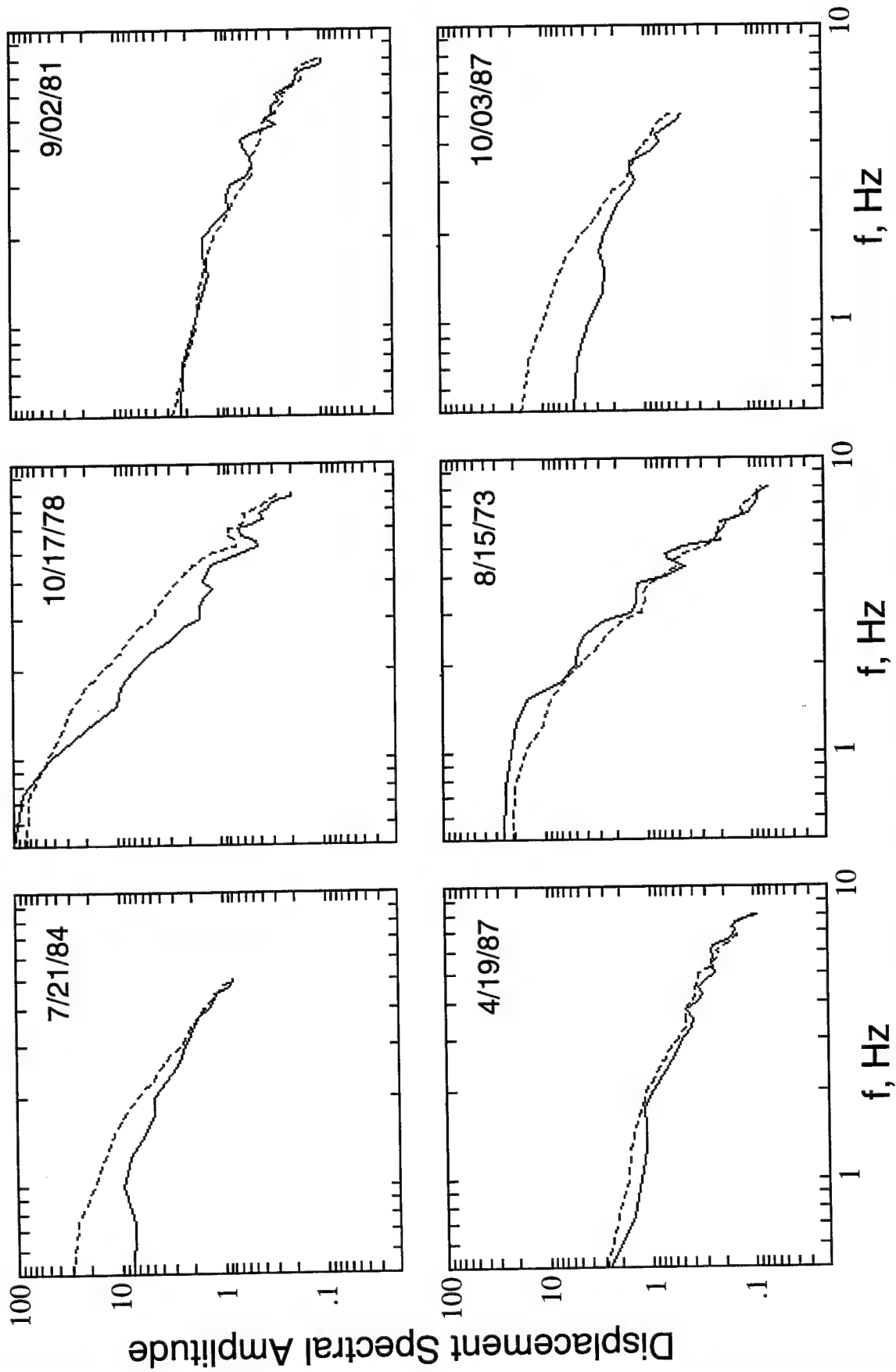


Figure C-8. Comparison of predicted (dashed) and observed (solid) Borovoye  $S_n$  amplitude spectra for the selected PNE events in the  $10.5^\circ$  distance range.

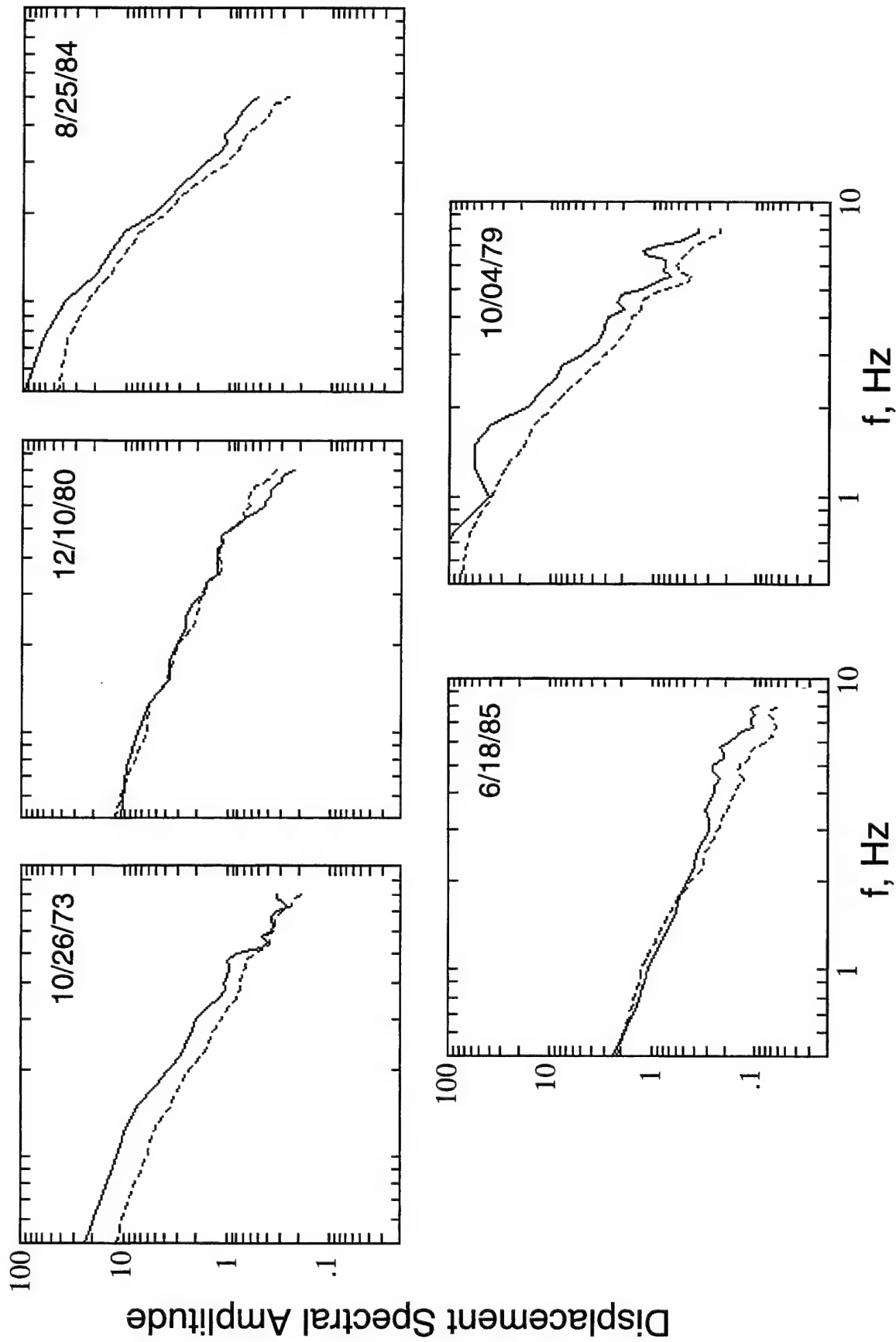


Figure C-9. Comparison of predicted (dashed) and observed (solid) Borovoye  $L_g$  amplitude spectra for the selected PNE events in the  $8^\circ$  distance range.

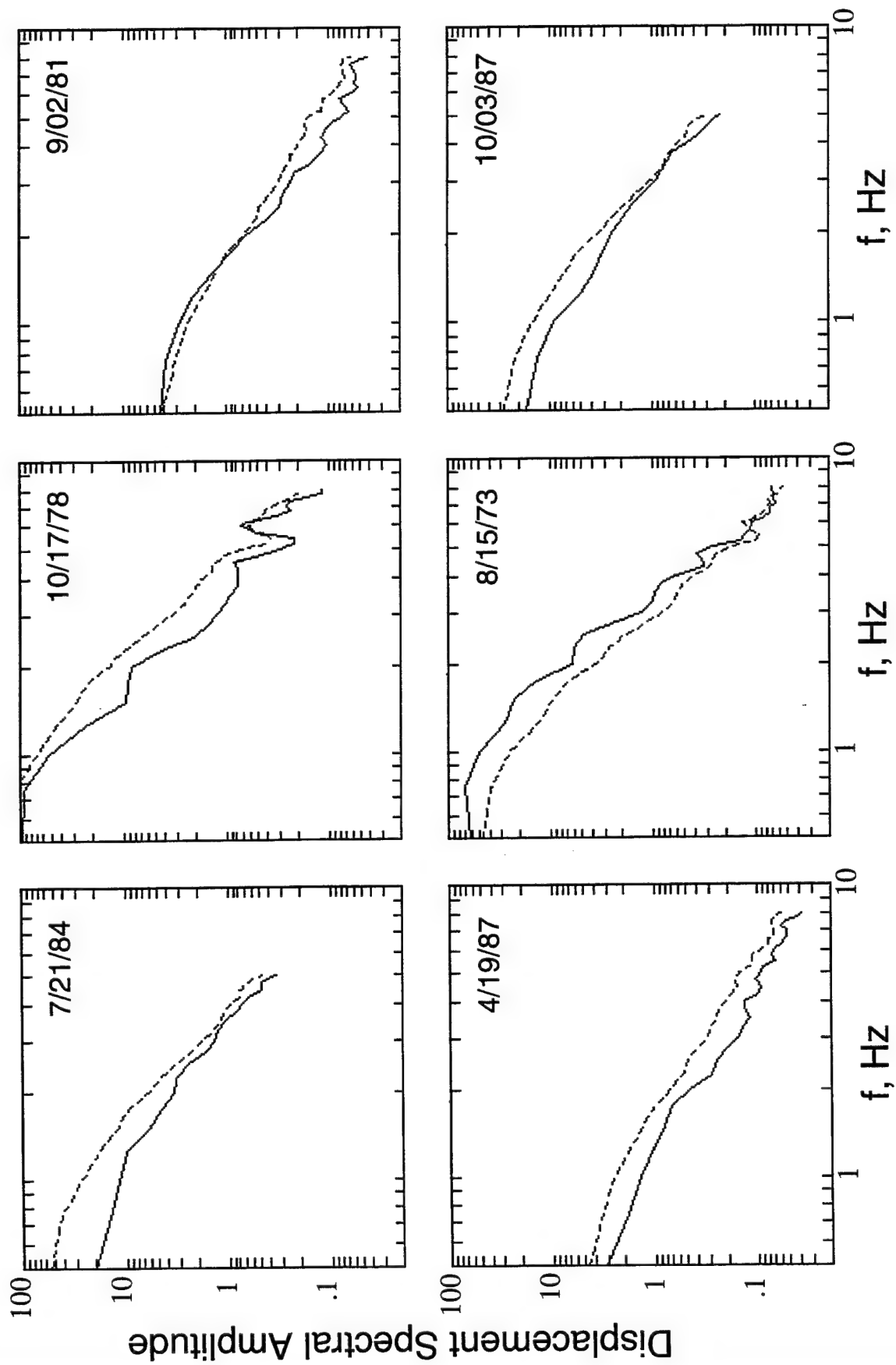


Figure C-10. Comparison of predicted (dashed) and observed (solid) Borovoye  $L_g$  amplitude spectra for the selected PNE events in the  $10.5^\circ$  distance range.

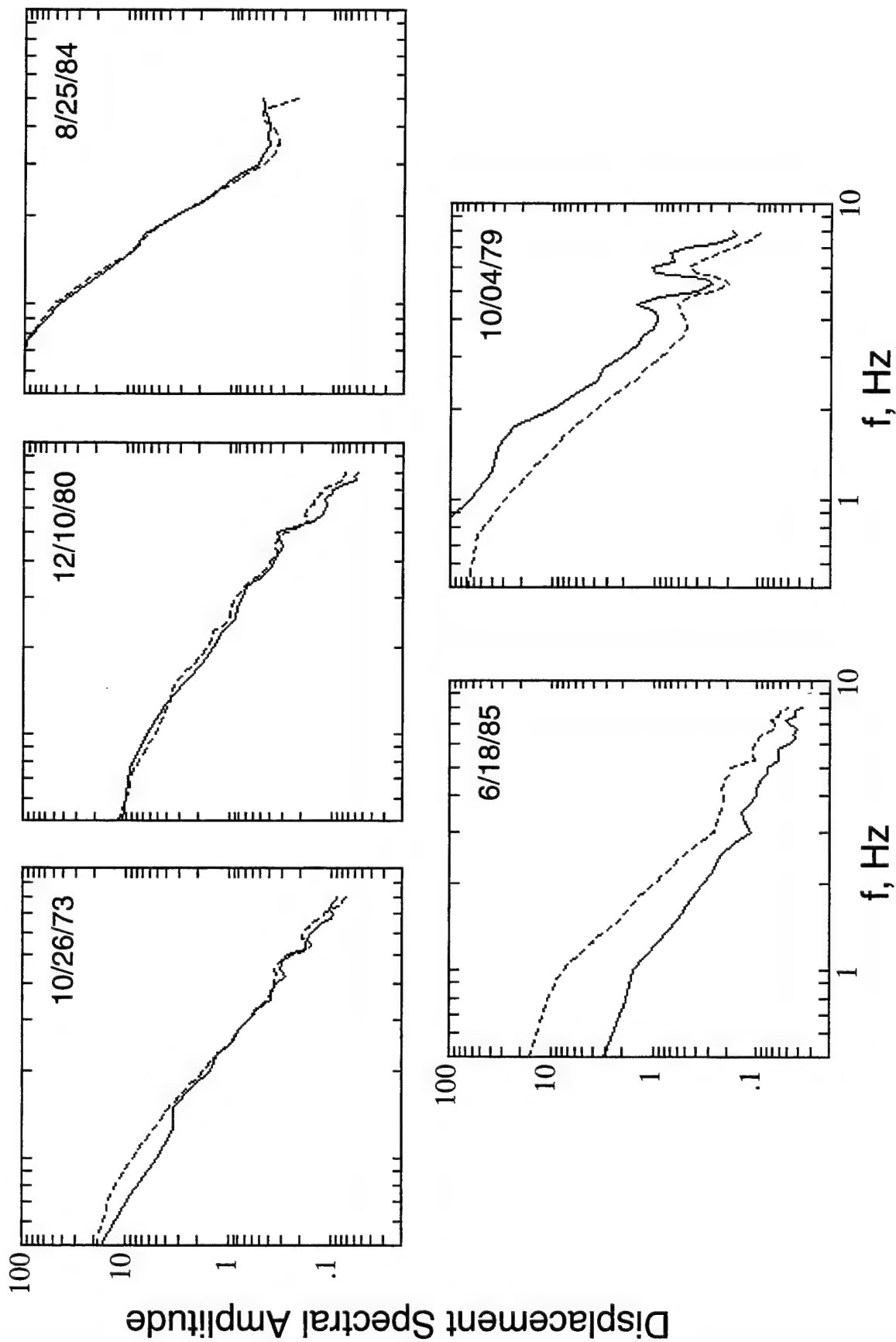


Figure C-11. Comparison of predicted (dashed) and observed (solid) Borovoye  $L_{gcoda}$  amplitude spectra for the selected PNE events in the  $8^\circ$  distance range.

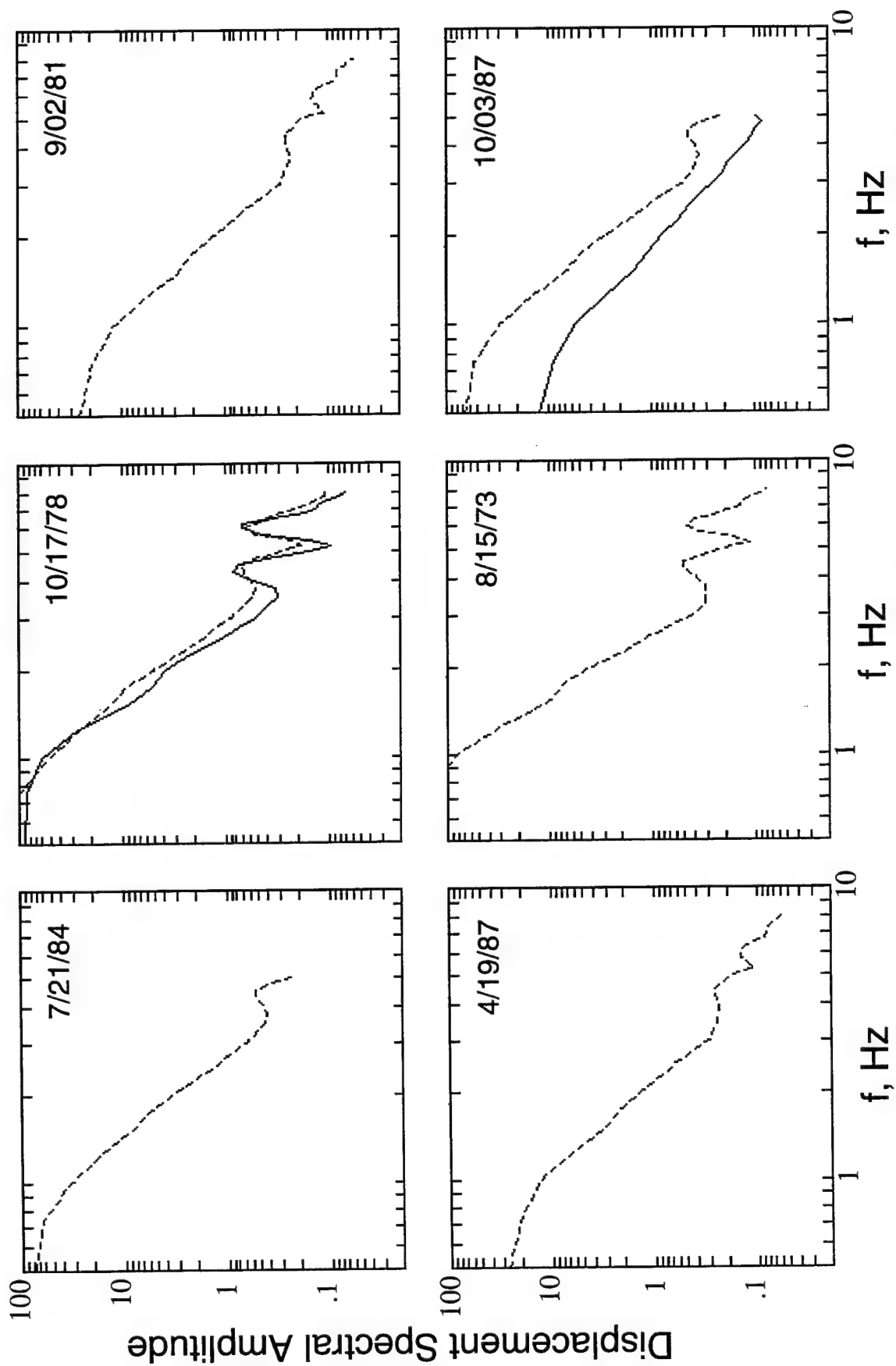


Figure C-12. Comparison of predicted (dashed) and observed (solid) Borovoye  $L_{gcoda}$  amplitude spectra for the selected PNE events in the  $10.5^\circ$  distance range.

THOMAS AHRENS  
SEISMOLOGICAL LABORATORY 252-21  
CALIFORNIA INSTITUTE OF TECHNOLOGY  
PASADENA, CA 91125

TECHNICAL STAFF:  
PLEASE ROUTE TO APPROPRIATE INDIVIDUALS  
LANL  
PO BOX 1663, MS F659  
LOS ALAMOS, NM 87545

MUAWIA BARAZANGI  
INSTITUTE FOR THE STUDY OF THE CONTINENTS  
3126 SNEE HALL  
CORNELL UNIVERSITY  
ITHACA, NY 14853

T.G. BARKER  
MAXWELL TECHNOLOGIES  
P.O. BOX 23558  
SAN DIEGO, CA 92123

TECHNICAL STAFF:  
PLEASE ROUTE TO APPROPRIATE INDIVIDUALS  
SNL, DEPT. 5791  
MS 0567, PO BOX 5800  
ALBUQUERQUE, NM 87185-0567

THERON J. BENNETT  
MAXWELL TECHNOLOGIES  
11800 SUNRISE VALLEY DRIVE SUITE 1212  
RESTON, VA 22091

JONATHAN BERGER  
UNIVERSITY OF CA, SAN DIEGO  
SCRIPPS INSTITUTION OF OCEANOGRAPHY IGPP, 0225  
9500 GILMAN DRIVE  
LA JOLLA, CA 92093-0225

TECHNICAL STAFF:  
PLEASE ROUTE TO APPROPRIATE INDIVIDUALS  
LANL  
PO BOX 1663, MS F665  
LOS ALAMOS, NM 87545

STEVEN BRATT  
NTPO  
1901 N. MOORE STREET, SUITE 609  
ARLINGTON, VA 22209

TECHNICAL STAFF:  
PLEASE ROUTE TO APPROPRIATE INDIVIDUALS  
LLNL  
PO BOX 808, MS L-221  
LIVERMORE, CA 94551

RALPH ALEWINE  
NTPO  
1901 N. MOORE STREET, SUITE 609  
ARLINGTON, VA 22209

TECHNICAL STAFF:  
PLEASE ROUTE TO APPROPRIATE INDIVIDUALS  
LLNL  
PO BOX 808, MS L-200  
LIVERMORE, CA 94551

RICHARD BARDZELL  
ACIS  
DCI/ACIS  
WASHINGTON, DC 20505

DOUGLAS BAUMGARDT  
ENSCO INC.  
5400 PORT ROYAL ROAD  
SPRINGFIELD, VA 22151

MARA BEGLEY  
ACIS  
NPIC/PO BOX 70967/SOUTHWEST STATION  
WASHINGTON, DC 20024-0967

WILLIAM BENSON  
NAS/COS  
ROOM HA372  
2001 WISCONSIN AVE. NW  
WASHINGTON, DC 20007

ROBERT BLANDFORD  
AFTAC  
1300 N. 17TH STREET  
SUITE 1450  
ARLINGTON, VA 22209-2308

TECHNICAL STAFF:  
PLEASE ROUTE TO APPROPRIATE INDIVIDUALS  
LLNL  
PO BOX 808, MS L-207  
LIVERMORE, CA 94551

TECHNICAL STAFF:  
PLEASE ROUTE TO APPROPRIATE INDIVIDUALS  
SNL, DEPT. 5704  
MS 0655, PO BOX 5800  
ALBUQUERQUE, NM 87185-0655

RHETT BUTLER  
IRIS  
1616 N. FORT MEYER DRIVE  
SUITE 1050  
ARLINGTON, VA 22209

TECHNICAL STAFF:  
PLEASE ROUTE TO APPROPRIATE INDIVIDUALS  
SNL, DEPT. 5736  
MS 0655, PO BOX 5800  
ALBUQUERQUE, NM 87185-0655

TECHNICAL STAFF:  
PLEASE ROUTE TO APPROPRIATE INDIVIDUALS  
SNL, DEPT. 9311  
MS 1159, PO BOX 5800  
ALBUQUERQUE, NM 87185-1159

SEAN DORAN  
ACIS  
DCI/ACIS  
WASHINGTON, DC 20505

TECHNICAL STAFF:  
PLEASE ROUTE TO APPROPRIATE INDIVIDUALS  
LLNL  
PO BOX 808, MS L-175  
LIVERMORE, CA 94551

RICHARD J. FANTEL  
BUREAU OF MINES  
DENVER FEDERAL CENTER  
DENVER, CO 80225

MARK D. FISK  
MISSION RESEARCH CORPORATION  
735 STATE STREET  
P.O. DRAWER 719  
SANTA BARBARA, CA 93102-0719

TECHNICAL STAFF:  
PLEASE ROUTE TO APPROPRIATE INDIVIDUALS  
PNL  
PO BOX 999, MS K6-48  
RICHLAND, WA 99352

LORI GRANT  
MULTIMAX, INC.  
311C FOREST AVE. SUITE 3  
PACIFIC GROVE, CA 93950

CATHERINE DE GROOT-HEDLIN  
SCRIPPS INSTITUTION OF OCEANOGRAPHY  
UNIVERSITY OF CALIFORNIA, SAN DIEGO  
INSTITUTE OF GEOPHYSICS AND PLANETARY PHYSICS  
LA JOLLA, CA 92093

TECHNICAL STAFF:  
PLEASE ROUTE TO APPROPRIATE INDIVIDUALS  
PNL  
PO BOX 999, MS K6-40  
RICHLAND, WA 99352

LESLIE A. CASEY  
DOE  
1000 INDEPENDENCE AVE. SW  
NN-40  
WASHINGTON, DC 20585-0420

DR. STANLEY DICKINSON  
AFOSR  
110 DUNCAN AVENUE  
SUITE B115  
BOLLING AFB, WASHINGTON D.C. 20332-001

DIANE I. DOSER  
DEPARTMENT OF GEOLOGICAL SCIENCES  
THE UNIVERSITY OF TEXAS AT EL PASO  
EL PASO, TX 79968

TECHNICAL STAFF:  
PLEASE ROUTE TO APPROPRIATE INDIVIDUALS  
SNL, DEPT. 4115  
MS 0329, PO BOX 5800  
ALBUQUERQUE, NM 87185-0329

JOHN FILSON  
ACIS/TMG/NTT  
ROOM 6T11 NHB  
WASHINGTON, DC 20505

TECHNICAL STAFF:  
PLEASE ROUTE TO APPROPRIATE INDIVIDUALS  
LLNL  
PO BOX 808, MS L-208  
LIVERMORE, CA 94551

ROBERT GEIL  
DOE  
PALAIS DES NATIONS, RM D615  
GENEVA 10, SWITZERLAND

HENRY GRAY  
SMU STATISTICS DEPARTMENT  
P.O. BOX 750302  
DALLAS, TX 75275-0302

TECHNICAL STAFF:  
PLEASE ROUTE TO APPROPRIATE INDIVIDUALS  
PNL  
PO BOX 999, MS K7-34  
RICHLAND, WA 99352

JAMES HAYES  
NSF  
4201 WILSON BLVD., ROOM 785  
ARLINGTON, VA 22230

THOMAS HEARN  
NEW MEXICO STATE UNIVERSITY  
DEPARTMENT OF PHYSICS  
LAS CRUCES, NM 88003

DONALD HELMBERGER  
CALIFORNIA INSTITUTE OF TECHNOLOGY  
DIVISION OF GEOLOGICAL & PLANETARY SCIENCES  
SEISMOLOGICAL LABORATORY  
PASADENA, CA 91125

ROBERT HERRMANN  
ST. LOUIS UNIVERSITY  
DEPARTMENT OF EARTH & ATMOSPHERIC SCIENCES  
3507 LACLEDE AVENUE  
ST. LOUIS, MO 63103

ANTHONY IANNACCHIONE  
BUREAU OF MINES  
COCHRANE MILL ROAD  
PO BOX 18070  
PITTSBURGH, PA 15236-9986

THORNE LAY  
UNIVERSITY OF CALIFORNIA, SANTA CRUZ  
EARTH SCIENCES DEPARTMENT  
EARTH & MARINE SCIENCE BUILDING  
SANTA CRUZ, CA 95064

DONALD A. LINGER  
DNA  
6801 TELEGRAPH ROAD  
ALEXANDRIA, VA 22310

KEITH MCLAUGHLIN  
MAXWELL TECHNOLOGIES  
P.O. BOX 23558  
SAN DIEGO, CA 92123

BRIAN MITCHELL  
DEPARTMENT OF EARTH & ATMOSPHERIC SCIENCES  
ST. LOUIS UNIVERSITY  
3507 LACLEDE AVENUE  
ST. LOUIS, MO 63103

JOHN MURPHY  
MAXWELL TECHNOLOGIES  
11800 SUNRISE VALLEY DRIVE SUITE 1212  
RESTON, VA 22091

CHARLES ODDENINO  
BUREAU OF MINES  
810 7TH ST. NW  
WASHINGTON, DC 20241

MICHAEL HEDLIN  
UNIVERSITY OF CALIFORNIA, SAN DIEGO  
SCRIPPS INSTITUTION OF OCEANOGRAPHY IGPP, 0225  
9500 GILMAN DRIVE  
LA JOLLA, CA 92093-0225

EUGENE HERRIN  
SOUTHERN METHODIST UNIVERSITY  
DEPARTMENT OF GEOLOGICAL SCIENCES  
DALLAS, TX 75275-0395

VINDELL HSU  
HQ/AFTAC/TTR  
1030 S. HIGHWAY A1A  
PATRICK AFB, FL 32925-3002

THOMAS JORDAN  
MASSACHUSETTS INSTITUTE OF TECHNOLOGY  
EARTH, ATMOSPHERIC & PLANETARY SCIENCES  
77 MASSACHUSETTS AVENUE, 54-918  
CAMBRIDGE, MA 02139

ANATOLI L. LEVSHIN  
DEPARTMENT OF PHYSICS  
UNIVERSITY OF COLORADO  
CAMPUS BOX 390  
BOULDER, CO 80309-0309

GARY MCCARTOR  
SOUTHERN METHODIST UNIVERSITY  
DEPARTMENT OF PHYSICS  
DALLAS, TX 75275-0395

TECHNICAL STAFF:  
PLEASE ROUTE TO APPROPRIATE INDIVIDUALS  
PNL  
PO BOX 999, MS K7-22  
RICHLAND, WA 99352

RICHARD MORROW  
USACDA/IVI  
320 21ST STREET, N.W.  
WASHINGTON, DC 20451

JAMES NI  
NEW MEXICO STATE UNIVERSITY  
DEPARTMENT OF PHYSICS  
LAS CRUCES, NM 88003

JOHN ORCUTT  
INSTITUTE OF GEOPHYSICS AND PLANETARY PHYSICS  
INSTITUTE OF GEOPHYSICS AND PLANETARY PHYSICS  
UNIVERSITY OF CALIFORNIA, SAN DIEGO  
LA JOLLA, CA 92093

FRANK PILOTTE  
HQ/AFTAC/TT  
1030 S. HIGHWAY A1A  
PATRICK AFB, FL 32925-3002

JAY PULLI  
RADIX SYSTEMS, INC.  
6 TAFT COURT  
ROCKVILLE, MD 20850

PAUL RICHARDS  
COLUMBIA UNIVERSITY  
LAMONT-DOHERTY EARTH OBSERVATORY  
PALISADES, NY 10964

TECHNICAL STAFF:  
PLEASE ROUTE TO APPROPRIATE INDIVIDUALS  
LLNL  
PO BOX 808, MS L-202  
LIVERMORE, CA 94551

THOMAS SERENO JR.  
SCIENCE APPLICATIONS INTERNATIONAL  
CORPORATION  
10260 CAMPUS POINT DRIVE  
SAN DIEGO, CA 92121

ROBERT SHUMWAY  
410 MRAK HALL  
DIVISION OF STATISTICS  
UNIVERSITY OF CALIFORNIA  
DAVIS, CA 95616-8671

TECHNICAL STAFF:  
PLEASE ROUTE TO APPROPRIATE INDIVIDUALS  
LANL  
PO BOX 1663, MS D460  
LOS ALAMOS, NM 87545

TECHNICAL STAFF:  
PLEASE ROUTE TO APPROPRIATE INDIVIDUALS  
LLNL  
PO BOX 808, MS L-195  
LIVERMORE, CA 94551

TECHNICAL STAFF:  
PLEASE ROUTE TO APPROPRIATE INDIVIDUALS  
LANL  
PO BOX 1663, MS C335  
LOS ALAMOS, NM 87545

DAVID THOMAS  
ISEE  
29100 AURORA ROAD  
CLEVELAND, OH 44139

KEITH PRIESTLEY  
DEPARTMENT OF EARTH SCIENCES  
UNIVERSITY OF CAMBRIDGE  
MADINGLEY RISE, MADINGLEY ROAD  
CAMBRIDGE, CB3 0EZ UK

TECHNICAL STAFF:  
PLEASE ROUTE TO APPROPRIATE INDIVIDUALS  
PNL  
PO BOX 999, MS K5-72  
RICHLAND, WA 99352

TECHNICAL STAFF:  
PLEASE ROUTE TO APPROPRIATE INDIVIDUALS  
PNL  
PO BOX 999, MS K6-84  
RICHLAND, WA 99352

CHANDAN SAIKIA  
WOODWARD-CLYDE FEDERAL SERVICES  
566 EL DORADO ST., SUITE 100  
PASADENA, CA 91101-2560

AVI SHAPIRA  
SEISMOLOGY DIVISION  
THE INSTITUTE FOR PETROLEUM RESEARCH AND  
GEOPHYSICS  
P.O.B. 2286, NOLON 58122 ISRAEL

TECHNICAL STAFF:  
PLEASE ROUTE TO APPROPRIATE INDIVIDUALS  
SNL, DEPT. 5704  
MS 0979, PO BOX 5800  
ALBUQUERQUE, NM 87185-0979

DAVID SIMPSON  
IRIS  
1616 N. FORT MEYER DRIVE  
SUITE 1050  
ARLINGTON, VA 22209

JEFFRY STEVENS  
MAXWELL TECHNOLOGIES  
P.O. BOX 23558  
SAN DIEGO, CA 92123

BRIAN SULLIVAN  
BOSTON COLLEGE  
INSITUTE FOR SPACE RESEARCH  
140 COMMONWEALTH AVENUE  
CHESTNUT HILL, MA 02167

NAFI TOKSOZ  
EARTH RESOURCES LABORATORY, M.I.T.  
42 CARLTON STREET, E34-440  
CAMBRIDGE, MA 02142

LAWRENCE TURNBULL  
ACIS  
DCI/ACIS  
WASHINGTON, DC 20505

GREG VAN DER VINK  
IRIS  
1616 N. FORT MEYER DRIVE  
SUITE 1050  
ARLINGTON, VA 22209

TECHNICAL STAFF:  
PLEASE ROUTE TO APPROPRIATE INDIVIDUALS  
LLNL  
PO BOX 808, MS L-205  
LIVERMORE, CA 94551

JAMES WHITCOMB  
NSF  
NSF/ISC OPERATIONS/EAR-785  
4201 WILSON BLVD., ROOM 785  
ARLINGTON, VA 22230

JIANG XIE  
ST. LOUIS UNIVERSITY  
DEPARTMENT OF EARTH & ATMOSPHERIC SCIENCES  
3507 LACLEDE AVENUE  
ST. LOUIS, MO 63103

TECHNICAL STAFF: PLEASE ROUTE TO APPROPRIATE  
INDIVIDUALS  
SNL, DEPT. 6116  
MS 0750, PO BOX 5800  
ALBUQUERQUE, NM 87185-0750

SECRETARY OF THE AIR FORCE  
(SAFRD)  
WASHINGTON, DC 20330

DEFENSE TECHNICAL INFORMATION CENTER  
8725 JOHN J. KINGMAN ROAD  
FT BELVOIR, VA 22060-6218 (2 COPIES)

PHILLIPS LABORATORY  
ATTN: XPG  
29 RANDOLPH ROAD  
HANSCOM AFB, MA 01731-3010

PHILLIPS LABORATORY  
ATTN: TSML  
5 WRIGHT STREET  
HANSCOM AFB, MA 01731-3004

FRANK VERNON  
UNIVERSITY OF CALIFORNIA, SAN DIEGO  
SCRIPPS INSTITUTION OF OCEANOGRAPHY IGPP, 0225  
9500 GILMAN DRIVE  
LA JOLLA, CA 92093-0225

TERRY WALLACE  
UNIVERSITY OF ARIZONA  
DEPARTMENT OF GEOSCIENCES  
BUILDING #77  
TUCSON, AZ 85721

DANIEL WEILL  
NSF  
EAR-785  
4201 WILSON BLVD., ROOM 785  
ARLINGTON, VA 22230

RU SHAN WU  
UNIVERSITY OF CALIFORNIA SANTA CRUZ  
EARTH SCIENCES DEPT.  
1156 HIGH STREET  
SANTA CRUZ, CA 95064

TECHNICAL STAFF:  
PLEASE ROUTE TO APPROPRIATE INDIVIDUALS  
PNL  
PO BOX 999, MS K5-12  
RICHLAND, WA 99352

JAMES E. ZOLLWEG  
BOISE STATE UNIVERSITY  
GEOSCIENCES DEPT.  
1910 UNIVERSITY DRIVE  
BOISE, ID 83725

OFFICE OF THE SECRETARY OF DEFENSE  
DDR&E  
WASHINGTON, DC 20330

TACTEC  
BATTELLE MEMORIAL INSTITUTE  
505 KING AVENUE  
COLUMBUS, OH 43201 (FINAL REPORT)

PHILLIPS LABORATORY  
ATTN: GPE  
29 RANDOLPH ROAD  
HANSCOM AFB, MA 01731-3010

PHILLIPS LABORATORY  
ATTN: PL/SUL  
3550 ABERDEEN AVE SE  
KIRTLAND, NM 87117-5776 (2 COPIES)